

EFFECTS OF DESIGN PARAMETERS ON THE AEROELASTIC
PERFORMANCE OF A CRUISE MISSILE WING

A THESIS SUBMITTED TO
THE GRADUATE SCHOOL OF NATURAL AND APPLIED SCIENCES
OF
MIDDLE EAST TECHNICAL UNIVERSITY



BY

BURAK ERTÜRK

IN PARTIAL FULFILLMENT OF THE REQUIREMENTS
FOR
THE DEGREE OF MASTER OF SCIENCE
IN
AEROSPACE ENGINEERING

AUGUST 2019

Approval of the thesis:

**EFFECTS OF DESIGN PARAMETERS ON THE AEROELASTIC
PERFORMANCE OF A CRUISE MISSILE WING**

submitted by **BURAK ERTÜRK** in partial fulfillment of the requirements for the degree of **Master of Science in Aerospace Engineering Department, Middle East Technical University** by,

Prof. Dr. Halil Kalıpçılar
Dean, Graduate School of **Natural and Applied Sciences**

Prof. Dr. İsmail Hakkı Tuncer
Head of Department, **Aerospace Engineering**

Prof. Dr. Yavuz Yaman
Supervisor, **Aerospace Engineering, METU**

Examining Committee Members:

Assoc. Prof. Dr. Ercan Gürses
Aerospace Engineering, METU

Prof. Dr. Yavuz Yaman
Aerospace Engineering, METU

Prof. Dr. Ender Ciğeroğlu
Mechanical Engineering, METU

Prof. Dr. Kürşad Melih Güleren
Flight Training, ESTÜ

Assist. Prof. Dr. Mustafa Kaya
Aerospace Engineering, AYBU

Date: 29.08.2019



I hereby declare that all information in this document has been obtained and presented in accordance with academic rules and ethical conduct. I also declare that, as required by these rules and conduct, I have fully cited and referenced all material and results that are not original to this work.

Name, Surname: Burak Ertürk

Signature:

ABSTRACT

EFFECTS OF DESIGN PARAMETERS ON THE AEROELASTIC PERFORMANCE OF A CRUISE MISSILE WING

Ertürk, Burak
Master of Science, Aerospace Engineering
Supervisor: Prof. Dr. Yavuz Yaman

August 2019, 104 pages

The design of a cruise missile wing is a multidisciplinary work since the wing has to provide enough aerodynamic forces while being structurally safe. Furthermore, the wing needs to satisfy other considerations such as propulsion, weight, flight performance, sizing for launch platform integration and other measures of merit. In order to meet these design requirements and achieve a successful design, several parameters of the wing need to be investigated at various flight conditions. In this thesis, aeroelastic characteristics of different wing geometries are investigated at various altitudes and speeds. The design of experiments is constructed by changing several variables of the wing systematically to have a better understanding of the effects of design parameters on the aeroelastic characteristics of the wings. Flutter speeds are calculated to examine the aeroelastic characteristics of the wings and the aeroelastic analyses for the determination of the flutter speed are conducted by using ZAERO package program.

Keywords: Aeroelasticity, Design Parameters, Flutter, Wing Design

ÖZ

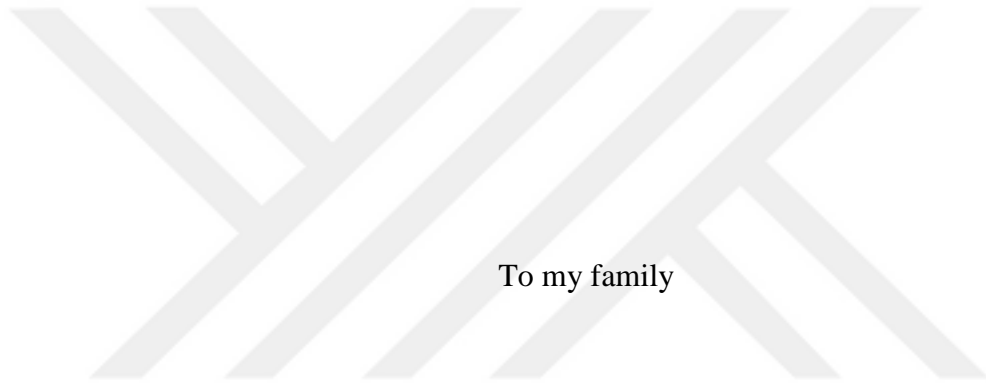
TASARIM DEĞİŞKENLERİNİN BİR SEYİR FÜZESİ KANADININ AEROELASTİK PERFORMANSI ÜZERİNDEKİ ETKİLERİ

Ertürk, Burak
Yüksek Lisans, Havacılık ve Uzay Mühendisliği
Tez Danışmanı: Prof. Dr. Yavuz Yaman

Ağustos 2019, 104 sayfa

Bir seyir füzesi kanadının tasarımı çok disiplinli bir çalışmadır, çünkü kanat yapısal olarak sağlıklı durumda gerekli aerodinamik kuvvetleri sağlamak zorundadır. Bunun yanı sıra kanat; itki, ağırlık, uçuş performansı, fırlatma platformuna entegrasyonu için olan boyutlandırması gibi diğer başarımlı ölçütlerini sağlamak zorundadır. Bu tasarım gereksinimlerini karşılamak ve başarılı bir tasarım elde etmek için, çeşitli uçuş koşullarında kanadın çeşitli parametrelerinin incelenmesi gerekmektedir. Bu tezde, farklı kanat geometrilerinin aeroelastik karakterleri çeşitli irtifalarda ve hızlarda incelenmiştir. Tasarım değişkenlerinin kanatların aeroelastik karakteristiklerine olan etkilerini daha iyi anlayabilmek için kanada ait birtakım değişkenler değiştirilerek bir deney tasarımı oluşturulmuştur. Kanatların aeroelastik karakteristiklerini incelemek için çarpınma hızları hesaplanmış ve çarpınma hızını elde etmek için aeroelastik analizler ZAERO paket programı ile gerçekleştirilmiştir.

Anahtar Kelimeler: Aeroelastisite, Çarpıntı, Kanat Tasarımı, Tasarım Değişkenleri



To my family

ACKNOWLEDGEMENTS

I would like to express my appreciation, indebtedness and gratitude to my supervisor Prof. Dr. Yavuz Yaman for his guidance, insight, encouragement, understanding and patience throughout this study.

I would also like to thank to my thesis committee members, Assoc. Prof. Dr. Ercan Gürses, Prof. Dr. Ender Ciğerođlu, Prof. Dr. Kürşad Melih Güleren, and Assist. Prof. Dr. Mustafa Kaya for their valuable and helpful comments and criticisms on the research.

I wish to thank to TÜBİTAK-SAGE for allowing me to make this investigation. I would also like to thank to Mr. Taylan Karaağaçlı for his support from beginning to end of the thesis. I would like to extend my thanks to my colleagues in Aerodynamics Division for their support to motivate me in order to complete my studies.

I am especially grateful to my parents Adile Ertürk and Mustafa Ertürk, and my brother Veli Can Ertürk for their endless support.

My acknowledgements will never end without special mention of a very valuable person for me. Special thanks also go to my wife Sinem for her endless love and motivation. She shared all of the difficulties of this work with me and showed understanding.

TABLE OF CONTENTS

ABSTRACT	v
ÖZ	vi
ACKNOWLEDGEMENTS	viii
TABLE OF CONTENTS	ix
LIST OF TABLES	xii
LIST OF FIGURES	xiii
LIST OF ABBREVIATIONS	xviii
LIST OF SYMBOLS	xix
CHAPTERS	
1. INTRODUCTION	1
1.1. Background of the Study	1
1.2. Introduction to the Aeroelasticity	2
1.3. Literature Survey	4
1.4. Contents of the Thesis	10
2. VARIATION OF DESIGN PARAMETERS	11
2.1. Design of Experiments	12
3. THEORY OF AEROELASTIC ANALYSES	15
3.1. Governing Equations	15
3.1.1. Modal Reduction Approach	17
3.1.2. Unified AIC of ZAERO	19

3.1.3. The Spline Matrix.....	21
3.2. Flutter Solution Techniques	23
3.2.1. The K-Method	23
3.2.2. The P-K Method	25
3.2.3. The g-Method	27
3.2.3.1. Solution Algorithm of the g-Method	28
3.3. Solution Procedure of the ZAERO	29
3.3.1. Brief Summary	29
3.3.2. Sections of the ZAERO Input File	31
3.3.2.1. Executive Control Section	32
3.3.2.2. Case Control Section	32
3.3.2.3. Bulk Data Section	33
4. ANALYSES OF THE WINGS	35
4.1. Generation of the Wing Solid Models	35
4.2. Finite Element Modeling and Analyses of the Wings	38
4.3. Aerodynamic Modeling of the Wings.....	44
4.4. Preparation of the ZAERO Solution Setup.....	46
4.4.1. Executive Control Section.....	46
4.4.2. Case Control Section	47
4.4.3. Bulk Data Section.....	47
4.5. Determination of the Flutter Speed.....	49
5. RESULTS AND DISCUSSIONS	51
5.1. Flutter Analysis Results	51
5.2. Effects of the Aspect Ratio	53

5.3. Effects of the Taper Ratio	54
5.4. Effects of the Sweep Angle	55
5.5. Effect of the Altitude	57
6. CONCLUSIONS	59
6.1. General Conclusions.....	59
6.2. Recommendations for Future Work	60
REFERENCES.....	61
APPENDICES	
A. Technical Drawing of the Wing Geometries	65
B. Mode Shapes of the Wings	75
C. Flutter Analysis Results	85

LIST OF TABLES

TABLES

Table 2.1. Variation of design parameters.....	13
Table 2.2. Flight conditions for the aeroelastic analyses.....	13
Table 4.1. Material properties of 2014-T6 aluminum alloy that used in finite element model	41
Table 4.2. Natural frequencies of the wings (in Hz).....	43
Table 4.3. A set of reduced frequencies (in Hz)	48

LIST OF FIGURES

FIGURES

Figure 1.1. Collar's Aeroelastic Triangle [4]	2
Figure 1.2. Aeroelasticity tree	3
Figure 1.3. Flutter test mechanism [5]	4
Figure 1.4. Flutter test wing geometries [5]	5
Figure 1.5. Effects of the aspect ratio on the flutter speed and frequency [5]	5
Figure 1.6. Effects of the sweepback angle on flutter speed and frequency [5]	6
Figure 1.7. Wingspan variation [6]	7
Figure 1.8. Effects of the span on the divergence characteristics of the wing [6]	7
Figure 1.9. UAV wingspan variation [7]	8
Figure 1.10. Effects of the span on the flutter speed and frequency [7]	8
Figure 1.11. The plan-form of the plate wing [8]	9
Figure 1.12. Effects of the taper ratio on the divergence and flutter speeds [8]	9
Figure 3.1. Aeroelastic Functional Diagram	16
Figure 3.2. Panel model of an aircraft	20
Figure 3.3. AGARD 445.6 K-method flutter results (ZONA6), M=0.9 [14]	24
Figure 3.4. AGARD 445.6 P-K method flutter results (ZONA6), M=0.9 [10]	26
Figure 3.5. Executive Control Section	32
Figure 3.6. Case Control Section	32
Figure 3.7. Bulk Data Section	33
Figure 4.1. A comparison of a conventional airfoil and the NASA supercritical airfoil [23]	36
Figure 4.2. Definition of the sweep angle	37
Figure 4.3. Technical drawing of the Wing 4 (AR=10, TR=0.75, SA=30°)	37
Figure 4.4. Different grids from coarse to fine	39
Figure 4.5. First mode frequency of the Wing 4 with respect to different grids	40

Figure 4.6. Second mode frequency of the Wing 4 with respect to different grids...	40
Figure 4.7. Surface mesh around the Wing 4 in finite element model	41
Figure 4.8. Schematic of the wing	42
Figure 4.9. First five mode shapes of the Wing 4 (AR=10, TR=0.75, SA=30°).....	44
Figure 4.10. Spanwise and chordwise divisions of the wing [22].....	45
Figure 4.11. Grid of the aerodynamic model for the Wing 4	46
Figure 4.12. Warning message for violation of the convergence criteria.....	46
Figure 4.13. Infinite Plate Spline Method	48
Figure 4.14. Determination of the speed of the aeroelastic problem.....	50
Figure 4.15. Determination of the frequency of the aeroelastic problem.....	50
Figure 5.1. Velocity vs. Damping plots for the Wing 4	52
Figure 5.2. Velocity vs. Frequency plots for the Wing 4	52
Figure 5.3. Effects of the aspect ratio on the flutter speed	54
Figure 5.4. Effects of the taper ratio on the flutter speed	55
Figure 5.5. Effects of the sweep angle on the flutter speed.....	56
Figure 5.6. Effect of the altitude on the flutter speed	57
Figure A.1. Technical drawing of the Wing 1	65
Figure A.2. Technical drawing of the Wing 2	65
Figure A.3. Technical drawing of the Wing 3	66
Figure A.4. Technical drawing of the Wing 4	66
Figure A.5. Technical drawing of the Wing 5	67
Figure A.6. Technical drawing of the Wing 6	67
Figure A.7. Technical drawing of the Wing 7	68
Figure A.8. Technical drawing of the Wing 8	68
Figure A.9. Technical drawing of the Wing 9	69
Figure A.10. Technical drawing of the Wing 10	69
Figure A.11. Technical drawing of the Wing 11	70
Figure A.12. Technical drawing of the Wing 12	70
Figure A.13. Technical drawing of the Wing 13	71
Figure A.14. Technical drawing of the Wing 14	71

Figure A.15. Technical drawing of the Wing 15	71
Figure A.16. Technical drawing of the Wing 16	72
Figure A.17. Technical drawing of the Wing 17	72
Figure A.18. Technical drawing of the Wing 18	72
Figure A.19. Technical drawing of the Wing 19	73
Figure A.20. Technical drawing of the Wing 20	73
Figure A.21. First five mode shapes of the Wing 1	75
Figure A.22. First five mode shapes of the Wing 2	75
Figure A.23. First five mode shapes of the Wing 3	76
Figure A.24. First five mode shapes of the Wing 4	76
Figure A.25. First five mode shapes of the Wing 5	77
Figure A.26. First five mode shapes of the Wing 6	77
Figure A.27. First five mode shapes of the Wing 7	78
Figure A.28. First five mode shapes of the Wing 8	78
Figure A.29. First five mode shapes of the Wing 9	79
Figure A.30. First five mode shapes of the Wing 10	79
Figure A.31. First five mode shapes of the Wing 11	80
Figure A.32. First five mode shapes of the Wing 12	80
Figure A.33. First five mode shapes of the Wing 13	81
Figure A.34. First five mode shapes of the Wing 14	81
Figure A.35. First five mode shapes of the Wing 15	82
Figure A.36. First five mode shapes of the Wing 16	82
Figure A.37. First five mode shapes of the Wing 17	83
Figure A.38. First five mode shapes of the Wing 18	83
Figure A.39. First five mode shapes of the Wing 19	84
Figure A.40. First five mode shapes of the Wing 20	84
Figure A.41. Velocity vs. Damping plots for the Wing 1	85
Figure A.42. Velocity vs. Frequency plots for the Wing 1	85
Figure A.43. Velocity vs. Damping plots for the Wing 2	86
Figure A.44. Velocity vs. Frequency plots for the Wing 2	86

Figure A.45. Velocity vs. Damping plots for the Wing 3.....	87
Figure A.46. Velocity vs. Frequency plots for the Wing 3.....	87
Figure A.47. Velocity vs. Damping plots for the Wing 4.....	88
Figure A.48. Velocity vs. Frequency plots for the Wing 4.....	88
Figure A.49. Velocity vs. Damping plots for the Wing 5.....	89
Figure A.50. Velocity vs. Frequency plots for the Wing 5.....	89
Figure A.51. Velocity vs. Damping plots for the Wing 6.....	90
Figure A.52. Velocity vs. Frequency plots for the Wing 6.....	90
Figure A.53. Velocity vs. Damping plots for the Wing 7.....	91
Figure A.54. Velocity vs. Frequency plots for the Wing 7.....	91
Figure A.55. Velocity vs. Damping plots for the Wing 8.....	92
Figure A.56. Velocity vs. Frequency plots for the Wing 8.....	92
Figure A.57. Velocity vs. Damping plots for the Wing 9.....	93
Figure A.58. Velocity vs. Frequency plots for the Wing 9.....	93
Figure A.59. Velocity vs. Damping plots for the Wing 10.....	94
Figure A.60. Velocity vs. Frequency plots for the Wing 10.....	94
Figure A.61. Velocity vs. Damping plots for the Wing 11.....	95
Figure A.62. Velocity vs. Frequency plots for the Wing 11.....	95
Figure A.63. Velocity vs. Damping plots for the Wing 12.....	96
Figure A.64. Velocity vs. Frequency plots for the Wing 12.....	96
Figure A.65. Velocity vs. Damping plots for the Wing 13.....	97
Figure A.66. Velocity vs. Frequency plots for the Wing 13.....	97
Figure A.67. Velocity vs. Damping plots for the Wing 14.....	98
Figure A.68. Velocity vs. Frequency plots for the Wing 14.....	98
Figure A.69. Velocity vs. Damping plots for the Wing 15.....	99
Figure A.70. Velocity vs. Frequency plots for the Wing 15.....	99
Figure A.71. Velocity vs. Damping plots for the Wing 16.....	100
Figure A.72. Velocity vs. Frequency plots for the Wing 16.....	100
Figure A.73. Velocity vs. Damping plots for the Wing 17.....	101
Figure A.74. Velocity vs. Frequency plots for the Wing 17.....	101

Figure A.75. Velocity vs. Damping plots for the Wing 18	102
Figure A.76. Velocity vs. Frequency plots for the Wing 18	102
Figure A.77. Velocity vs. Damping plots for the Wing 19	103
Figure A.78. Velocity vs. Frequency plots for the Wing 19	103
Figure A.79. Velocity vs. Damping plots for the Wing 20	104
Figure A.80. Velocity vs. Frequency plots for the Wing 20	104



LIST OF ABBREVIATIONS

AIC	Aerodynamic Influence Coefficient
AR	Aspect Ratio
DOE	Design of Experiments
DOF	Degrees of Freedom
FEM	Finite Element Method
IPS	Infinite Plate Spline
SA	Sweep Angle
SAGE	Defense Industries Research and Development Institute
TR	Taper Ratio
TÜBİTAK	The Scientific and Technological Research Council of Turkey

LIST OF SYMBOLS

A	Area of the wing
C	Damping matrix
c_{root}	Root chord of the wing
c_{tip}	Tip chord of the wing
f	Frequency
F	Aerodynamic force
ft	Feet
g	Damping
G	Spline matrix
γ	Decay rate
h	Structural deformation
k	Reduced frequency
K	Stiffness matrix
kft	1000 feet
L	Reference length
λ	Eigenvalue
M	Mass matrix
p	Laplace parameter
Φ	Modal matrix

Q	Aerodynamic forces matrix
q_{∞}	Dynamic pressure
ρ	Density
S	Span of the wing
V	Velocity
$V-f$	Velocity versus frequency
$V-g$	Velocity versus damping
x	Structural deformation
ξ	Modal coordinates
ω	Harmonic oscillatory frequency

CHAPTER 1

INTRODUCTION

1.1. Background of the Study

In the beginning of the design process, the customer defines the mission (or scenario) of the desired missile. This scenario consists of flight conditions such as altitude, speed, angles of attack/sideslip, etc. The design requirements that must be satisfied to perform defined mission emerge as a result of studies in different disciplines [1].

In order to meet the design requirements and achieve a successful design, multidisciplinary design optimization needs to be performed. This design process comprises of sizing of different components of the missile. Various parameters of the missile components are investigated during the design phase. Since it is a multidisciplinary process, different disciplines must work together in the design of the missile.

The wing may be pointed as the most important component of a cruise missile because it is needed to reach long range. The primary function of the wing is to generate sufficient aerodynamic force. While looking to aerodynamic forces during the design phase, structural health of the wing should also be considered. That's why a cruise missile wing design involves fundamental trade-offs between different disciplines. These fundamental trade-offs can have complex interactions, especially as the wing design problem includes additional design parameters [2].

In this complexity, predicting the effects of the design parameters to estimate the geometric constraints is highly important. Besides, these effects may not be the same at different flight conditions on which the cruise missile flying. In this thesis, it is aimed that increasing awareness about the aeroelastic effects of various design parameters on a cruise missile wing. Thus, analyses have been conducted in such a

way that in each group of runs, one design parameter has been varied while the other relevant parameters have been kept constant.

1.2. Introduction to the Aeroelasticity

Aeroelasticity is an important consideration in cruise missile design. Its studying area includes the mutual interaction between inertial, elastic and aerodynamic forces on cruise missile structure. Since the cruise missile structure has flexibility, aeroelastic problems may occur. If the structure were perfectly rigid, there would not be any aeroelastic problem but it is not possible in reality.

In order to categorize aeroelastic problems, Collar defined his famous triangle [3]. Bisplinghoff et al. recreated this triangle as given in Figure 1.1 [4]. In this figure, the symbols of I, E, and A represent the inertial, elastic, and aerodynamic forces respectively.

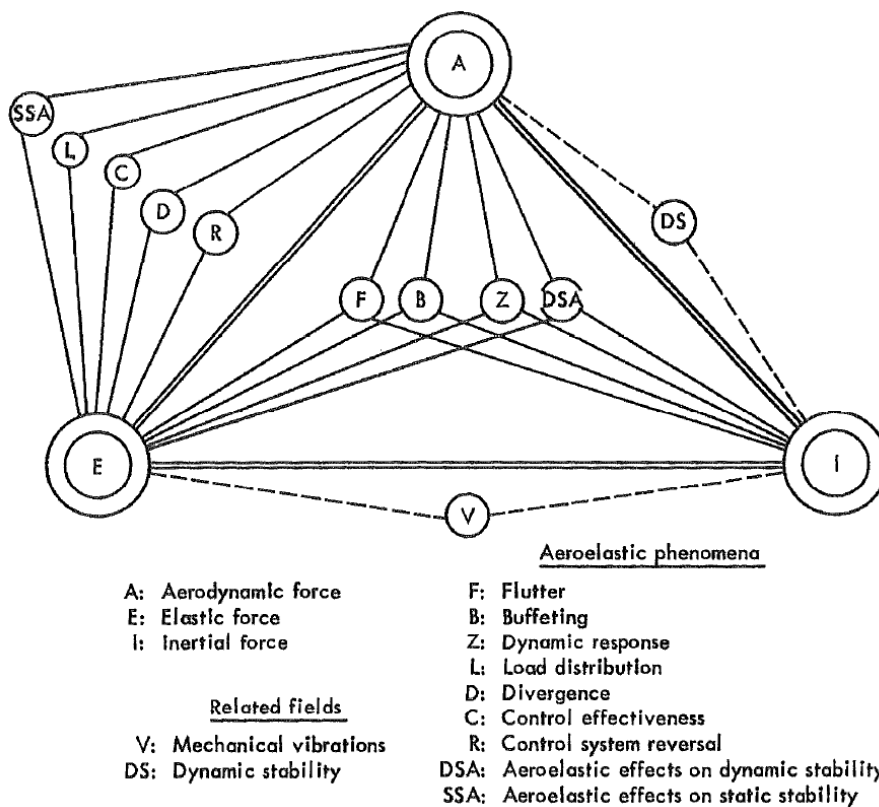


Figure 1.1. Collar's Aeroelastic Triangle [4]

Furthermore, aeroelastic problems are divided into two categories as static and dynamic aeroelasticity. The aeroelastic problems occurring as a result of interaction between elastic and aerodynamic forces are named as static aeroelastic problems while the aeroelastic problems occurring as a result of interaction between inertial, elastic and aerodynamic forces are named as dynamic aeroelastic problems. Schematic of this categorization is given in Figure 1.2.

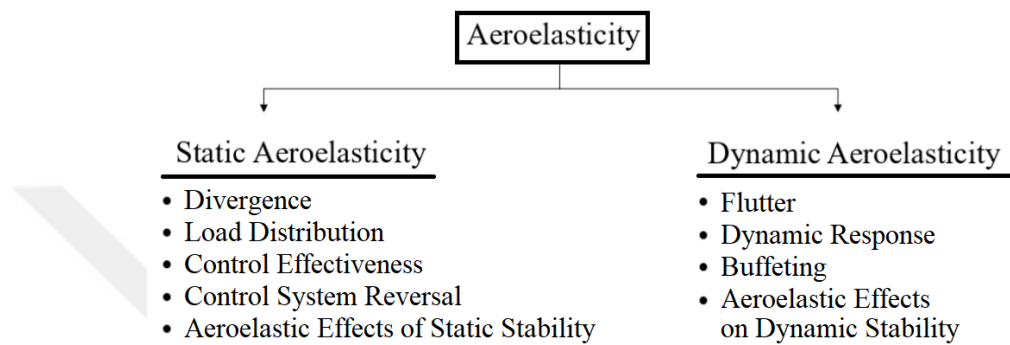


Figure 1.2. Aeroelasticity tree

The aeroelastic problems occur when additional aerodynamic forces are induced as a result of deformation of the structure. These increased aerodynamic forces also increase the deformation of the structure. Then, this greater deflection of the structure results in greater aerodynamic forces. This interaction between deformation of the structure and induced aerodynamic forces are continuing up to reach the stable equilibrium or failure of the structure.

In this thesis, the dynamic aeroelastic problem of flutter is observed. Flutter is a self-excited dynamic instability and elasticity of the structure plays an essential role. In the flutter instability, the structure extracts negative damping from air. The structure already has a fixed structural damping in itself. The negative damping extracted from the air is proportional with the speed and the frequency. Once the air vehicle attains a certain speed, total damping it has become nearly zero. Therefore, upon any excitation, the structure vibrates with increasing amplitude which results in catastrophic failure. That speed is known as the flutter speed and the flutter should be considered in the design of any air vehicle including cruise missile.

1.3. Literature Survey

Molyneux and Hall made several tests to find the flutter speeds of different wings which differ in aspect ratio and sweepback angle [5]. Flutter test mechanism is given in Figure 1.3.

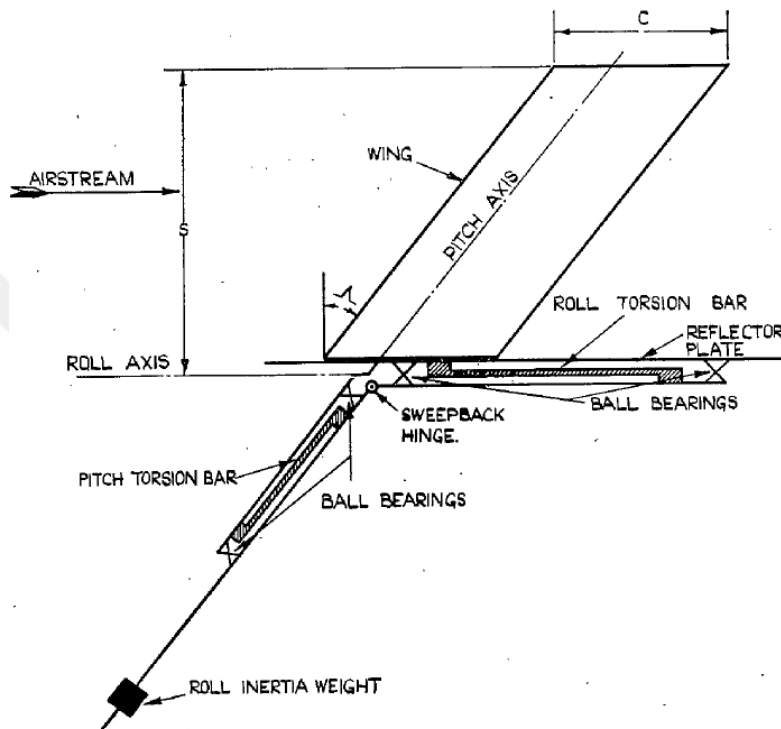


Figure 1.3. Flutter test mechanism [5]

The tests were made by changing the aspect ratio and the sweepback angle systematically while the other parameters were keeping constant. Tested wing geometries are given in Figure 1.4.

In order to investigate the effects of the aspect ratio on the flutter speed, the wingspan was changed from 6 in to 18 in. The aspect ratio of the wing was changed from 2 to 6 since the wing did not have a taper. Tests were made for 0 and 45° sweepback angle. Results of these tests are given in Figure 1.5.

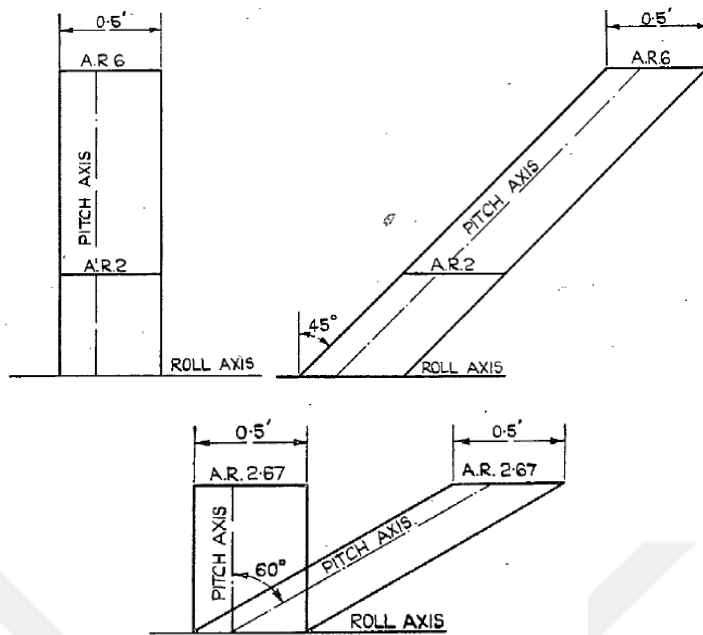


Figure 1.4. Flutter test wing geometries [5]

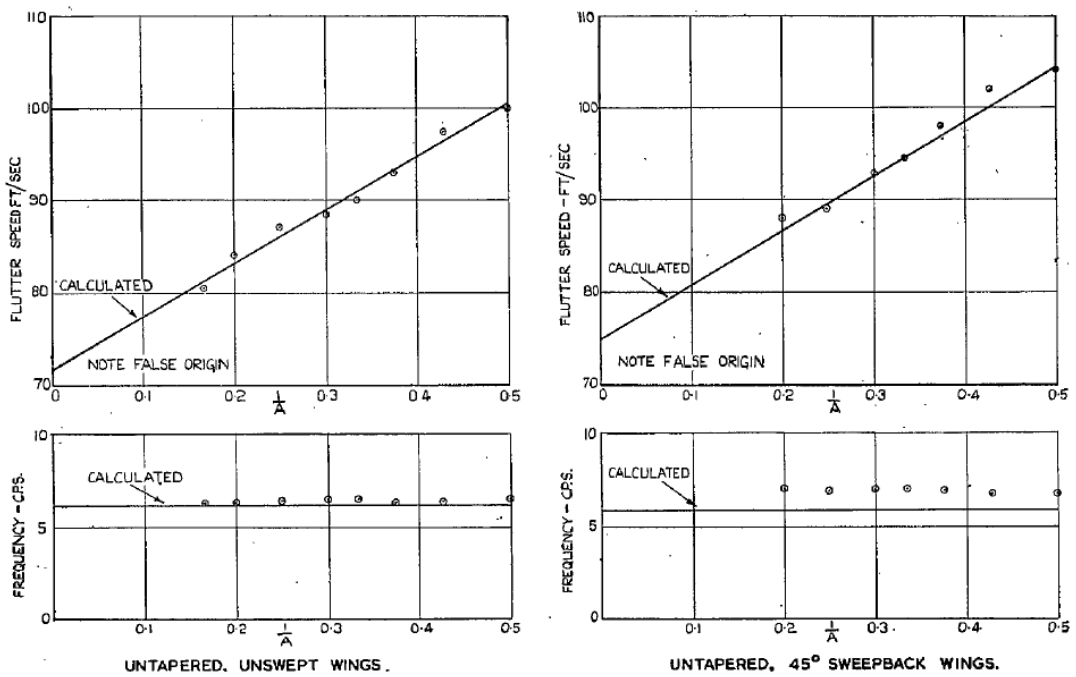


Figure 1.5. Effects of the aspect ratio on the flutter speed and frequency [5]

It can be easily seen from Figure 1.5 that increasing of the aspect ratio decreases the flutter speed. The other tests were made for different wing sweepback angles while the aspect ratio was keeping constant. The sweepback angle was changed from 0 to 60°. The flutter speeds and frequencies were obtained as given in Figure 1.6. It can be easily concluded that the increase in the sweepback angle also increases the flutter speed.

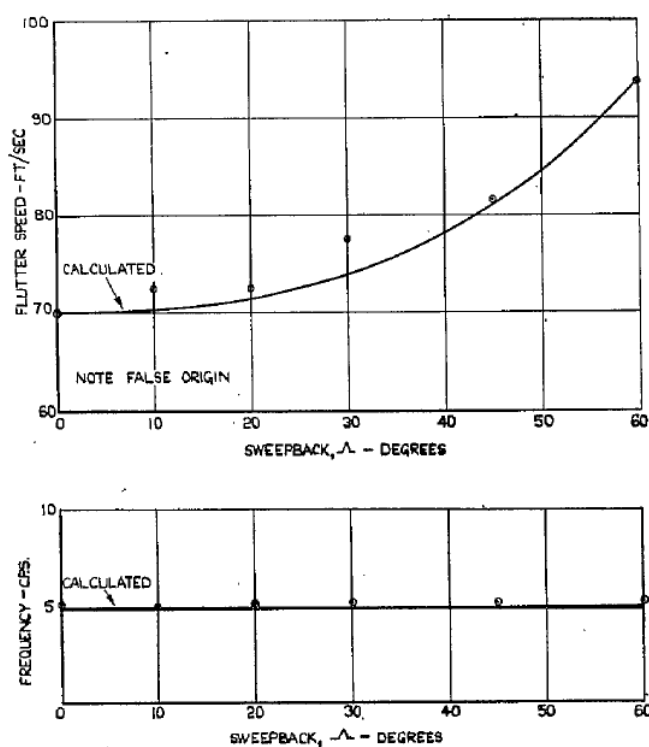


Figure 1.6. Effects of the sweepback angle on flutter speed and frequency [5]

Furthermore, Bae et. al. studied on the aerodynamic and aeroelastic characteristics of the variable-span morphing wing. The span was increased by 50 percent from its original size. By changing the span, the aspect ratio was changed naturally. The size of the wing and variation of the aspect ratio are given in Figure 1.7 [6].

As expected, with the increase of the span, lift is increased and induced drag is decreased. Moreover, deformations of the wing are increased. Bae at al. analyzed the divergence characteristic of the structure as given in Figure 1.8 [6].

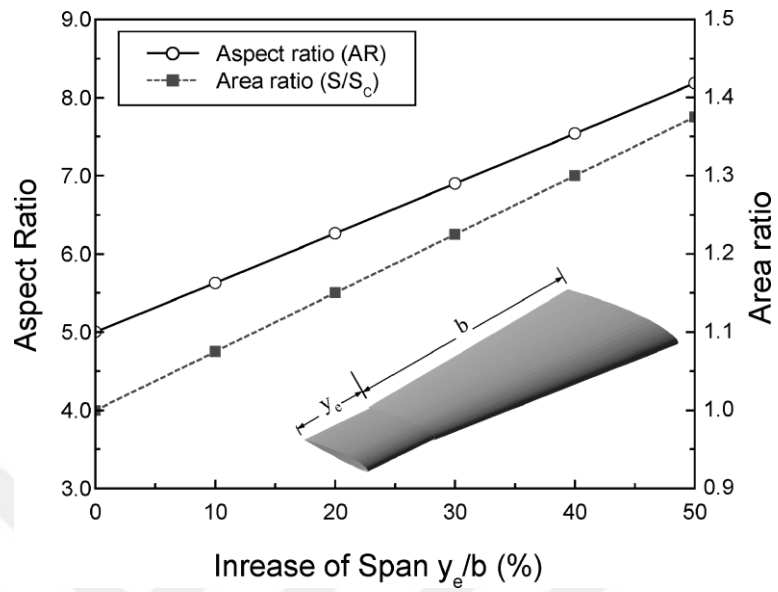


Figure 1.7. Wingspan variation [6]

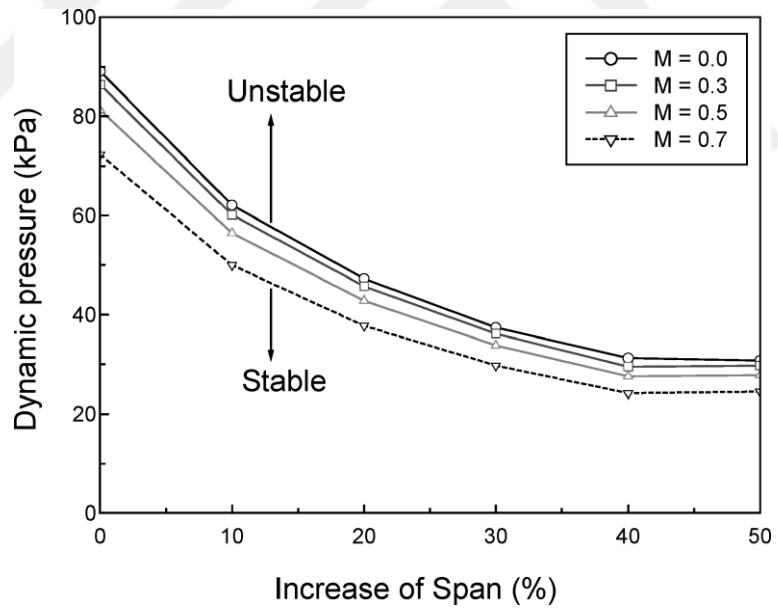


Figure 1.8. Effects of the span on the divergence characteristics of the wing [6]

As seen from Figure 1.8, increasing the span to gain lift and range results in a significant decrease in the stability of the wing.

Another work is performed by Ren and Zhiping. They calculated the flutter speeds of the morphing wing given in Figure 1.9 [7].

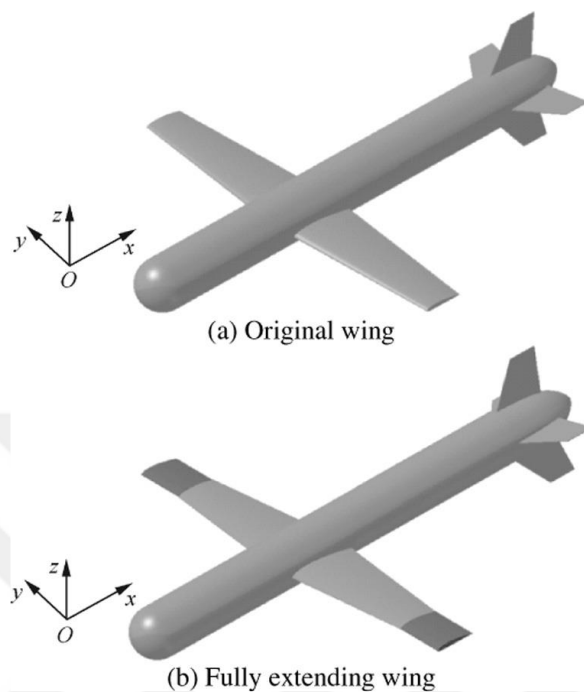


Figure 1.9. UAV wingspan variation [7]

Similar to the Bae’s results, this work shows the effects of the span on the aeroelastic characteristics of the wing. Figure 1.10 shows the significant change in the flutter speed and frequency with the change of the span.

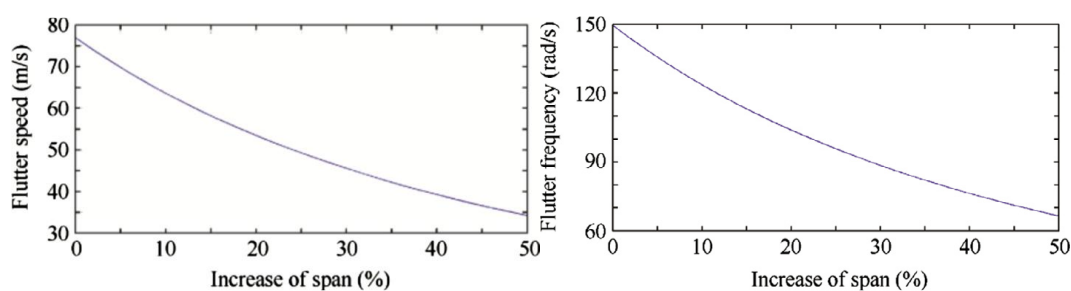


Figure 1.10. Effects of the span on the flutter speed and frequency [7]

It can be concluded from both two works that changing design parameters in order to gain several advantages in one discipline may affect another disciplines in a negative way. Thus, different disciplines must work together in the design process.

Lastly, Mahran et. al. analyzed plate wings by using the FEM [8]. They performed aeroelastic analyses to find divergence and flutter speeds for different plate wing geometries. The tip chord of the plate wing was altered to differentiate the taper ratio of the wing. The plan-form of the plate wing is given in Figure 1.11.

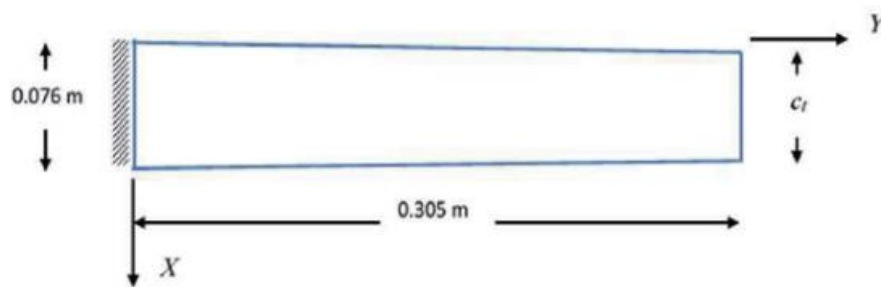


Figure 1.11. The plan-form of the plate wing [8]

Results are presented in Figure 1.12. Decreasing the taper ratio by decreasing the tip chord results in increasing in the divergence and flutter speeds. It means that the plate wing structure becomes healthier with decreasing the taper ratio.

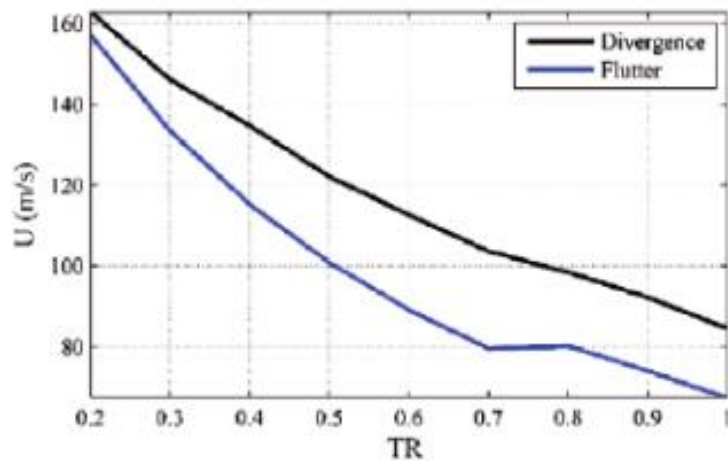


Figure 1.12. Effects of the taper ratio on the divergence and flutter speeds [8]

In brief, if the studies mentioned above are considered, the following conclusions can be drawn:

1. Increasing the wingspan and the aspect ratio decrease the flutter speed of the wing.
2. Increasing the sweepback angle also increases the flutter speed of the wing.
3. Increasing the taper ratio decreases both the divergence and flutter speeds of the wing.

1.4. Contents of the Thesis

In this thesis, in order to investigate the effects of the design parameters, the aeroelastic analyses were performed for different cruise missile wing geometries by using the ZAERO software.

Chapter 2 introduces the variation of design parameters and geometries used in the aeroelastic analyses. This chapter also gives information about the flight conditions used in the analyses.

In Chapter 3, the theory behind the aeroelastic analyses is described. Governing equations for aeroelastic analyses are provided and some of the flutter solution techniques are briefly introduced. At the end of the chapter, the solution procedure of the aeroelastic analyses are given.

Chapter 4 is composed of the methodology followed in the aeroelastic analyses. This chapter gives information about the finite element and aerodynamic modeling of the wings. This chapter also includes information about vibrational analyses and preparation of the ZAERO input file. At the end of the chapter, determination of the flutter speed is explained.

In Chapter 5, the results of the aeroelastic analyses of different wing configurations are given. Moreover, the effects of the aspect ratio, taper ratio, sweep angle and altitude on the flutter speed are discussed.

Lastly, conclusions and recommendations for future work are given in Chapter 6.

CHAPTER 2

VARIATION OF DESIGN PARAMETERS

In order to meet the design requirements mentioned in Chapter 1, several parameters need to be optimized for the wing. These parameters can be listed as:

1. Reference area
2. Cross section
3. Root chord
4. Tip chord
5. Incidence
6. Span
7. Sweep angle
8. Aspect ratio
9. Taper ratio
10. Twist angle
11. Dihedral angle
12. Vertical and horizontal position

Among these parameters; the taper ratio, the aspect ratio, and the sweep angle are worthy to be examined. It should be noted that due to geometric limitations dictated by the missile body, the root chord of the wing is taken as constant. Thus, the taper ratio and the aspect ratio is varied by changing the tip chord and span during the design process.

Since the root chord of the wing is constant, changing the tip chord of the wing results in the tapered wing that has a spanwise chord variation. These wings are better than the rectangular wings in terms of structure and aerodynamics. As structure, the root

section is stiffer than the tip section and as aerodynamics it is the nearest wing shape to the elliptical wing which gives the optimum aerodynamic lift distribution [8].

Since the aspect ratio defined as the ratio of wingspan to its mean chord, varying the wingspan is also changing the aspect ratio. For a cruise missile wing, change of the aspect ratio affects the aerodynamic and aeroelastic characteristics in a number of ways. It is known that flutter speed is changing with the change of the aspect ratio. Additionally, it was observed from the experimental and numerical studies that the changing of the aspect ratio also affects the lift force [9].

As the last parameter, wings may have forward or backward sweep angle. The swept wings are commonly seen in high-speed cruise missiles since they reduce the effective flow speed below the critical speeds at which shock waves form on the upper wing surface. Moreover, the backward sweep reduces the drag effect. In addition to the aerodynamic effects, it is known that the sweep angle also affects the aeroelastic characteristics of the wing. In this study, the sweep angle represents the quarter-chord sweep angle.

2.1. Design of Experiments

Design of experiments (DOE) is a statistical tool that widely used in design processes. It is a helpful tool for optimization and product development. DOE is used in various circumstances for identification of input variables and their relations with response variables. In order to investigate the effects of design parameters on the flutter speed, such parameters as the taper ratio, the aspect ratio, and the sweep angle are selected and applied as given in Table 2.1.

Wings in the first seven rows are used to examine the effects of the aspect ratio on the flutter speed. The effects of the taper ratio are studied using wings between Wing 8 and Wing 13. Lastly, wings between Wing 14 and Wing 20 are used to observe the effects of the sweep angle. It should be noted that Wing 4 is included in both of the studies on the effects of the taper ratio and the sweep angle.

Table 2.1. *Variation of design parameters*

Wing Number	<i>Taper Ratio</i>	<i>Aspect Ratio</i>	<i>Sweep Angle</i>
1	0.75	4	30
2	0.75	6	30
3	0.75	8	30
4	0.75	10	30
5	0.75	12	30
6	0.75	14	30
7	0.75	16	30
8	0.50	10	30
9	0.60	10	30
10	0.70	10	30
11	0.80	10	30
12	0.90	10	30
13	1.00	10	30
14	0.75	10	0
15	0.75	10	5
16	0.75	10	10
17	0.75	10	15
18	0.75	10	20
19	0.75	10	40
20	0.75	10	50

Wings given in Table 2.1 are used in aeroelastic analyses to estimate flutter speeds and analyses are performed at different altitudes given in Table 2.2 by using ZAERO which is a commercial code having different aeroelastic solution methods.

Table 2.2. *Flight conditions for the aeroelastic analyses*

Wing Number	<i>Altitude (kft)</i>
1 to 20	0, 10, 20, 30, 40

CHAPTER 3

THEORY OF AEROELASTIC ANALYSES

In this study, ZAERO software developed by ZONA Inc. is used for aeroelastic analyses. This chapter provides the theory behind this software [10].

3.1. Governing Equations

The aeroelastic response of flying vehicles consists of aerodynamic forces, structural forces, and external forces. The structural forces can be divided into inertial and elastic forces. The equilibrium condition of these forces represents the general equation of motion.

$$\begin{aligned} \bar{M}\ddot{x}(t) + \bar{K}x(t) &= F(t) \\ \text{(Inertial forces)} + \text{(Elastic forces)} &= \text{(Aerodynamic forces)} \end{aligned} \quad (3.1)$$

where

\bar{M} is the mass matrix generated by the structural FEM,

$x(t)$ is the structural deformation,

\bar{K} is the stiffness matrix generated by the structural FEM,

$F(t)$ is the aerodynamic forces.

The aerodynamic forces are generally originated from the structural deformation, $F_a(x)$, and external effects, $F_e(t)$.

$$F(t) = F_a(x) + F_e(t) \quad (3.2)$$

The impulsive type gusts, forces coming from control surfaces because of pilot's command, continuous atmospheric turbulence, and store ejection forces are several

examples for the external aerodynamic forces. Since the aerodynamic forces are a function of the $x(t)$, the iterative process given in Figure 3.1 is needed.

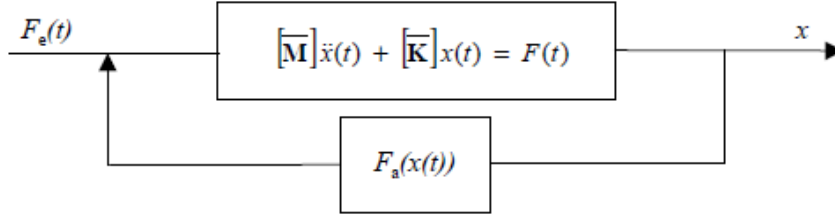


Figure 3.1. Aeroelastic Functional Diagram

Rearranging the Equation (3.1) gives:

$$\bar{M}\ddot{x}(t) + \bar{K}x(t) - F_a(x) = F_e(t) \quad (3.3)$$

Actually, the system of Equation (3.3) is a self-excited system. The flutter can be defined as the stability problem of this system. When $F_a(x)$ is a nonlinear function, the aeroelastic analysis should be done by solving the equation given below using initial conditions of $x(0)$ and $\dot{x}(0)$ at $t = 0$.

$$\bar{M}\ddot{x}(t) + \bar{K}x(t) - F_a(x) = 0 \quad (3.4)$$

By assuming the magnitude of the structural deformation is small, $F_a(x)$ can be written as:

$$F_a(x) = \int_0^t q_\infty H \left(\frac{V}{L}(t - \tau) \right) x(\tau) d\tau \quad (3.5)$$

where

q_∞ is the dynamic pressure,

L is the reference length which is the half of the chord,

V is the velocity of undisturbed flow,

$q_\infty H$ is the aerodynamic transfer function.

Equation (3.5) can also be written in the Laplace domain as:

$$F_a(x(s)) = q_\infty \bar{H} \left(\frac{sL}{V} \right) x(s) \quad (3.6)$$

Substituting Equation (3.6) into Equation (3.4) in Laplace domain gives:

$$\left[s^2 \bar{M} + \bar{K} - q_\infty \bar{H} \left(\frac{sL}{V} \right) \right] x(s) = 0 \quad (3.7)$$

Solving the eigenvalues of Equation (3.7) is hard and costly since the mass and stiffness matrices have larger sizes. This is due to the huge amount of DOF the FEM model of flying vehicle has. Thus, aeroelastic analysis takes a long time to complete. The modal reduction approach helps to cope with this problem.

3.1.1. Modal Reduction Approach

The modal reduction approach defines the transformation between the global coordinates and modal coordinates as given below:

$$x(s) = \Phi \xi(s) \quad (3.8)$$

In Equation (3.8) given above, Φ represents the modal matrix whose columns contain the lower order natural modes while $\xi(s)$ represents the modal coordinates. For example, if there are 1000 DOF in the FEM, the size of the $x(s)$ will be 1000x1. If structural deformation is expressed as the first 10 superposition of natural modes of structure, the size of the modal matrix Φ will be 1000x10 and the size of modal coordinates matrix $\xi(s)$ will be 10x1. In fact, no more than ten numbers of the natural modes are needed for the aeroelastic analysis of a wing.

Substitution of Equation (3.8) into Equation (3.4) yields:

$$\bar{M} \Phi \ddot{\xi} + \bar{K} \Phi \xi - F_a(x) = 0 \quad (3.9)$$

Pre-multiplying Equation (3.9) by Φ^T and substituting the term $F_a(x)$ with Equation (3.6) in the Laplace domain gives:

$$\Phi^T \bar{M} \Phi s^2 \xi + \Phi^T \bar{K} \Phi \xi - q_\infty \Phi^T \bar{H} \left(\frac{sL}{V} \right) \Phi \xi = 0 \quad (3.10)$$

Simplifying Equation (3.10) with generalized matrices yields:

$$\left[s^2 M + K - q_\infty Q \left(\frac{sL}{V} \right) \right] \{\xi\} = 0 \quad (3.11)$$

where

$M = \Phi^T \bar{M} \Phi$ is the generalized mass matrix,

$K = \Phi^T \bar{K} \Phi$ is the generalized stiffness matrix,

$Q \left(\frac{sL}{V} \right) = \Phi^T \bar{H} \left(\frac{sL}{V} \right) \Phi$ is the generalized aerodynamic forces matrix.

In order to determine the flutter range, the eigenvalue problem of Equation (3.11) is needed to solve for different speeds and altitudes.

The advantage of the modal reduction approach can be seen by comparing the sizes of the matrices in Equation (3.11) and Equation (3.7). For example, for the structural model having 1000 DOF, the size of mass and stiffness matrices will be 1000x1000. It means that the 1000 equations with 1000 unknowns need to be solved. However, considering that the response of structure can be expressed as the superposition of the first 10 natural modes of the structure using the modal reduction approach, the sizes of the matrices in Equation (3.11) will be 10x10. Using Equation (3.11) instead of Equation (3.7) for aeroelastic calculations is a very cost-effective approach.

The modal reduction approach is advantageous for the reason mentioned above. However, since the solution of the aerodynamic part in the Laplace domain is difficult, the aerodynamic part is formulated in the frequency domain which is named as Aerodynamic Influence Coefficient (AIC).

3.1.2. Unified AIC of ZAERO

There are six unsteady aerodynamic methods for creating the AIC matrices incorporated in ZAERO. These methods can be briefly introduced as:

1. ZONA6: Subsonic unsteady aerodynamics.
2. ZONA7: Supersonic unsteady aerodynamics.
3. ZTAIC: Transonic unsteady aerodynamics using a Transonic Equivalent Strip Method.
4. ZTRAN: Transonic unsteady aerodynamics using an Overset Field-Panel Method.
5. ZSAP: Sonic Acceleration Potential Method for M=1.
6. ZONA7U: Hypersonic unsteady aerodynamics.

All methods mentioned above use the panel method to solve unsteady flow equations in integral form. The reduced frequency k is defined as:

$$k = \frac{\omega L}{V} \quad (3.12)$$

where

ω is the harmonic oscillatory frequency.

In the panel method, the flying vehicle is modelled with small panel elements named as aerodynamic box shown in Figure 3.2. In the center of each panel element, there is a control point where the boundary condition is imposed.

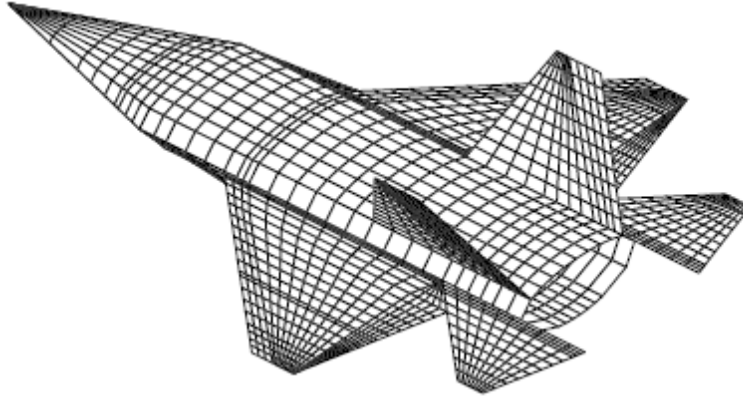


Figure 3.2. Panel model of an aircraft

For a certain reduced frequency k , when the integral equations are solved, the AIC is obtained. The AIC includes the contribution of all remaining panel elements to the aerodynamic force formed at the control point of a certain panel element. The AIC defines the relation between structural deformation and aerodynamic forces as:

$$F_h = q_\infty [AIC(ik)]h \quad (3.13)$$

where

F_h is the resultant aerodynamic forces,

h is the structural deformation.

Note that the AIC matrix is computed in the k -domain. In addition, the AIC matrix depends on the aerodynamic panel model, Mach number and reduced frequency. Since it is calculated based on the panel model, it is independent of the vibrational analysis results computed from the structural FEM. The problem here is displacement and force transferal. The solution of the problem is a spline matrix which relates the structural and aerodynamic panel model.

3.1.3. The Spline Matrix

The aerodynamic forces in Equation (3.13) are written in terms of h which represents the deformations of control points of panel elements belonging to the aerodynamic model. Besides, in order to solve aeroelastic equations, the aerodynamic forces should be written in terms of x which represents deformations of grid points in structural FEM. In order to do this, the relation must be expressed between h and x . The spline matrix G is created from ZAERO's spline module as:

$$h = Gx \quad (3.14)$$

where

h is the aerodynamic grid points,

x is the structural grid points.

The beam spline method, infinite plate spline method, thin-plate spline method and rigid-body attachment method are four different methods to construct the spline matrix G in ZAERO. Substituting Equation (3.14) into Equation (3.13) gives:

$$F_h = q_\infty [AIC(ik)]Gx \quad (3.15)$$

F_h is the resultant aerodynamic forces at the aerodynamic control points. It should be transferred to the structural model. This force transferal can be performed according to the principle of virtual work as:

$$F_a = G^T F_h \quad (3.16)$$

According to the principle of virtual work, the virtual work of the force acting on the aerodynamic panel elements along the displacement of the panel elements should be equal to the virtual work of the equivalent aerodynamic force acting on the grid points of the FEM along the displacement of the grid points. In other words, F_h and F_a need to have the same work.

$$\delta h^T F_h = \delta x^T F_a \quad (3.17)$$

where

F_a is the aerodynamic forces acting to the grid points of the FEM.

Substituting Equation (3.17) into Equation (3.14) yields:

$$\delta x^T (F_a - G^T F_h) = 0 \quad (3.18)$$

Since the δx is different from zero, the equation in the bracket must be zero. So that:

$$F_a = G^T F_h \quad (3.19)$$

Substituting Equation (3.15) into Equation (3.19) yields:

$$F_a = q_\infty G^T [AIC(ik)] G x \quad (3.20)$$

If Equation (3.20) will be substituted into Equation (3.4) and the modal reduction approach will be used, the below equation will be obtained:

$$\Phi^T \bar{M} \Phi s^2 \xi + \Phi^T \bar{K} \Phi \xi - q_\infty \Phi^T G^T [AIC(ik)] G \Phi \xi = 0 \quad (3.21)$$

Equation (3.21) can be simplified as:

$$[s^2 M + K - q_\infty Q(ik)] \xi = 0 \quad (3.22)$$

where

$Q(ik) = \Phi^T G^T [AIC(ik)] G \Phi$ is the generalized aerodynamic forces matrix in the k -domain.

As mentioned before, ZAERO makes the flutter prediction by solving the eigenvalue problem of Equation (3.22).

3.2. Flutter Solution Techniques

ZAERO has three different flutter solution techniques as the K-method, the P-K method and the g-method. In fact, the g-method is derived from the P-K method and it is quite similar to the P-K method. Therefore, in this section, these three different flutter solution methods are discussed. These methods are:

- The K-method
- The P-K method
- The g-method

Moreover, the theoretical validity of each method will be discussed. This discussion explains why the g-method is used in aeroelastic analyses.

3.2.1. The K-Method

The K-method is firstly introduced by Scanlan and Rosenbaum in 1951 as a brief overview of the techniques introduced by Theodorsen in the 1940s [11][12][13]. The equation of the K-method can be obtained by replacing s by $i\omega$ in Equation (3.22) as:

$$[-\omega^2 M + (1 + i\zeta_s)K - q_\infty Q(ik)]\{\xi\} = 0 \quad (3.23)$$

The dynamic pressure q_∞ can be expressed as:

$$q_\infty = \frac{1}{2}\rho V^2 = \frac{1}{2}\rho \left(\frac{\omega L}{k}\right)^2 \quad (3.24)$$

where

ρ is the density of air.

Substitution of Equation (3.24) into Equation (3.23) and dividing the whole equation by ω^2 gives the main K-method equation as:

$$\left[M + \frac{\rho}{2} \left(\frac{L}{k}\right)^2 Q(ik) - \lambda K \right] \{\xi\} = 0 \quad (3.25)$$

where

$\lambda = \frac{1+i\varrho_s}{\omega^2}$ is the eigenvalue of Equation (3.25).

$Q(ik)$ is dependent on the reduced frequency k and it should be calculated at a given Mach number. For the given reduced frequencies, the solution of the eigenvalue problem of Equation (3.25) gives λ . After λ is calculated, the artificial damping ϱ_s , the flutter frequency ω_f , and the airspeed V_f can be calculated as:

$$\omega_f = \frac{1}{\sqrt{\text{Re}(\lambda)}}$$

$$\varrho_s = \omega_f^2 \text{Im}(\lambda) = \frac{\text{Im}(\lambda)}{\text{Re}(\lambda)} \quad (3.26)$$

$$V_f = \frac{\omega_f L}{k}$$

For the given reduced frequencies, velocity versus damping (V-g) and velocity versus frequency (V-f) diagrams can be derived. The typical results for the AGARD 445.6 wing computed by the K-method are given in Figure 3.3.

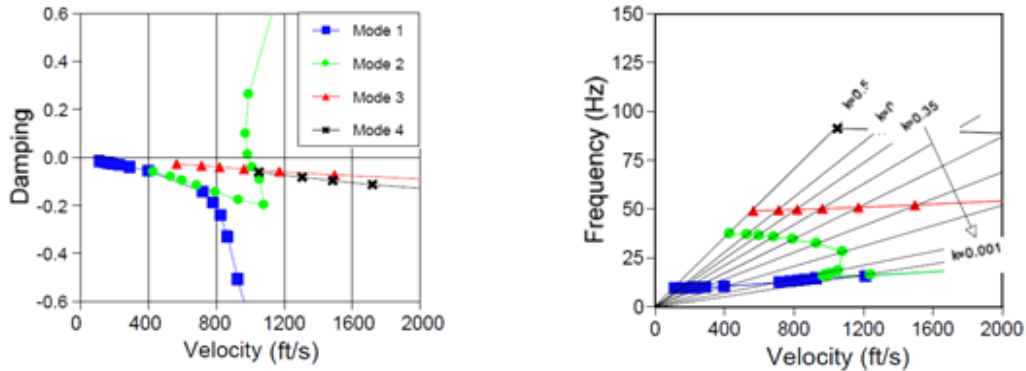


Figure 3.3. AGARD 445.6 K-method flutter results (ZONA6), M=0.9 [14]

The K-method does not require iteration for solving the eigenvalue problem. It is a numerical procedure performing for each reduced frequency. Thus, the K-method is efficient and robust. However, due to the reasons stated below, the K-method is a less attractive method for flutter analysis:

- The K-method can be used for only $\varrho_s = 0$. Other $\varrho_s \neq 0$ values are not representing the correct damping of the system.
- The velocities (and also frequencies) are evaluated for a specific Mach number and density couple. In general, points in the flutter range calculated by K-method do not satisfy the $V_f = Ma_\infty$. If this condition is not satisfied, the calculated flutter speed has no physical meaning. In order to reach the true flutter speed with K-method, flutter analysis should be performed iteratively for a constant Mach number by changing the density or for a constant density by changing the Mach number up to $V_f = Ma_\infty$ is satisfied.
- Since the term $1/k$ in Equation (3.25) is not defined for $k = 0$, the K-method cannot perform aeroelastic analysis at $k = 0$. Thus, the K-method does not have the ability to predict the divergence phenomena.

3.2.2. The P-K Method

The P-K method is developed in 1965 by Irwin and Guyet [15]. Nowadays, this method is widely used in aeroelastic analyses by aeroelasticians. Hassig explains the advantage of the P-K method over the K-method and gives the equation of the P-K method as [16]:

$$\left[\left(\frac{V^2}{L^2} \right) Mp^2 + K - \frac{1}{2} \rho V^2 Q(ik) \right] \{\xi\} = 0 \quad (3.27)$$

where

$p = \gamma k + ik$ is the Laplace parameter,

γ is the decay rate.

Hassig's P-K method equation is modified by Rodden by adding an aerodynamic damping matrix into Equation (3.27). The modified P-K method equation is [17][18]:

$$\left[\left(\frac{V^2}{L^2} \right) Mp^2 + K - \frac{1}{2} \rho V^2 \frac{Q^I}{k} p - \frac{1}{2} \rho V^2 Q^R \right] \{\xi\} = 0 \quad (3.28)$$

where

$$Q(ik) = Q^R + iQ^I$$

ZAERO uses Equation (3.28) given above for the P-K method aeroelastic solutions. This equation is solved for a given pair of V and ρ , for complex roots p . The iterative solution continues up matching the reduced frequency k to the imaginary part of p for every structural mode. The typical results for the AGARD 445.6 wing computed by P-K method are given in Figure 3.4.

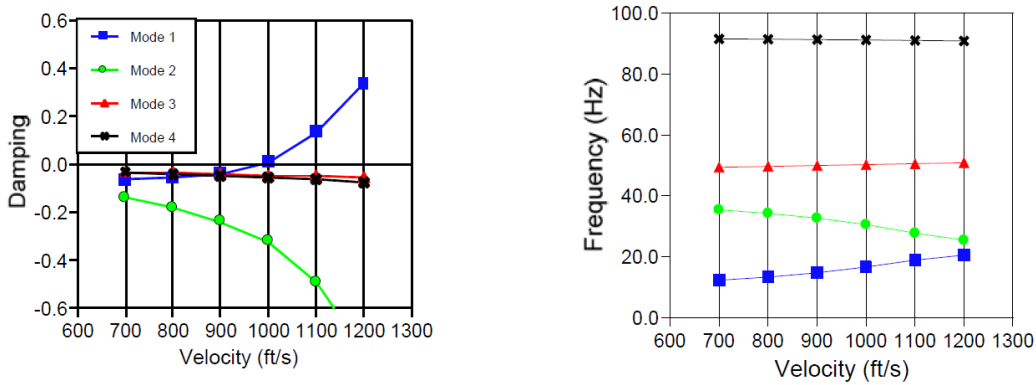


Figure 3.4. AGARD 445.6 P-K method flutter results (ZONA6), M=0.9 [10]

The P-K method results in a more realistic solution in comparison to the K-method. Also, this method can accurately predict the damping of the structure. Moreover, since the P-K method gives solution for $k = 0$, it can predict the divergence characteristics of the structure.

The other advantage of the P-K method is that it computes directly flutter speed for a given velocity while the K-method needs iterative process to find physically meaningful flutter speed. Besides, the P-K method is valid only for small reduced frequencies k or for linearly varying $Q(ik)$ matrices. If not so, the P-K method may give unrealistic solution [19].

3.2.3. The g-Method

Addition of the aerodynamic damping matrix in the P-K method is a simple way to predict $Q(ik)$ matrix. Another way to estimate this aerodynamic matrix is including a first-order damping term into the flutter equation. This method, which is called the g-method, is suggested by Chen and the first order damping term is rigorously derived from the Laplace domain aerodynamic [20].

The term $Q(p)$ is defined as:

$$Q(p) = Q(g + ik) \quad (3.29)$$

where

$$g = \gamma k$$

For small values of g , $Q(p)$ can be expanded along the imaginary axis using a damping perturbation method as:

$$Q(p) \approx Q(ik) + g \left. \frac{\partial Q(p)}{\partial g} \right|_{g=0} \quad (3.30)$$

Equation (3.30) is valid for only $g \ll 1$. Also, the term $\left. \frac{\partial Q(p)}{\partial g} \right|_{g=0}$ does not exist in k -domain unsteady aerodynamic methods. Assuming that $Q(p)$ is analytic, Cauchy-Riemann equations claims:

$$\begin{aligned} \frac{\partial(\operatorname{Re}Q(p))}{\partial g} &= \frac{\partial(\operatorname{Im}Q(p))}{\partial k} \\ \frac{\partial(\operatorname{Im}Q(p))}{\partial g} &= -\frac{\partial(\operatorname{Re}Q(p))}{\partial k} \end{aligned} \quad (3.31)$$

Combining two equations in Equation (3.31) yields:

$$\frac{\partial Q(p)}{\partial g} = \frac{\partial Q(p)}{\partial(ik)} \quad (3.32)$$

Note that Equation (3.32) is not valid for the negative real axis where discontinuity due to a branch cut in subsonic flow occurs. Except that, Equation (3.32) is valid in the complete p -domain. Therefore, $\left. \frac{\partial Q(p)}{\partial g} \right|_{g=0}$ can be expressed as:

$$\left. \frac{\partial Q(p)}{\partial g} \right|_{g=0} = \left. \frac{\partial Q(p)}{\partial (ik)} \right|_{g=0} = Q'(ik) \quad (3.33)$$

Substituting Equation (3.33) into Equation (3.30) gives:

$$Q(p) \approx Q(ik) + gQ'(ik) \quad (3.34)$$

Substituting the term $Q(p)$ into the flutter equation gives the g -method equation as:

$$\left[\left(\frac{V^2}{L^2} \right) Mp^2 + K - \frac{1}{2} \rho V^2 \frac{Q^I}{k} Q'(ik)g - \frac{1}{2} \rho V^2 Q(ik) \right] \{\xi\} = 0 \quad (3.35)$$

3.2.3.1. Solution Algorithm of the g -Method

If the substitution of $p = g + ik$ is done in Equation (3.35), a second-order linear system can be obtained as:

$$[g^2A + gB + C]\{\xi\} = 0 \quad (3.36)$$

where

$$A = \left(\frac{V}{L} \right)^2 M$$

$$B = 2ik \left(\frac{V}{L} \right)^2 M - \frac{1}{2} \rho V^2 Q'(ik) + \left(\frac{V}{L} \right) Z$$

$$C = -k^2 \left(\frac{V}{L} \right)^2 M + K - \frac{1}{2} \rho V^2 Q(ik) + ik \left(\frac{V}{L} \right) Z$$

When $\text{Im}(g) = 0$, there is a solution for Equation (3.36). In order to find the solution, the state space form of Equation (3.36) should be written as:

$$[D - gI]\{X\} = 0 \quad (3.37)$$

where

$$D = \begin{bmatrix} 0 & I \\ -A^{-1}C & -A^{-1}B \end{bmatrix}$$

Solving the eigenvalues of D by using the reduced-frequency-sweep technique gives the flutter frequency ω_f and damping 2γ as:

$$\begin{aligned} \omega_f &= k \left(\frac{V}{L} \right) \\ 2\gamma &= 2 \frac{\text{Re}(g)}{k} \end{aligned} \quad (3.38)$$

Also, Rodden defines the damping equation for the value of $k = 0$ as [21]:

$$2\gamma = \frac{\text{Re}(g) \left(\frac{L}{V} \right)}{\ln(2)} \quad (3.39)$$

3.3. Solution Procedure of the ZAERO

In this section, the solution procedure of the ZAERO is summarized briefly. Then, since ZAERO has no graphical user interface, the sections of the ZAERO input file are introduced.

3.3.1. Brief Summary

1. When the ZAERO input file is created by the user, the name and extension of the vibrational analysis result file of the structural FEM of the flying vehicle are entered in the Executive Control Section. ZAERO reads the following data from this file:
 - i. ID numbers and coordinates of the grid points,
 - ii. Modal mass and stiffness values,
 - iii. Natural frequencies and mode shapes.

2. ZAERO creates the M and K matrices in Equation (3.22) using modal mass and stiffness data. It also creates modal matrix Φ by using the mode shapes (eigenvalue vectors).
3. The user specifies the type of analysis using the necessary commands in the Case Control Section of the ZAERO input file, whichever one of the aeroelastic analyzes, such as flutter, trim, etc. For example, the “FLUTTER =” data card is used for the flutter analysis. After ZAERO receives this command, it seeks the parameters as Mach number, reduced frequency, altitude, etc. related to the flutter analysis in the Bulk Data Section of the input file.
4. The user inputs the geometric data to form the aerodynamic panel model in the Bulk Data Section. Using this data, ZAERO creates the aerodynamic panel elements and their control points. Then, it calculates the $AIC(ik)$ matrix in Equation (3.21) using this model with the Mach number and reduced frequency data received from the input file. The user should specify the solver type such as ZONA6, ZONA7, ZTRAN, etc. in the input file. Integral equations that calculate the matrix $AIC(ik)$ differ from one solver to another.
5. In the next step, the user inputs the data required by the Spline module again in the Bulk Data Section. Using this data, ZAERO's Spline module calculates the matrix G in Equation (3.21).
6. After the above steps, ZAERO calculates the aerodynamic force matrix $Q(ik)$ in Equation (3.22) using the Φ , G , and $AIC(ik)$ matrices. ZERO should know the density of air in order to calculate dynamic pressure q_∞ . ZAERO can derive the density of air from the altitude data specified by the user in the input file. In some cases, for example, for the analyses performed for wind tunnel tests, the user may also choose to input directly the density of the air. With this last step, all matrices in Equation (3.22) are calculated.

7. If the user wishes to calculate the flutter range of the flying vehicle, he/she must enter the all Mach numbers and altitudes in the range into the input file. Using this data, ZAERO generates an analysis matrix comprising of Mach numbers and altitudes. For each pair of Mach number and altitude in this matrix, the aerodynamic force matrix $Q(ik)$ in Equation (3.22) is calculated separately. After that, it solves the eigenvalue problem of Equation (3.22) for each pair of Mach number and altitude. The eigenvalues obtained from the solution of this eigenvalue problem are complex numbers. The real part of these complex numbers is the damping in the aeroelastic system and the imaginary part is the vibration frequency. The real part of the eigenvalues is a negative number indicates that the aeroelastic system is stable. This means that the system will not face flutter problem at the subjected Mach number and altitude. If the real part of at least one eigenvalue is zero or positive, it indicates that the system is unstable. In other words, the vibration amplitude of the aeroelastic structure is expected to increase uncontrollably at the smallest excitation. This means that the structure will go into a flutter. Consequently, for each Mach number and altitude combination, ZAERO determines whether there will be a flutter or not by looking at the results of the eigenvalue problem. When this process is completed for all Mach number and altitude combinations, the flutter range of the flying vehicle appears.

3.3.2. Sections of the ZAERO Input File

The input file of the ZAERO has three sections that describe the aeroelastic problem to be analyzed [22]. These three sections are the Executive Control Section, the Case Control Section, and the Bulk Data Section.

3.3.2.1. Executive Control Section

ZAERO input file should be started with the Executive Control Section. The finite element analysis result is assigned in this section. Moreover, print options and the type of analysis to be performed, such as symmetric, anti-symmetric boundary condition, can be defined in this section. The delimiters of ASSIGN and CEND are required for the operation of the software. ASSIGN is an important delimiter for starting the solution since it triggers the input file. Moreover, diagnostic routines can be indicated in this section. Preview of the Executive Control Section is given in Figure 3.5.

```
ASSIGN FEM = <filename>, FORM = <form>, BOUNDARY = <type>, PRINT = <print>
DIAG <values>
CEND
```

Figure 3.5. Executive Control Section

3.3.2.2. Case Control Section

After the Executive Control Section is completed with the delimiter of CEND, the next section in the input file should be the Case Control Section. This section is used to specify conditions to be performed. Each case should be defined by a subcase which indicates flutter conditions to be performed. Also, the titles as input file title and subcase titles are defined in this section. Preview of the Case Control Section is given in Figure 3.6.

```
TITLE = <title>
ECHO = <sort/nosort>
SUBCASE = <number>
  SUBTITLE = <subtitle>
  LABEL = <label>
  FLUTTER = <number>
  .
  .
  .
BEGIN BULK
```

Figure 3.6. Case Control Section

3.3.2.3. Bulk Data Section

The Bulk Data Section is the last section of the input file. The important delimiters in this section are BEGIN BULK and ENDDATA, which state the begin and end of the Bulk Data Section respectively. The biggest section in the input file is this section. It includes all the data required to perform the cases defined in the Case Control Section. These data can be listed as:

- Flight conditions,
- Parameters such as density, reference lengths, etc.
- The geometry of the aerodynamic model,
- Spline information between the structural and the aerodynamic models for displacement and force transferal,

Preview of the Bulk Data Section is given in Figure 3.7.

```

$      ACSID  XZSYM  FLIP   FMMUNIT  FMLUNIT  REFC   REFB   REFS   $
AEROZ  0      YES    NO     SLIN    IN      100.0  200.  10500. +AERO
$      REFY   REFZ
+AERO  33.333  0.    0.
.
.
.
ENDDATA
```

Figure 3.7. Bulk Data Section

CHAPTER 4

ANALYSES OF THE WINGS

The aeroelastic analyses of the wings given in Table 2.1 are comprised of four steps:

1. Generation of the wing solid models
2. Finite element modeling and analyses of the wings
3. Aerodynamic modeling of the wings
4. Preparation of the solution setup

First of all, the wing solid models are generated by using ANSYS DesignModeler. Then, finite element models of the wings are prepared by using MSC Patran and vibrational analyses of the wings are done by using MSC Nastran. Aerodynamic modeling of the wings is done in ZAERO input file by considering several rules. Lastly, the solution setup is built by preparing the ZAERO input files.

In order to determine the flutter speeds, the V-g plots are used and methodology is given at the end of this chapter.

4.1. Generation of the Wing Solid Models

In order to create 3D wing geometries given in Table 2.1, ANSYS DesignModeler software is used. During the design of the wing, many airfoil alternatives are investigated. Consequently, 10-percent thick supercritical airfoil SC(2)-1010 designed by NASA is selected. A comparison of supercritical flow phenomena for a conventional airfoil and the NASA supercritical airfoil is given in Figure 4.1 [23]. The NASA supercritical airfoil produces expansion waves or waves that tend to reduce pressure and increase velocity starting near the leading edge. For this reason, supercritical airfoils are better than conventional airfoils for cruise missiles that operating in transonic speed regime.

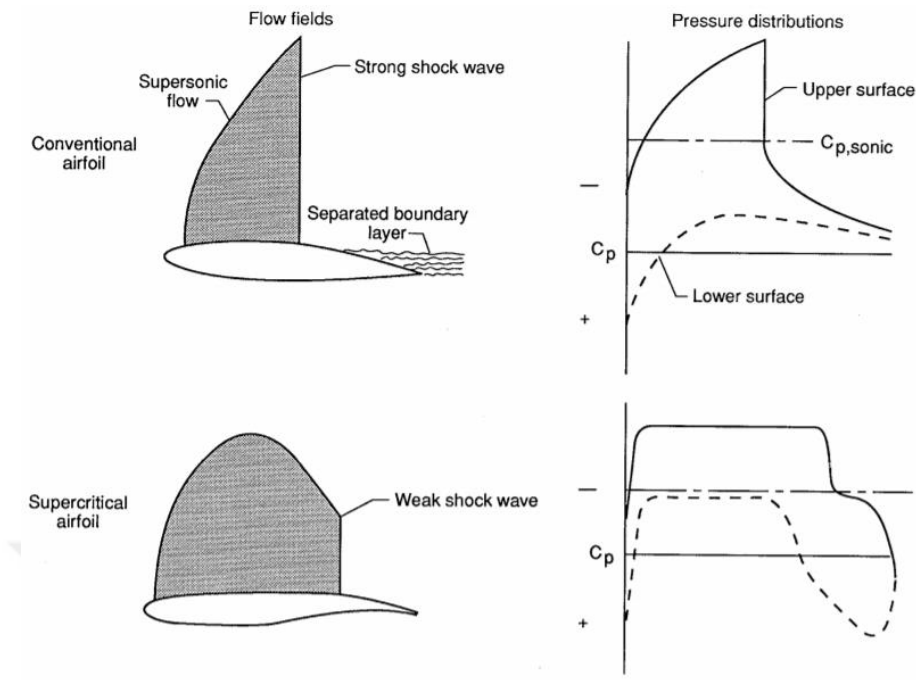


Figure 4.1. A comparison of a conventional airfoil and the NASA supercritical airfoil [23]

After selecting the airfoil profile, the parametric half-wing model is created by using ANSYS DesignModeler. The aspect ratio, the taper ratio, and the sweep angle are defined as design parameters of the wing. Since the root chord of the wing is constant, the span and the tip chord of the wing are changed to differentiate the aspect ratio and the taper ratio. Definitions of the aspect ratio and the taper ratio are given in the Equation (4.1) and Equation (4.2).

$$AR = \frac{S^2}{A} \quad (4.1)$$

where

A is the total area of the wing

S is the full-span of the wing

$$TR = \frac{c_{tip}}{c_{root}} \quad (4.2)$$

where

c_{root} is the root chord of the wing

c_{tip} is the tip chord of the wing

Furthermore, the swept wings are obtained by changing the location of the tip chord of the wing. It should be noted that the sweep angle represents the angle between the quarter-chord line and the lateral axis as seen from Figure 4.2.

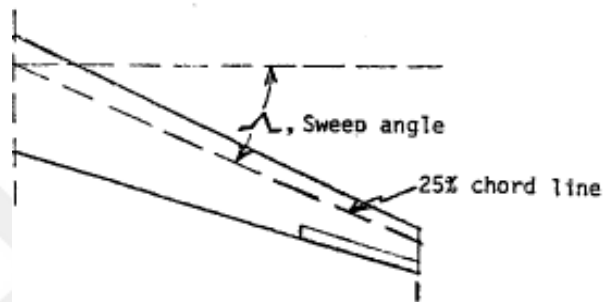


Figure 4.2. Definition of the sweep angle

All 3D wing geometries given in Table 2.1 are created by using this parametric model. Preview of one of the sample wing geometry, which is Wing 4, in DOE is given in Figure 4.3 as an example. In addition, technical drawings of all wing geometries are given in Appendix A between Figure A.1 and Figure A.20.

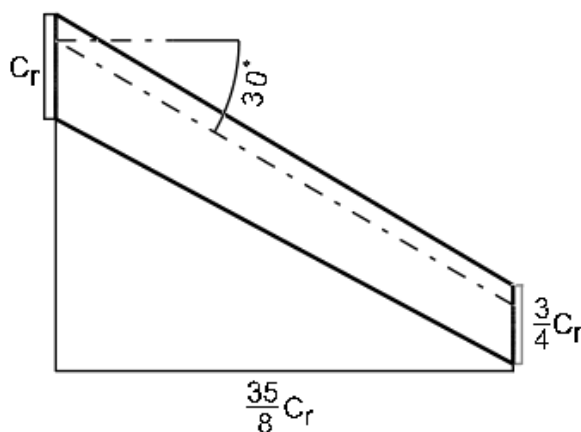


Figure 4.3. Technical drawing of the Wing 4 (AR=10, TR=0.75, SA=30°)

4.2. Finite Element Modeling and Analyses of the Wings

Finite element models are formed for each wing geometry separately by using MSC Patran. Firstly, computational grids for the wings are constructed by using Tet10 topology method. By using this method, surfaces are meshed with triangular elements and solid is meshed with ten-noded tetrahedral elements.

Grid independence study is performed to eliminate (or reduce) the influence of the grid size on the computational results. In other words, this study is performed to investigate how the mesh quality affects finite element analysis results. There exists a relationship between the accuracy of the results and computational costs [24]. It is important to find the optimum grid size before vibrational analyses.

The grid independence study is performed by developing ten different meshes for Wing 4. Systematically, the element size is decreased by changing division numbers of the root chord of the wing. While the grid cells become smaller, the number of cells in the finite element model increases. The surface meshes around the wings, for selected five ones, are represented in Figure 4.4 from coarsest to finest. The analyses also included five more intermediate grid sizes whose pictures have not been included for simplicity.

Vibrational analyses are performed to find the first two mode frequencies by using Wing 4. The results of grid independence study are shown in Figure 4.5 and Figure 4.6.

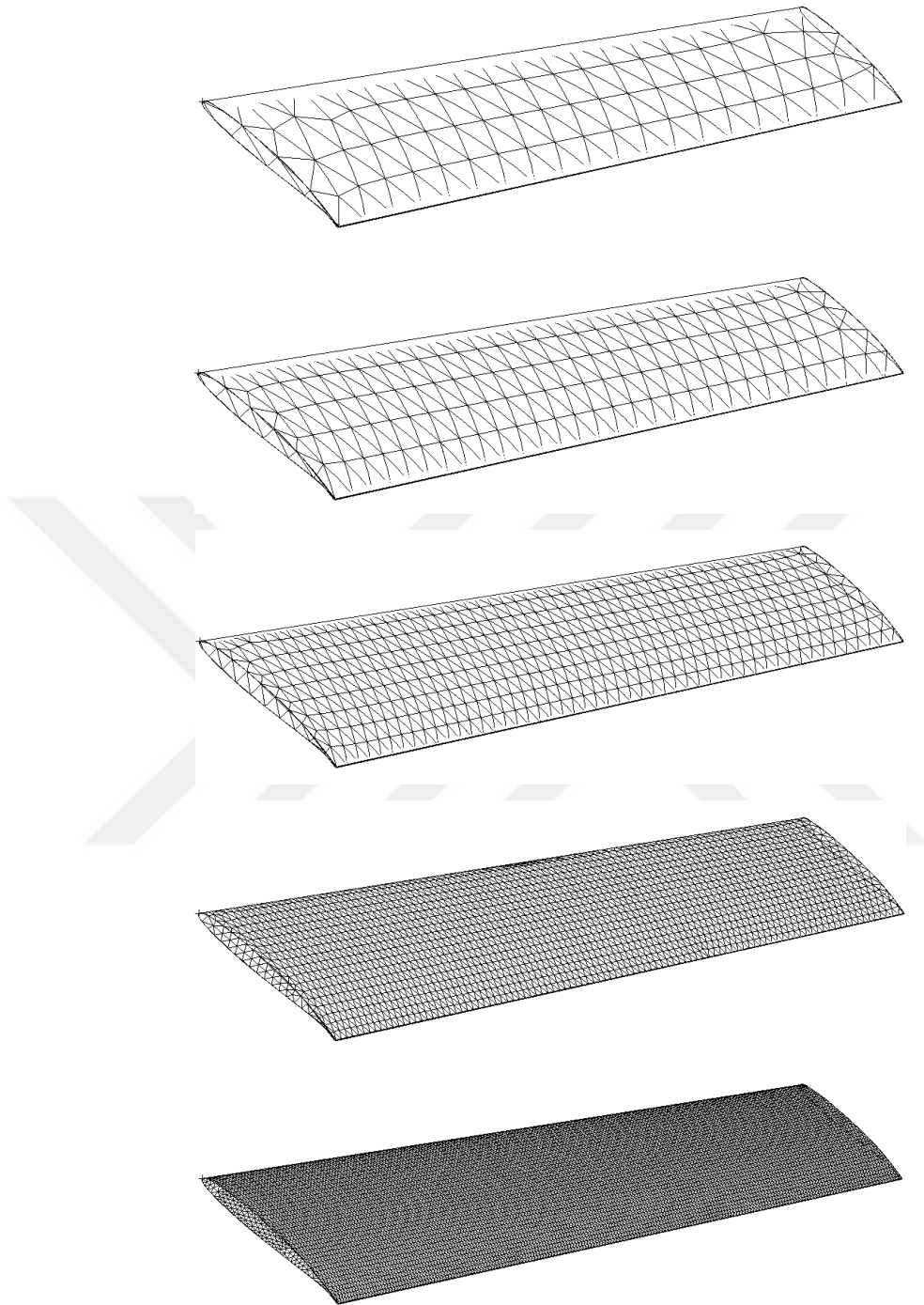


Figure 4.4. Different grids from coarse to fine

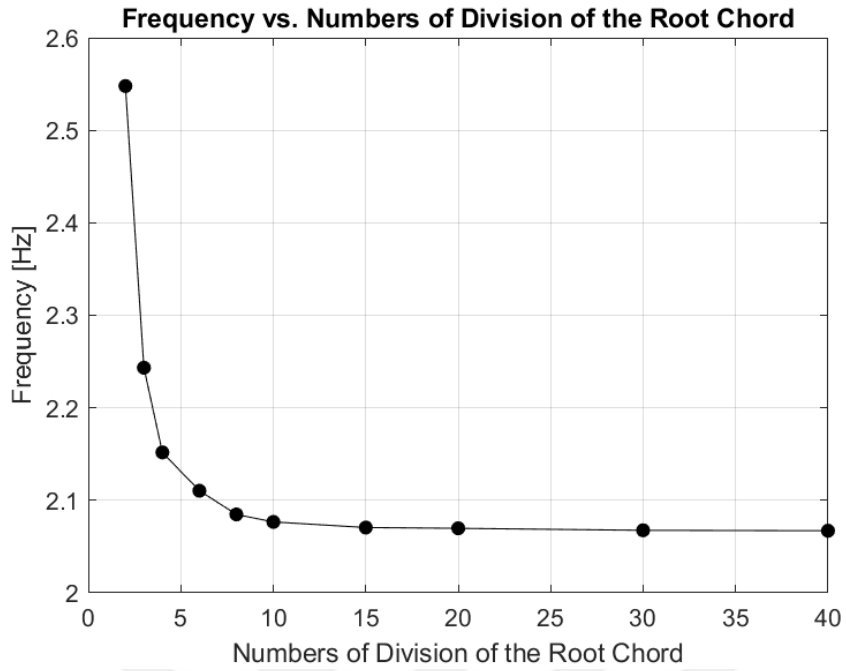


Figure 4.5. First mode frequency of the Wing 4 with respect to different grids

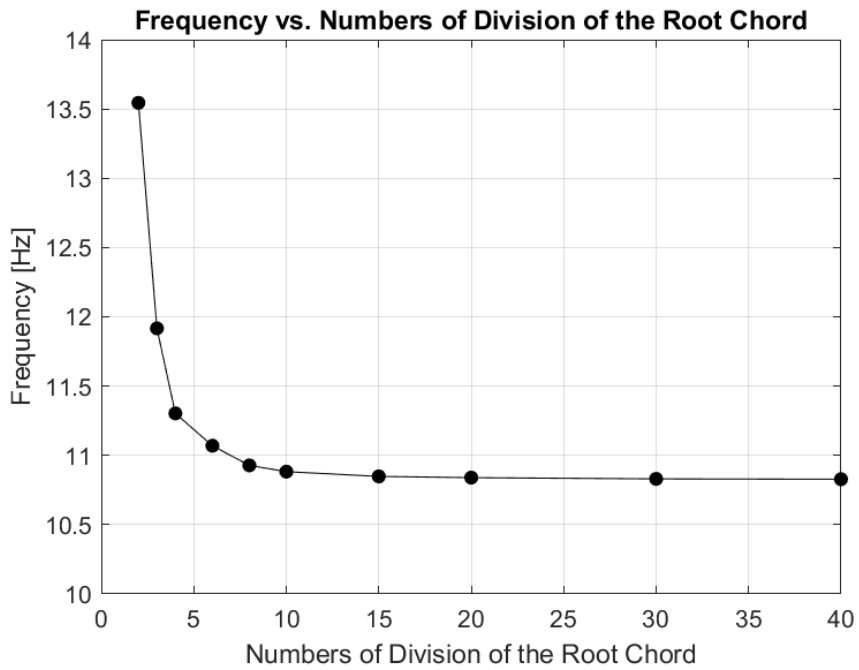


Figure 4.6. Second mode frequency of the Wing 4 with respect to different grids

By considering the frequencies obtained for the first two modes of Wing 4 with different grids, global edge length of one-tenth of the root chord is decided to be used for vibrational analyses. Preview of the surface mesh for one of the sample wing geometry in DOE, which is Wing 4, is given in Figure 4.7 as an example.

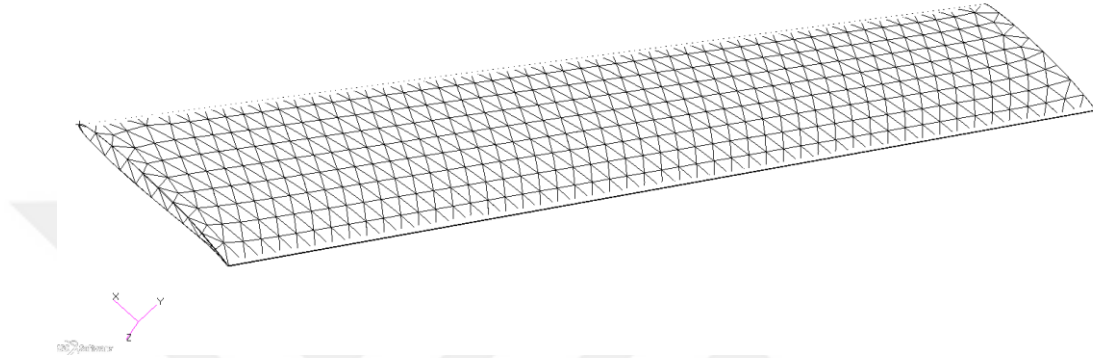


Figure 4.7. Surface mesh around the Wing 4 in finite element model

Secondly, the material properties of the wing are inputted to the software. The material of the wing is 2014-T6 aluminum alloy and properties used in finite element model are given in Table 4.1.

Table 4.1. Material properties of 2014-T6 aluminum alloy that used in finite element model

Properties	Value
Modulus of Elasticity	73.1 GPa
Shear Modulus of Elasticity	28 GPa
Poisson's Ratio	0.33
Density	2800 kg/m ³

Thirdly, the boundary condition of the wing is inputted as fixed at the root chord and free at the tip chord. This type of boundary condition is known as cantilever condition. In fact, the boundary conditions are inputted into the software in such a way that there are no translations and no rotations in three coordinates at the root chord. Schematic of the wing with boundary conditions is given in Figure 4.8.

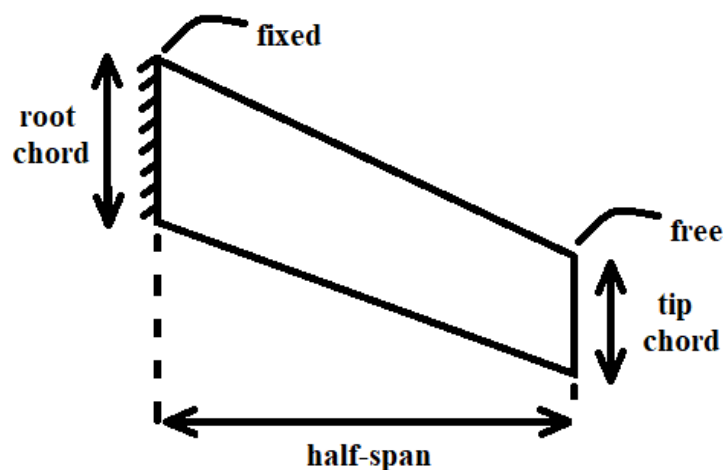


Figure 4.8. Schematic of the wing

Lastly, vibrational analyses are performed, for all the wing geometries existing in DOE, by using MSC Nastran. The normal modes are calculated for each wing geometry and the first five relevant modes are decided to use in aeroelastic analyses. Results of the vibrational analyses are given in Table 4.2.

Table 4.2. *Natural frequencies of the wings (in Hz)*

Wing Number	Mode 1	Mode 2	Mode 3	Mode 4	Mode 5
1	13.42	67.01	83.63	105.23	170.01
2	5.86	30.40	46.76	53.45	79.44
3	3.26	17.06	26.21	39.49	44.98
4	2.08	10.88	16.68	28.75	31.42
5	1.44	7.53	11.53	19.96	26.05
6	1.05	5.52	8.44	14.65	22.25
7	0.80	4.22	6.44	11.20	19.41
8	3.07	12.97	23.90	32.09	46.93
9	2.60	12.07	20.53	30.75	39.72
10	2.23	11.25	17.86	29.40	33.85
11	1.94	10.53	15.62	28.09	29.27
12	1.69	9.87	13.80	25.30	27.01
13	1.49	9.28	12.23	22.26	25.86
14	2.73	14.28	24.25	31.82	37.73
15	2.71	14.18	24.12	31.74	37.46
16	2.65	13.87	23.49	31.66	36.67
17	2.55	13.38	22.37	31.60	35.37
18	2.42	12.70	20.83	31.50	33.60
19	1.64	8.61	11.79	22.79	31.17
20	1.17	6.12	7.07	16.24	29.86

The first five mode shapes of one of the sample wing geometry in DOE, which is Wing 4, is given in Figure 4.9 as an example. As seen from the figure, for the Wing 4, the first mode is the first out of plane bending mode, the second mode is the second out of plane bending mode, the third mode is the first in plane bending mode, the fourth mode is the third out of plane bending mode, and the fifth mode is the first torsion mode. In addition, the first five mode shapes of all wing geometries are given in Appendix B between Figure A.21 and Figure A.40.

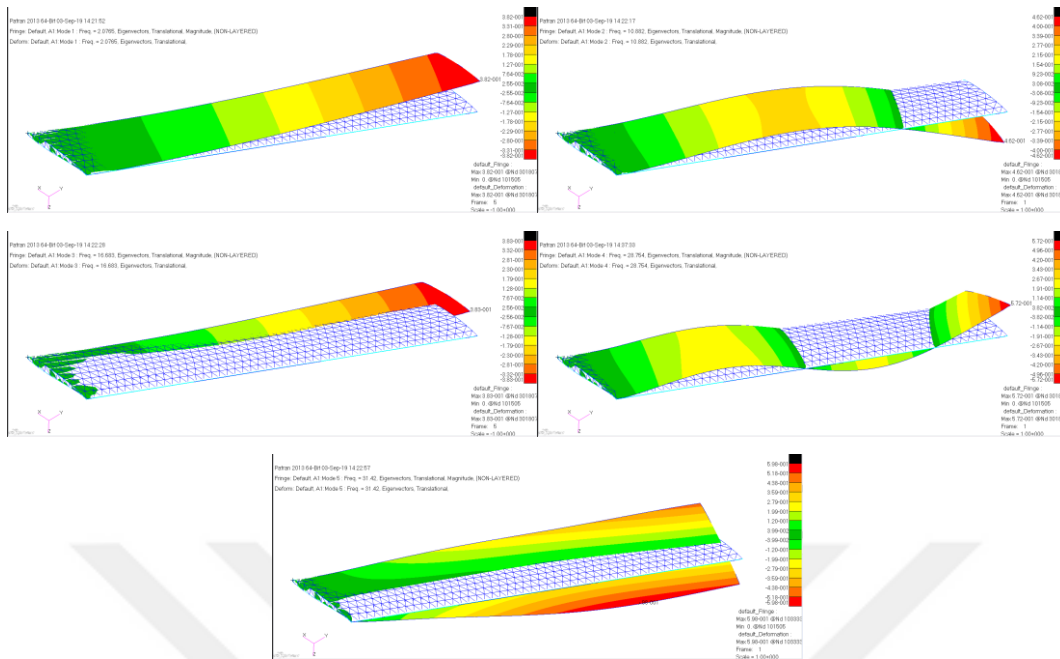


Figure 4.9. First five mode shapes of the Wing 4 (AR=10, TR=0.75, SA=30°)

4.3. Aerodynamic Modeling of the Wings

In order to perform the aeroelastic analyses, ZAERO needs aerodynamic models in addition to the finite element models. Aerodynamic models of the wings can be defined in the input files of ZAERO. For this, geometric properties of the aerodynamic model for the wings need to be inputted. These geometric properties can be listed as:

- X, Y, and Z locations of the root and tip chord leading edges,
- Length of the root and tip chords,
- Number of spanwise and chordwise divisions of the wing component shown in Figure 4.10 [22],
- Other detailed properties such as the distribution of divisions, element numbers, etc.

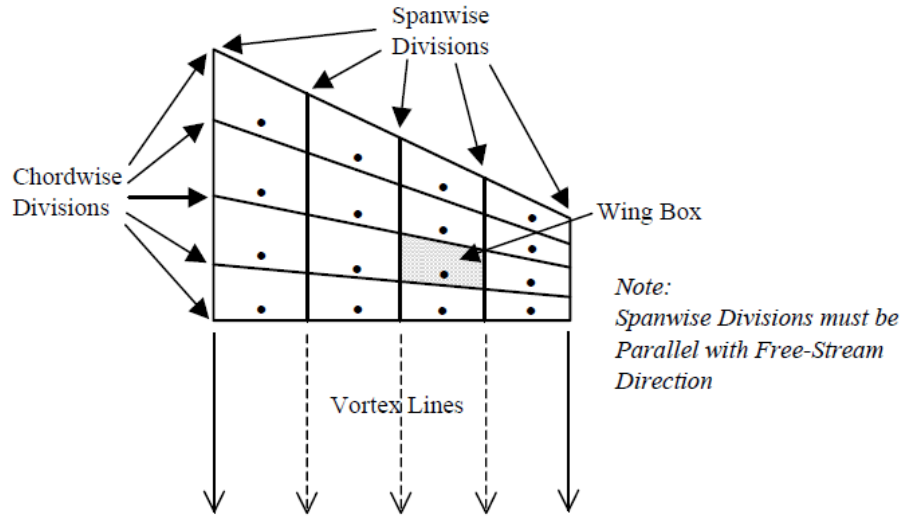


Figure 4.10. Spanwise and chordwise divisions of the wing [22]

ZAERO unsteady aerodynamics solves the frequency domain based unsteady small disturbance equation. The resulting unsteady pressure distribution computed by ZAERO is oscillatory in nature. The number of waves of the oscillatory pressure increases as the frequency increases. Because of this oscillatory nature, the convergence of the solution with respect to the number of aerodynamic boxes of the aerodynamic model becomes an important consideration. In order to have convergent solution, the maximum element size can be calculated as:

$$\Delta x < 0.08 \left(\frac{V}{f} \right) \frac{1}{\left(\frac{M}{\sqrt{|M^2 - 1|}} \right)^2} \quad (4.3)$$

Considering the maximum element size formula for convergent solution and element size of finite element model meshes, the element size for aerodynamic meshes is decided as one-tenth of the root chord of the wing. Preview of the grid of the aerodynamic model for one of the sample wing geometry in DOE, which is Wing 4, is given in Figure 4.11 as an example.

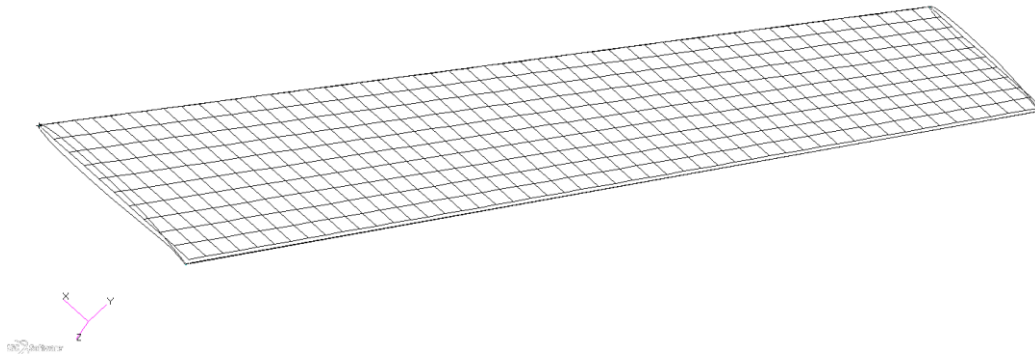


Figure 4.11. Grid of the aerodynamic model for the Wing 4

It should be noted that ZAERO prints out the warning message given in Figure 4.12 when the convergence criterion is violated. Since it helps to prevent possible convergence errors, it should not be ignored when it is encountered.

```
**** WARNING **** AT MACH=XXX, K=XXX, THE CHORD LENGTH (DX=XXX) OF
BODY (OR WING) BOX (ID=XXX) IS TOO LARGE
```

Figure 4.12. Warning message for violation of the convergence criteria

4.4. Preparation of the ZAERO Solution Setup

The aeroelastic analyses are performed by using ZAERO which executes his own input file. Input files are prepared for each wing geometry and each case. Remember that the ZAERO input file has three sections as:

1. Executive Control Section
2. Case Control Section
3. Bulk Data Section

In this part, the preparation of these three sections is explained.

4.4.1. Executive Control Section

In this section, only the finite element analysis result file is introduced. Input file includes the name of the finite element solution file and the form of the solution.

4.4.2. Case Control Section

This section is another short section of the ZAERO input file. Title for the aeroelastic analysis is given in this section. This section also includes some information about the subcases such as subtitle, label, etc.

4.4.3. Bulk Data Section

The most important section in the ZAERO input file is the Bulk Data Section. Many of the settings related to analyses are done in this section.

Firstly, using the input data card of AEROZ, the basic aerodynamic reference parameters are defined. These parameters include reference length and areas, identification numbers, units of length and mass, and location of aerodynamic moment center.

Then, the local coordinate system is defined by using ACOORD data card. This data card has information of identification number, location of the origin, and pitch and roll angle of the local coordinate system.

One of the important data cards in the Bulk Data Section is CAERO7 because the aerodynamic model is constructed with respect to values inputted here. As mentioned before, the aerodynamic grid is generated by using the size of elements as one-tenth of the root chord.

Another important data card is SPLINE1. In order to perform aeroelastic analyses, the finite element model and the aerodynamic model must be connected. SPLINE1 data card provides displacements and loads transferal between aerodynamic structural grid points by using the Infinite Plate Spline (IPS) method shown in Figure 4.13. This data card needs information that the node numbers of aerodynamic and structural grids. By knowing the spline method, ZAERO creates the spline matrix in its own.

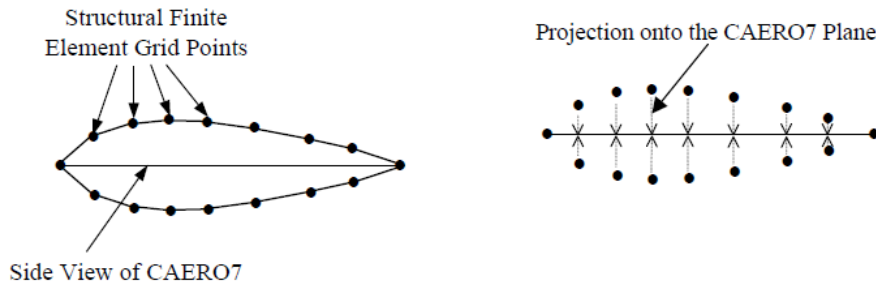


Figure 4.13. Infinite Plate Spline Method

In order to generate the AIC matrix, MKAEROZ data card is used. This data card includes information about Mach number, mean flow conditions, and reduced frequencies list. Moreover, the solution type of the aerodynamics can be selected in this data card. The required reduced frequencies can be calculated as:

$$k = \frac{\omega \left(\frac{REFC}{2} \right)}{V_{\infty}} \quad (4.4)$$

Since aeroelastic analyses are performed for different wing configurations, which have different natural modes and flutter speeds, the reduced frequency range has a large interval. The maximum reduced frequency is calculated for maximum natural frequency and minimum velocity. A set of reduced frequencies used in aeroelastic analyses is given in Table 4.3.

Table 4.3. A set of reduced frequencies (in Hz)

0.00	0.03	0.06	0.09	0.12	0.15
0.20	0.25	0.30	0.35	0.40	0.45
0.50	0.60	0.70	0.80	0.90	1.00
1.20	1.40	1.60	1.80	2.00	

Lastly, FLUTTER data card defines the aeroelastic analyses to obtain the flutter speed. This data card refers to one of the flutter solution methods. The aeroelastic analyses are performed by using FIXMDEN data card, which performs non-matched point

flutter analysis at fixed Mach number and the density with varying velocities by using both the K-Method and the g-Method. For the aeroelastic analyses, velocity is increased by 10 m/s until the flutter speed is obtained. Furthermore, analyses are performed for different altitudes by changing the density in this data card.

Results are obtained from the output file of ZAERO. The output file includes V-g and V-f data for the requested cases. By utilizing this data and founding where g is changing sign, the flutter speed can be estimated.

4.5. Determination of the Flutter Speed

The flutter is a dynamic aeroelastic problem and the V-g plot methodology is commonly used for its determination [25]. Since the aerodynamic forces are those which introduce energy into the system and their value depends on the speed for a given configuration (characteristic mass, elastic and geometric structure), it is possible to calculate the critical flutter speed, speed which if exceeded, the system becomes unstable dynamically and virtually destroyed [26].

In the V-g plot methodology, both V-g and V-f plots are drawn. Examples of these plots are given in Figure 4.14 and Figure 4.15. Unfortunately, these plots are using in both determinations of the flutter and the divergence speeds. First of all, the aeroelastic problem is detected by using the V-g plot. As seen from Figure 4.14, when the curve crosses the x-axis and damping value changes from negative to positive, this crossing point will be determined as flutter or divergence speed. In order to distinguish these two different aeroelastic problems, the V-f plot is used. Since the flutter is a dynamic aeroelastic problem, it should occur at a certain frequency. On the other hand, divergence occurs at zero frequency because it is a static aeroelastic problem. By using Figure 4.15, checking the frequency values for the velocities at the crossing points detected in Figure 4.14, it can be found that the first intersection point in Figure 4.14 is the flutter speed and the second intersection point in Figure 4.14 is the divergence speed.

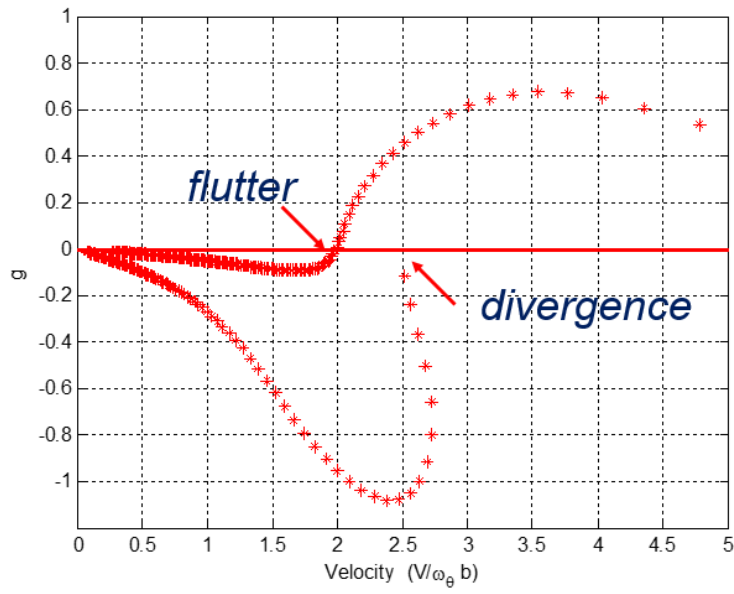


Figure 4.14. Determination of the speed of the aeroelastic problem

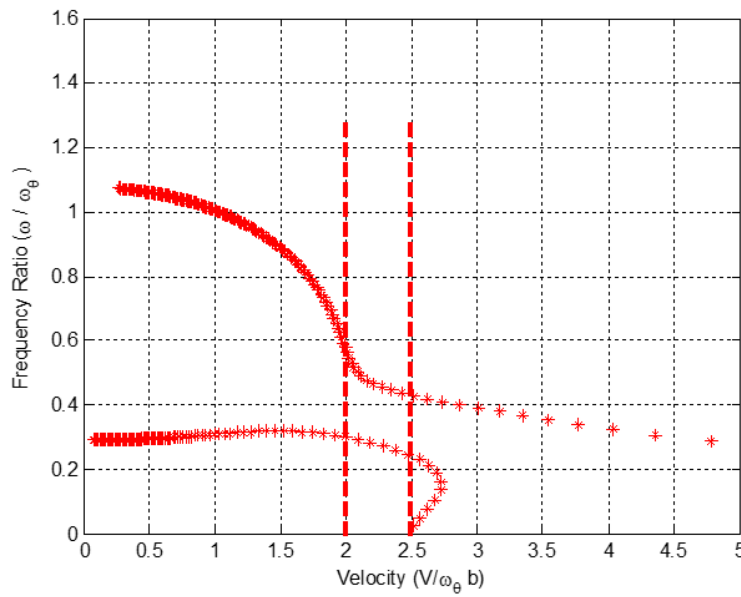


Figure 4.15. Determination of the frequency of the aeroelastic problem

CHAPTER 5

RESULTS AND DISCUSSIONS

In order to investigate the effects of the aspect ratio on the flutter speed, wings between Wing 1 and Wing 7 are analyzed. Moreover, wings between Wing 8 and Wing 13 are analyzed to examine the effects of the taper ratio. Lastly, wings between Wing 14 and Wing 20 are used to observe the effects of the sweep angle. It should be noted that Wing 4 is included in both studies in order to investigate the effects of the taper ratio and the sweep angle.

5.1. Flutter Analysis Results

The aeroelastic analyses are performed for 20 different wing geometries given in Table 2.1 at five different altitudes as sea level, 10 kft, 20 kft, 30 kft, and 40 kft. For the aeroelastic analyses, velocity is increased by 10 m/s until the flutter speed is obtained. In order to determine flutter speeds, the V-g and the V-f curves are plotted for all geometries and given in Appendix C between Figure A.41 and Figure A.80.

For example, the V-g and the V-f plots are given in Figure 5.1 and Figure 5.2 for Wing 4 which has the aspect ratio of 10, the taper ratio of 0.75 and the sweep angle of 30° . In Figure 5.1, the V-g plot is drawn for five different altitudes by selecting relevant modes that flutter occurred. If the curve belongs to the sea level condition is examined, the intersection point can be detected as 190 m/s. In order to distinguish whether it is a flutter speed or a divergence speed, the frequency value at the speed of 190 m/s should be checked from Figure 5.2. Since the frequency has a non-zero value at 190 m/s, it can be chosen as the flutter speed. Similarly, the flutter speeds at different altitudes can be found by determining the intersection points of V-g curves and checking the frequencies at the intersection points.

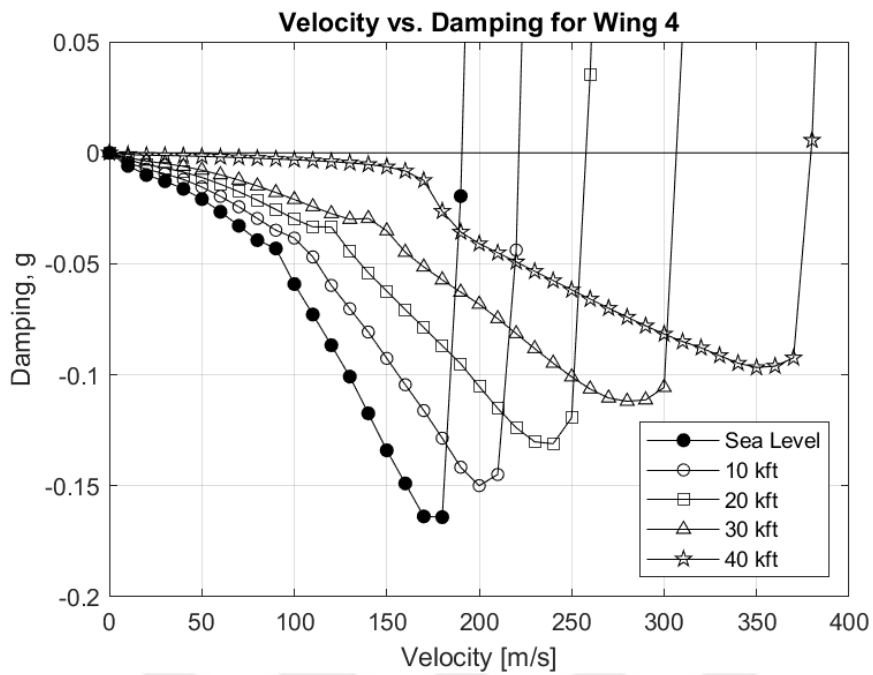


Figure 5.1. Velocity vs. Damping plots for the Wing 4

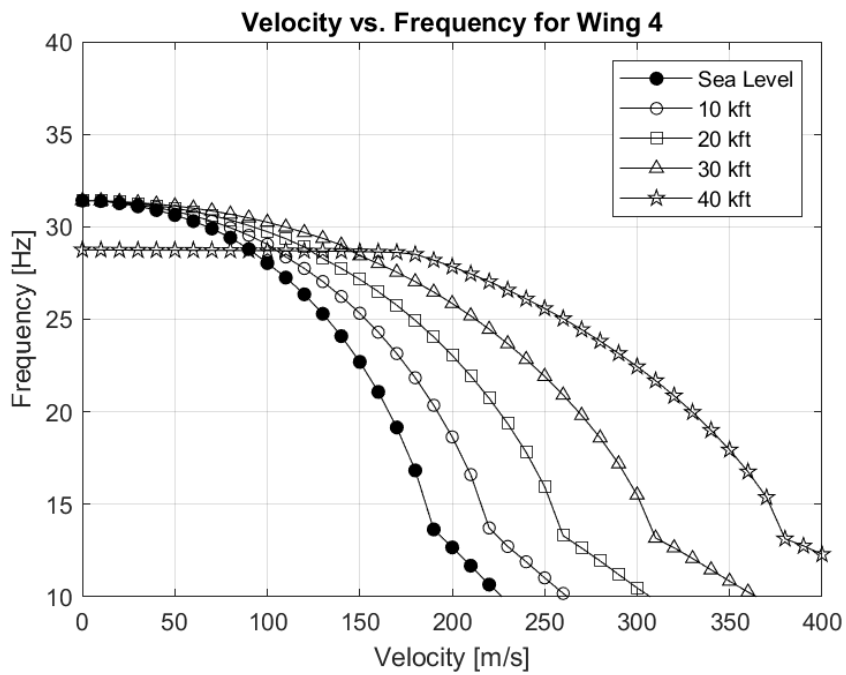


Figure 5.2. Velocity vs. Frequency plots for the Wing 4

For Wing 4, it should be also noted that the flutter occurs in the fifth mode, which is the first torsion mode, for the altitudes of sea level, 10 kft, 20 kft, and 30 kft. This is why the frequency curves except for 40 kft start from the same point in Figure 5.2. Since the flutter occurs in the fourth mode, which is the third out of plane bending mode, at the 40 kft, the starting point of the curve in Figure 5.2 is different from the others.

5.2. Effects of the Aspect Ratio

Wings between Wing 1 and Wing 7 are analyzed to investigate the effects of the aspect ratio on the flutter speed. From Wing 1 to Wing 7, the aspect ratios of the wings are linearly changing from 4 to 16. The other relevant parameters are kept constant when changing the aspect ratios. Technical drawings of these wings are given in figures between Figure A.1 and Figure A.7. By considering the results of vibrational analyses given in Table 4.2, it can be concluded that the natural frequencies of the wings decrease with the increase of the aspect ratio. Therefore, the structure of the wings becomes more flexible.

Figures between Figure A.41 and Figure A.54 show both the V-g and the V-f curves of the wings that have different aspect ratios. The flutter speeds are obtained by estimating the location of sign change, where the sign has a positive value, of the V-g curves and checking the non-zero value of the frequency at this velocity as mentioned before. The results of the aeroelastic analyses are combined and given in Figure 5.3 to investigate the effects of the aspect ratio on the flutter speed.

Since the disturbing aerodynamic forces on the wing is increasing with the increase of the aspect ratio, the flutter speed decreases significantly. The highest decrease is shown between the aspect ratio of 4 and the aspect ratio of 6. The flutter speed falls by nearly half between these two. After the aspect ratio of 6, the flutter speeds continue to decrease, but not as dramatically as between the aspect ratio of 4 and the aspect ratio of 6. Moreover, this decrease is almost linear after the aspect ratio of 6.

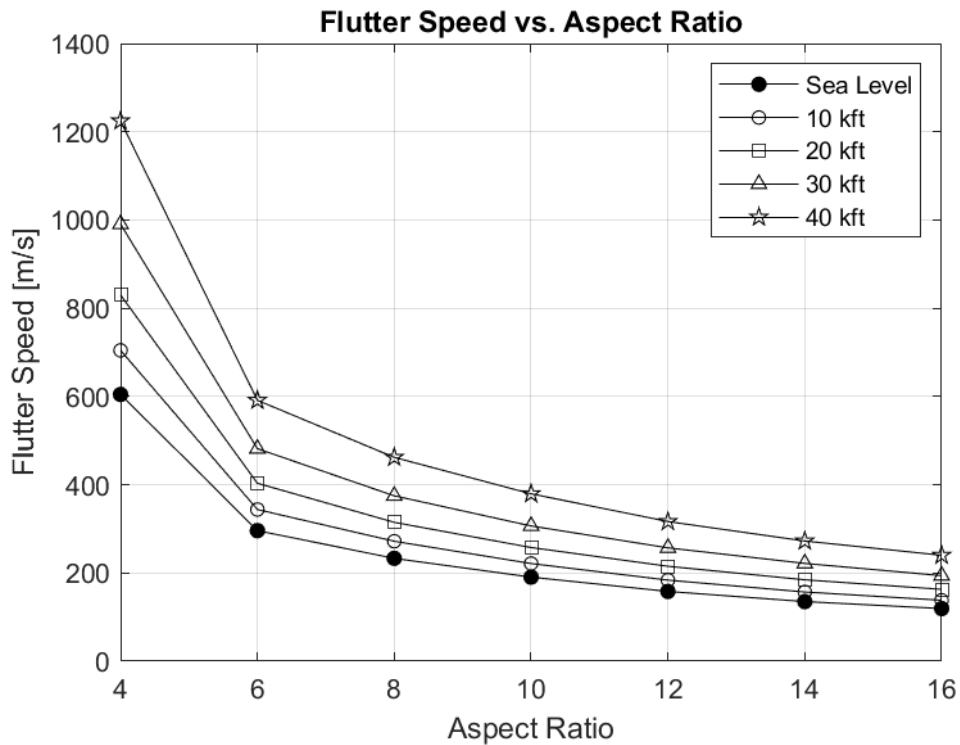


Figure 5.3. Effects of the aspect ratio on the flutter speed

5.3. Effects of the Taper Ratio

In order to investigate the effects of the taper ratio on the flutter speed, wings between Wing 8 and Wing 13 are analyzed. The taper ratios of the wings are linearly changing from 0.5 to 1 from Wing 8 to Wing 13. When changing the taper ratios, the other relevant parameters remained constant. In figures between Figure A.8 and Figure A.13, technical drawings of these wings are given. By considering the results of vibrational analyses given in Table 4.2, it can be concluded that the natural frequencies of the wings decrease with the increase of the taper ratio. Therefore, the structure of the wings becomes more flexible.

The V-g and the V-f curves of the wings that have different taper ratios are given in figures between Figure A.55 and Figure A.66. The flutter speeds are obtained by using the same procedure as mentioned before. The results of the aeroelastic analyses are

combined with the results of Wing 4 which has the taper ratio of 0.75 and given in Figure 5.4 to investigate the effects of the taper ratio on the flutter speed.

This figure shows clearly that with the increase of the taper ratio, the flutter speed decreases. In other words, the tapering increases the flutter speed. This increase is the result of the increase of the bending and torsional stiffness of the structure. Furthermore, the change of the flutter speeds with the change of the taper ratio has approximately linear behavior.

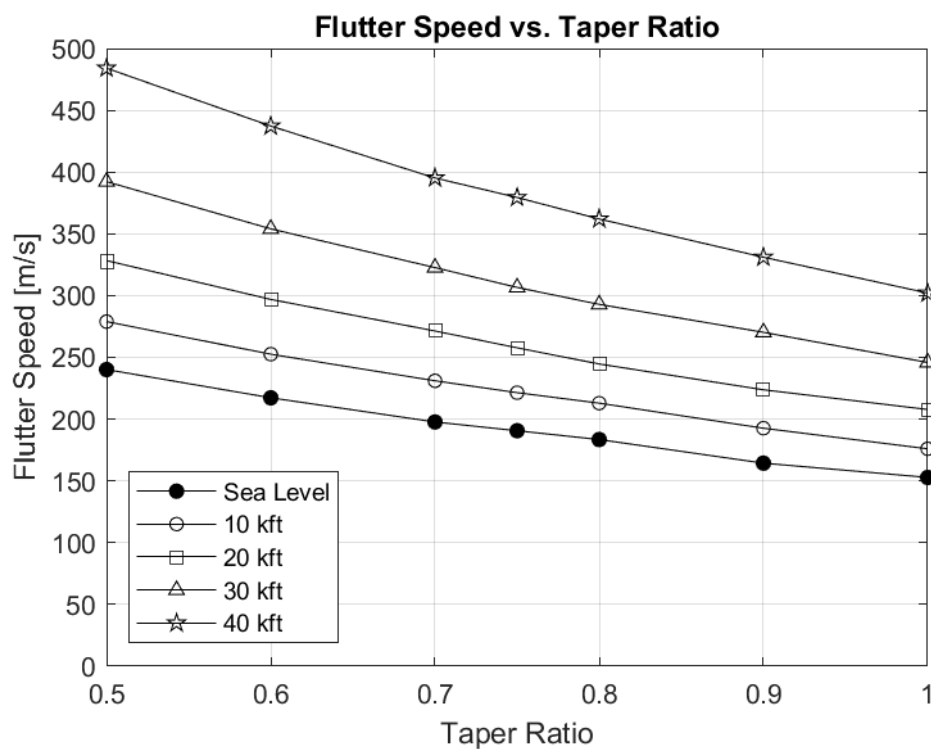


Figure 5.4. Effects of the taper ratio on the flutter speed

5.4. Effects of the Sweep Angle

Wings between the Wing 14 and Wing 20 are analyzed to investigate the effects of the quarter-chord sweep angle on the flutter speed. From Wing 14 to Wing 20, the sweep angles of the wings are changing from 0 to 50°. The other relevant parameters are kept constant when changing the sweep angles. In figures between Figure A.14 and Figure A.20, technical drawings of these wings are given. By considering the

results of vibrational analyses given in Table 4.2, it can be concluded that the natural frequencies of the wings decrease with the increase of the sweep angle. Therefore, the structure of the wings becomes more flexible.

The V-g and the V-f curves of the wings that have different sweep angles are given in figures between Figure A.67 and Figure A.80. The flutter speeds are obtained by using the same procedure as mentioned before. The results of the aeroelastic analyses are combined with the results of Wing 4 which has the sweep angle of 30° and given in Figure 5.5 to investigate the effects of the sweep angle on the flutter speed.

In contrast to the trend seen in the effects of the aspect ratio and the taper ratio, the flutter speed is not changing linearly with the sweep angle. It can be seen that flutter speed increases from 0 to 10°, decreases between 10° and 15°, and increases after 15° up to 50° for wing configuration studied.

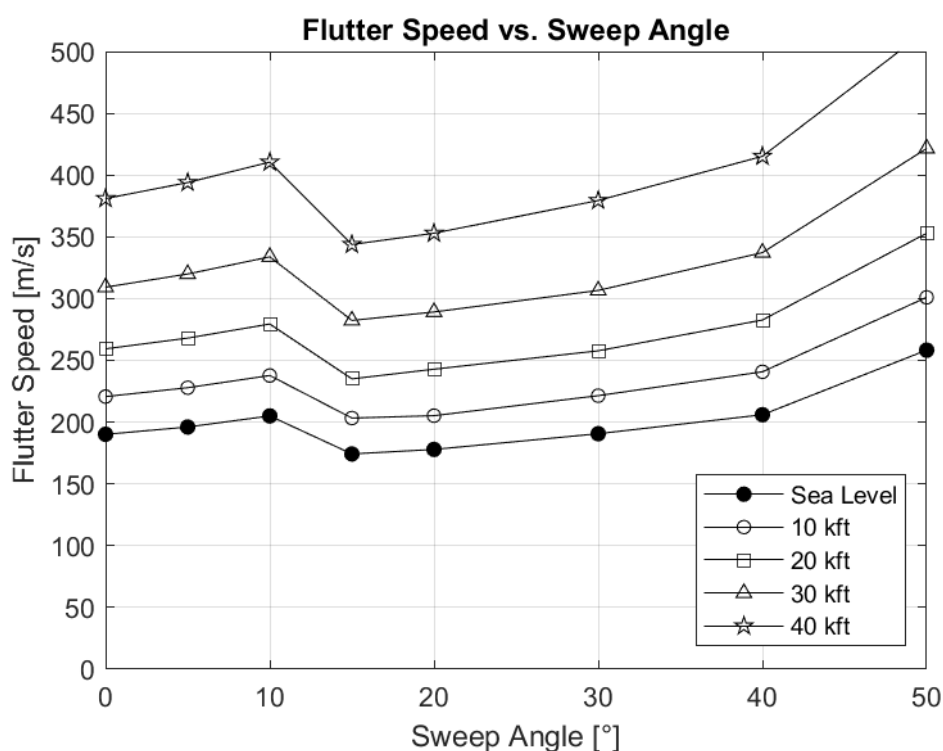


Figure 5.5. Effects of the sweep angle on the flutter speed

5.5. Effect of the Altitude

Since all wings from Wing 1 to Wing 20 have the same trend for the flutter speed versus altitude curves, the effect of the altitude on the flutter speed is investigated using the results of Wing 4 given in Figure 5.6. It can be concluded that the flutter speed increases with the increase of the altitude. By increasing the altitude, density of air decreases. In such a case, aerodynamic disturbing forces acting on the wing decrease. Therefore, the flutter speed increases with the increase of altitude.

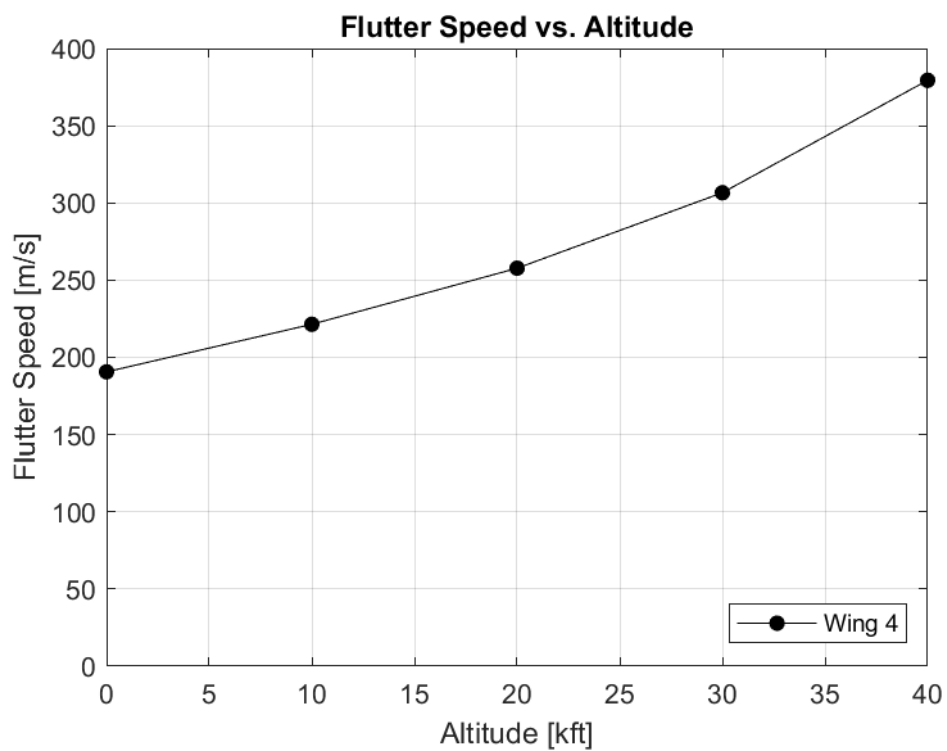


Figure 5.6. Effect of the altitude on the flutter speed

CHAPTER 6

CONCLUSIONS

6.1. General Conclusions

In this thesis, in order to obtain the aeroelastic effects of design parameters such as the aspect ratio, the taper ratio, and the sweep angle; different wing geometries were created by changing these design parameters systematically. The flutter speeds were estimated to determine the aeroelastic effects of design parameters.

The DOE was generated as a custom design. It consisted of 20 different wing geometries. The flutter speeds were obtained for these 20 different wing geometries in the DOE at various altitudes.

Before starting the aeroelastic analyses to obtain flutter speeds, the theory of aeroelastic analyses was discussed. It included governing equations, flutter solution techniques and solution procedure of the ZAERO.

Aeroelastic analyses of the wings have had four steps. Firstly, for all wings in the DOE, solid models were generated by using the ANSYS DesignModeler. Then, finite element models were composed and vibrational analyses were performed for each wing geometry. Thirdly, aerodynamic models of the wings were formed by inputting the chord-wise and span-wise number of divisions. Lastly, aeroelastic solution setup was constituted by preparing the ZAERO input files.

Moreover, the methodology of determination of the flutter speeds was given. For each wing geometry, V-g and V-f curves were obtained. The flutter speeds were estimated by determining the intersection point of V-g curves with x-axis and checking the frequency at the intersection velocity from V-f curves.

Results were obtained and discussed in Chapter 5 for each case. It can be concluded that the aspect ratio and the taper ratio has a substantial effect on the aeroelastic characteristics of the wing. The sweep angle shows different characteristics on the flutter speed of the wing. Moreover, it is shown that increasing the altitude increases the flutter speed. Therefore, this wing configuration will be safe when the missile is climbing to the higher altitudes.

In this study, the effects of design parameters such as the aspect ratio, the taper ratio, and the sweep angle on the flutter speed of the wing were investigated. In fact, it should not be forgotten that these effects may be different in other disciplines. For this reason, the design process of the missile needs to be multidisciplinary and the designer should consider aeroelastic problems in the design of a cruise missile wing. In this complex multidisciplinary design process, predicting the effects of individual design parameters in different aspects is highly important.

The results are applicable for considered missile wings only. The fuselage was assumed rigid and the wings were analyzed in cantilever condition. The consideration of the whole missile dynamics and inclusion of those of fuselage may alter the results.

6.2. Recommendations for Future Work

This study included the aeroelastic analyses to obtain effects of design parameters such as the aspect ratio, the taper ratio and the sweep angle on the flutter speed. The study may be extended for the other design parameters such as incidence, twist angle, airfoil type, etc. Moreover, this study is performed at cruise condition of the missile. The study may be extended to include different flight conditions. Finally, this study may be extended to show effects of design parameters on different disciplines as aerodynamics, flight mechanics, etc.

REFERENCES

1. Fleeman, E. L., "Tactical Missile Design," American Institute of Aeronautics and Astronautics, 2001.
2. Ning, A., and Kroo, I., "Multidisciplinary Considerations in the Design of Wings and Wing Tip Devices," *Journal of Aircraft*, Vol. 47, pp. 534–543, 2010.
3. Collar, A. R., "The Expanding Domain of Aeroelasticity," *Journal of the Royal Aeronautical Society*, Vol. 1, pp. 613-636, 1946.
4. Bisplinghoff, R. L., Ashley, H., and Halfman, R. L., "Aeroelasticity," Dover Publications Inc., New York, 1955.
5. Molineux, W. G., and Hall, H., "The aerodynamic effects of aspect ratio and sweepback on wing flutter," HM Stationery Office, 1957.
6. Bae, J. S., Seigler, M., and Inman, D. J., "Aerodynamic and static aeroelastic characteristics of a variable-span morphing wing," *Journal of Aircraft*, Vol. 42, No. 2, 2005.
7. Ren, H., and Zhiping, Q., "Transient aeroelastic responses and flutter analysis of a variable-span wing during the morphing process," *Chinese Journal of Aeronautics*, Vol. 26, No. 6, 2013.
8. Mahran, M., Negm, H., and Elsabbagh, A., "Aero-elastic Analysis of Plate Wings Using the Finite Element Method," LAP LAMBERT Academic Publishing, 2015.
9. Askan, A., and Tangoz, S., "The Effect of Aspect Ratio on Aerodynamic Performance and Flow Separation Behavior of a Model Wing Composed from Different Profiles," *Journal of Energy Systems*, Vol. 2, pp. 224–237, 2018.
10. "ZAERO Theoretical Manual," Version 8.5, ZONA 02 – 12.4, Zona Technology Inc., 2011.
11. Theodorsen, T., "General Theory of Aerodynamic Instability and the Mechanism of Flutter," NACA Report 496, 1935.

12. Hodges, D. H., and Pierce, G.A., "Introduction to Structural Dynamics and Aeroelasticity," Cambridge University Press, 2002.
13. Rodden, W. P., and Johnson, E. H., "User's Guide of MSC/NASTRAN Aeroelastic Analysis," MSC/NASTRAN v68, 1994.
14. Yates, E. C., Jr., Land, N.S. and Foughner, J.T., Jr., "Measured and Calculated Subsonic and Transonic Flutter Characteristics of a 45° Sweptback Wing Planform in Air and in Freon-12 in the Langley Transonic Dynamics Tunnel," NASA TN-D-1616, Mar. 1963.
15. Irwin, C. A. and Guyett, P.R., "The Subcritical Response and Flutter of a Swept Wing Model," Technical Report 65186, Royal Aircraft Establishment, Farnborough, U.K., Aug. 1965.
16. Hassig, H. J., "An Approximate True Damping Solution of the Flutter Equation by Determinant Iteration," Journal of Aircraft, Vol. 8, No. 11, Nov. 1971.
17. Rodden, W. P., Harder, R.L. and Bellinger, E.D., "Aeroelastic Addition to NASTRAN," NASA CR 3094, 1979.
18. Rodden, W. P. and Stahl, B., "A Strip Method for Prediction of Damping in Subsonic Wind Tunnel and Flight Flutter Test," Journal of Aircraft, Vol. 6, No. 1, pp. 9-17, Jan.-Feb. 1969.
19. Chen, P. C., "Damping Perturbation Method for Flutter Solution," AIAA Journal, Vol. 38, No. 9, pp. 1519-1524, Sep. 2000.
20. Chen, P. C., "A Damping Perturbation Method for Flutter Solution: The g-Method," International Forum on Aeroelasticity and Structural Dynamics, Hampton, VA, Jun. 22-25, 1999. Also in AIAA Journal, Vol. 38, No. 9, pp. 1519-1524, Sep. 2000.
21. Rodden, W. P., "Handbook for Aeroelastic Analysis," Vol. 1, MSC.NASTRAN Version 65.
22. "ZAERO User's Manual," Version 8.5, ZONA 02 – 12.4, Zona Technology Inc., June 2011.

23. Harris, C. D., "NASA Supercritical Airfoils: A Matrix of Family-Related Airfoils," NASA Technical Paper 2969, 1990.
24. Kulkarni, S. S., Chapman, C., and Shah, H., "Computational Fluid Dynamics (CFD) Mesh Independency Study of a Straight Blade Horizontal Axis Tidal Turbine," Sciprints, 2016.
25. Lind, R., and Brenner, M., "Robust aeroservoelastic stability analysis," Springer, London, 1999.
26. Stanciu, V., Stroe, G., and Andrei, I. C., "Linear Models and Calculation of Aeroelastic Flutter," UPB Sci. Bull, Vol. 74, pp. 29-38, 2012.



APPENDICES

A. Technical Drawing of the Wing Geometries

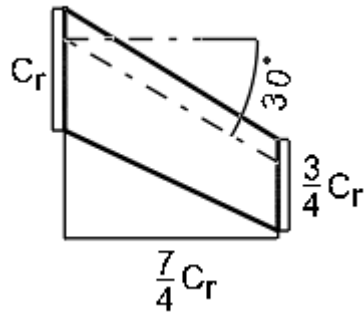


Figure A.1. Technical drawing of the Wing 1

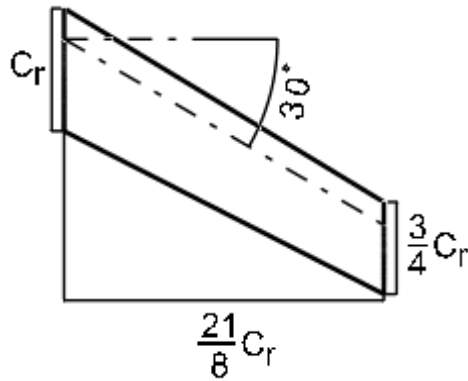


Figure A.2. Technical drawing of the Wing 2

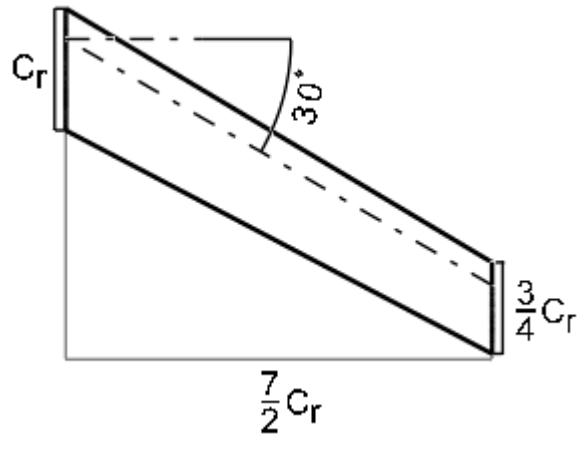


Figure A.3. Technical drawing of the Wing 3

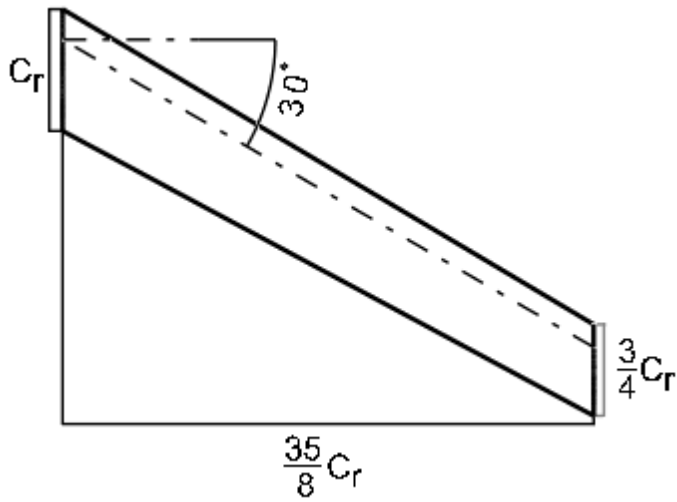


Figure A.4. Technical drawing of the Wing 4

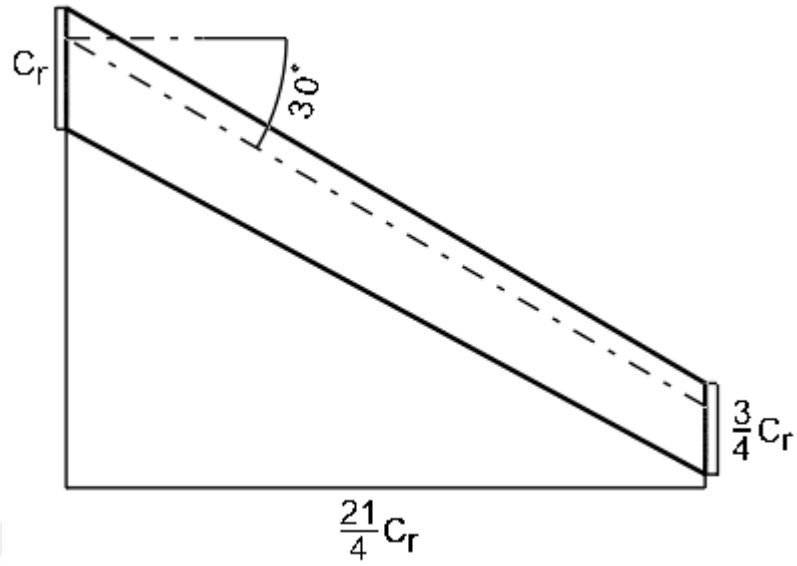


Figure A.5. Technical drawing of the Wing 5

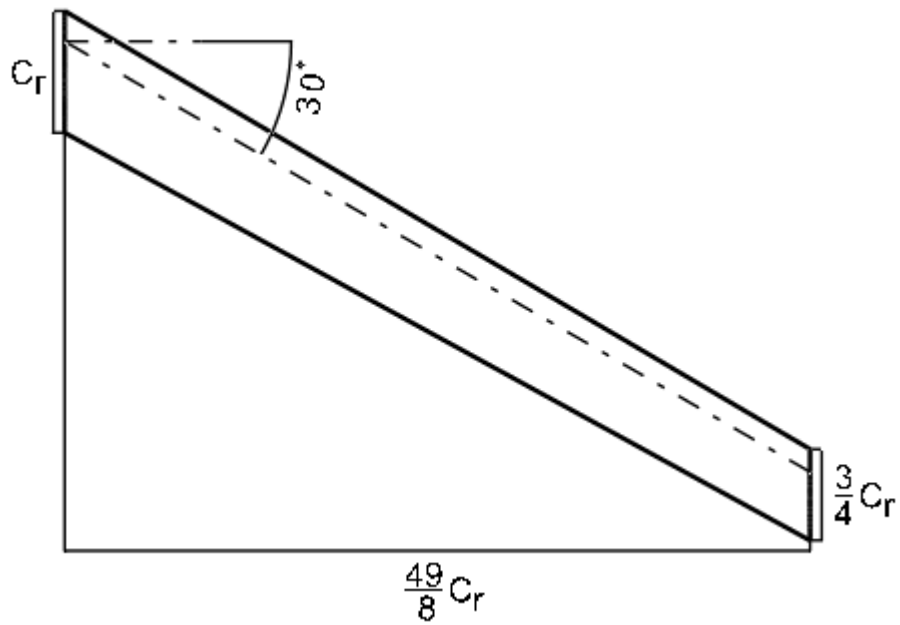


Figure A.6. Technical drawing of the Wing 6

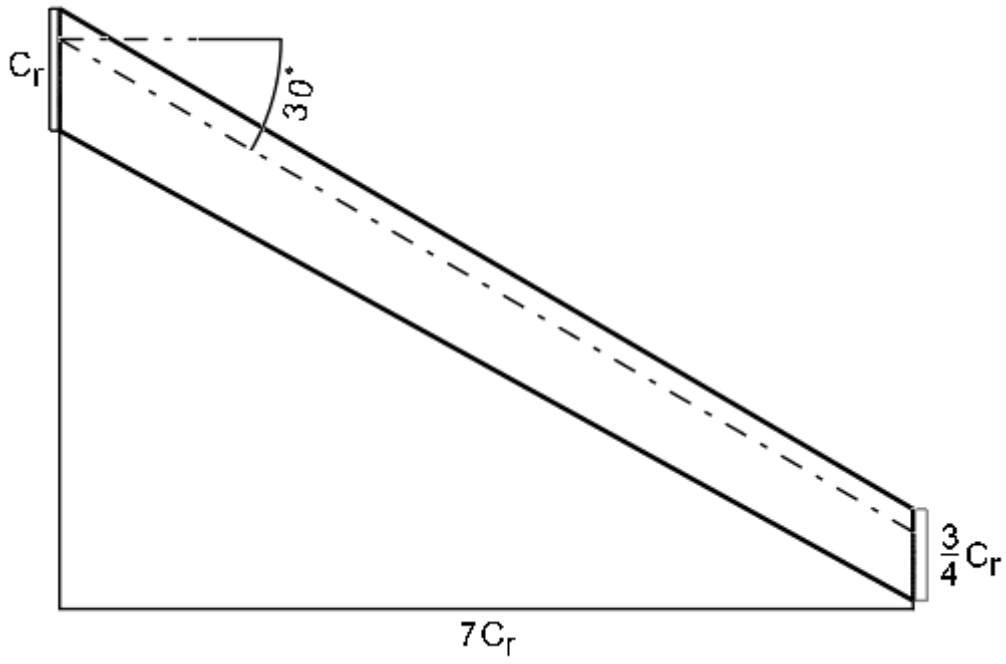


Figure A.7. Technical drawing of the Wing 7

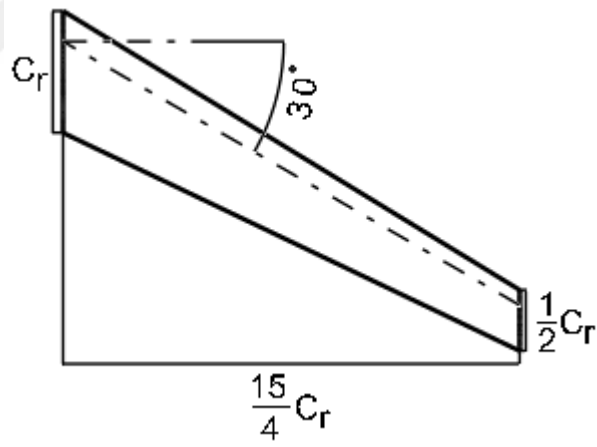


Figure A.8. Technical drawing of the Wing 8

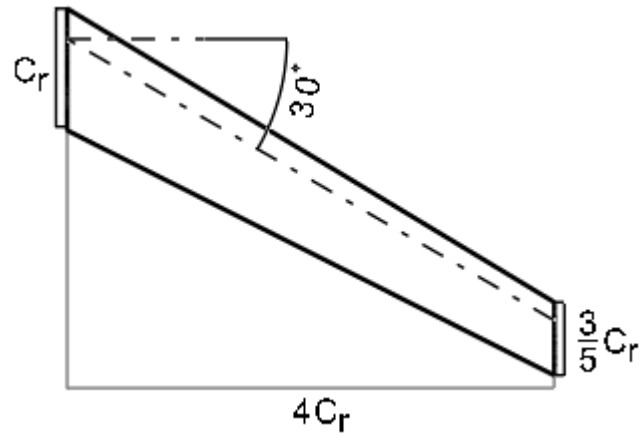


Figure A.9. Technical drawing of the Wing 9

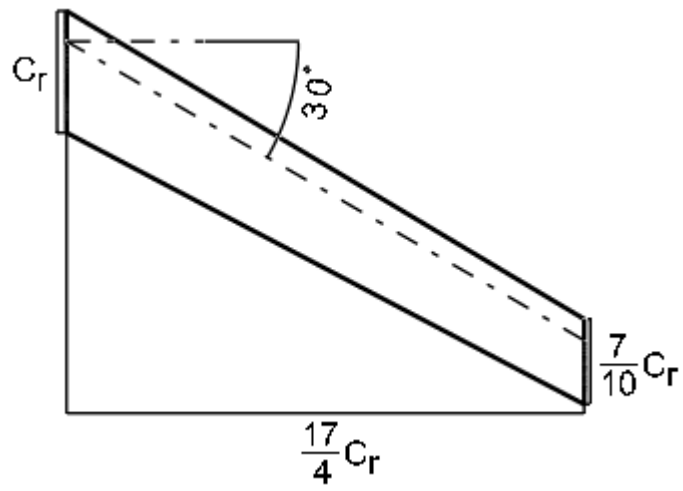


Figure A.10. Technical drawing of the Wing 10

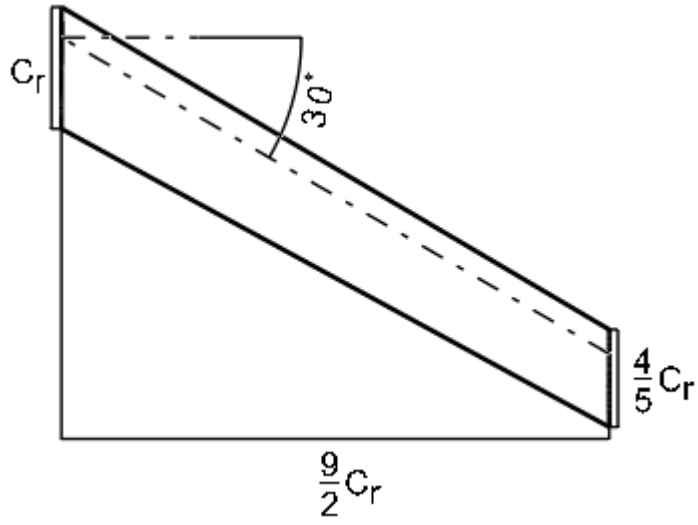


Figure A.11. Technical drawing of the Wing 11

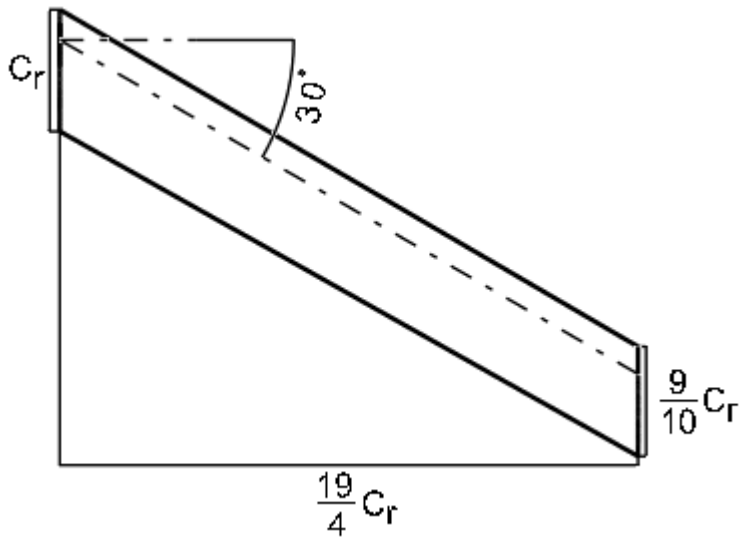


Figure A.12. Technical drawing of the Wing 12

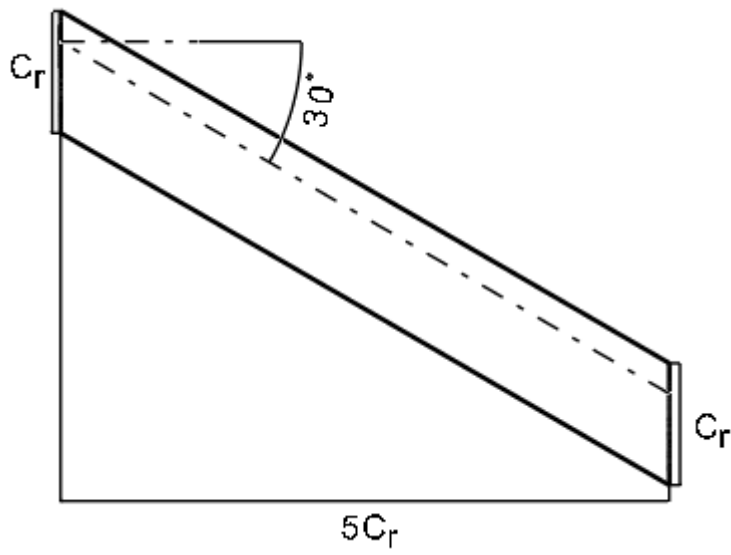


Figure A.13. Technical drawing of the Wing 13

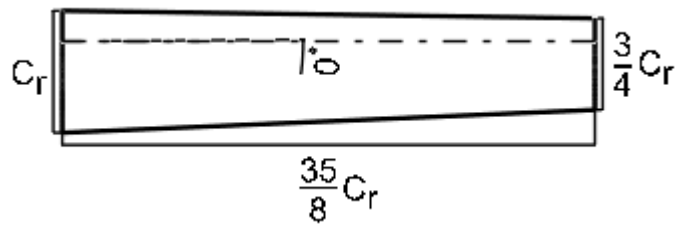


Figure A.14. Technical drawing of the Wing 14

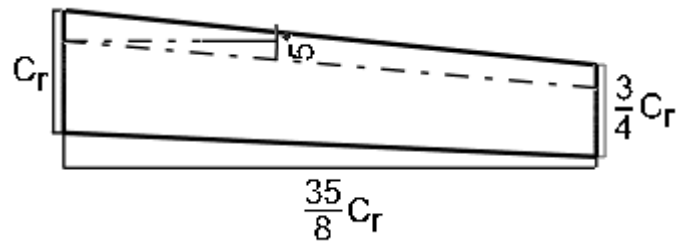


Figure A.15. Technical drawing of the Wing 15

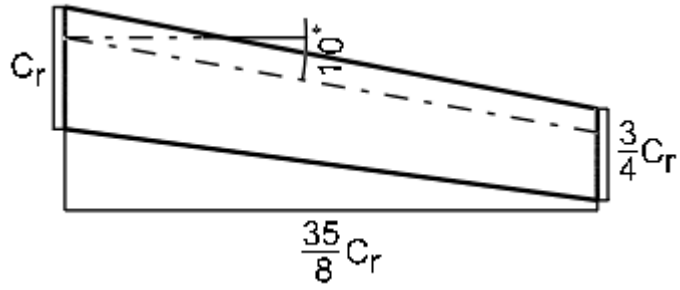


Figure A.16. Technical drawing of the Wing 16

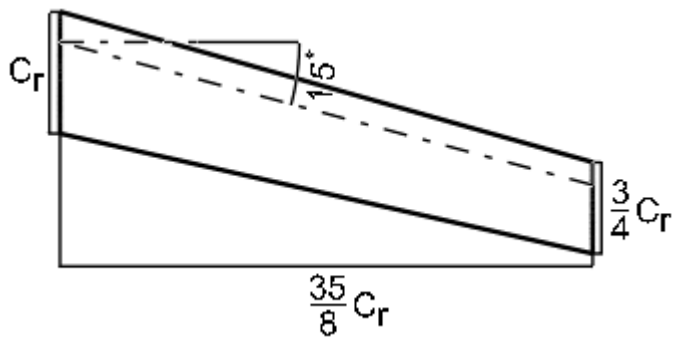


Figure A.17. Technical drawing of the Wing 17

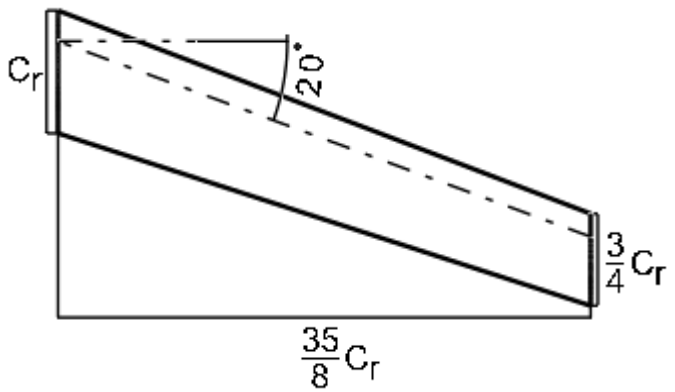


Figure A.18. Technical drawing of the Wing 18

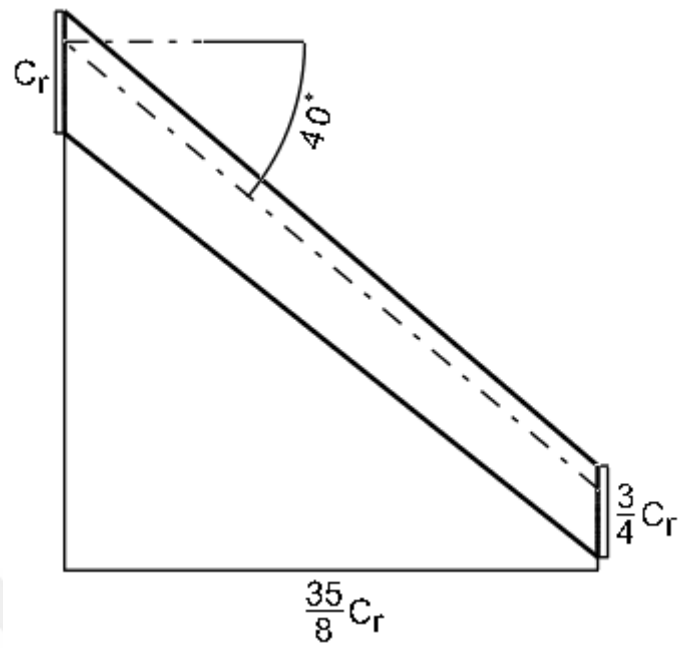


Figure A.19. Technical drawing of the Wing 19

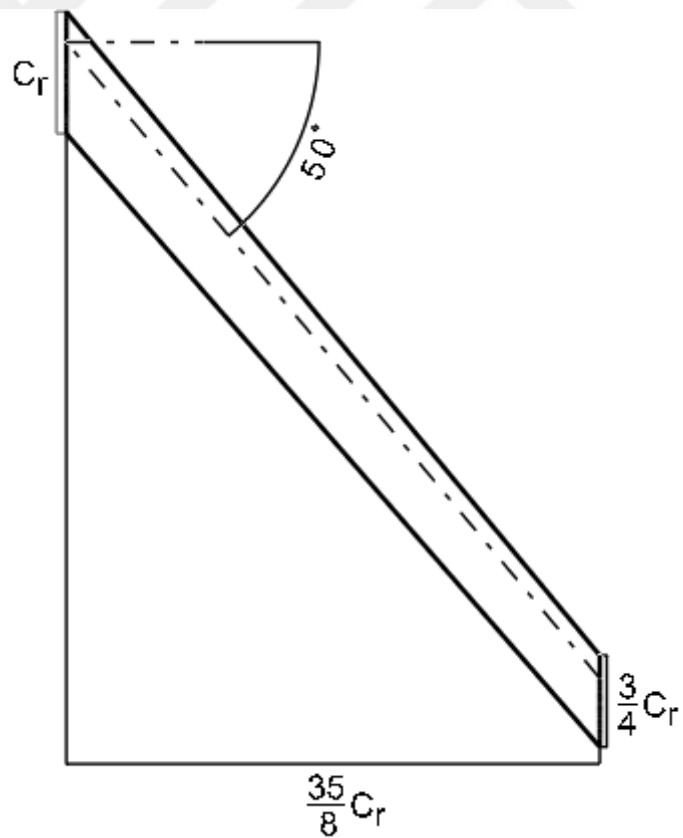


Figure A.20. Technical drawing of the Wing 20

B. Mode Shapes of the Wings

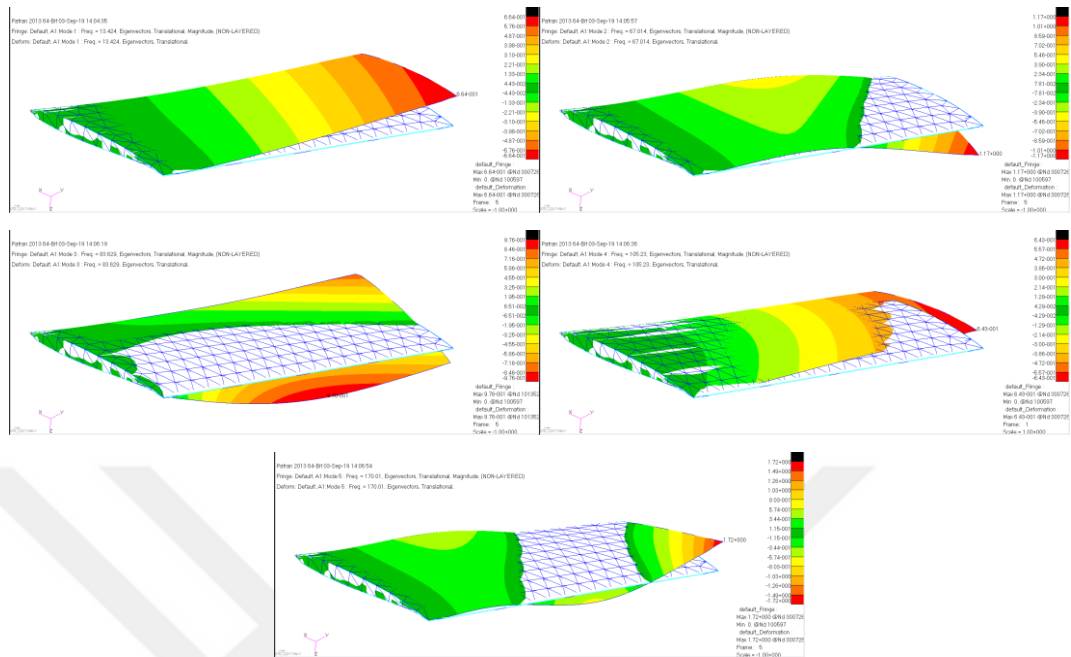


Figure A.21. First five mode shapes of the Wing 1

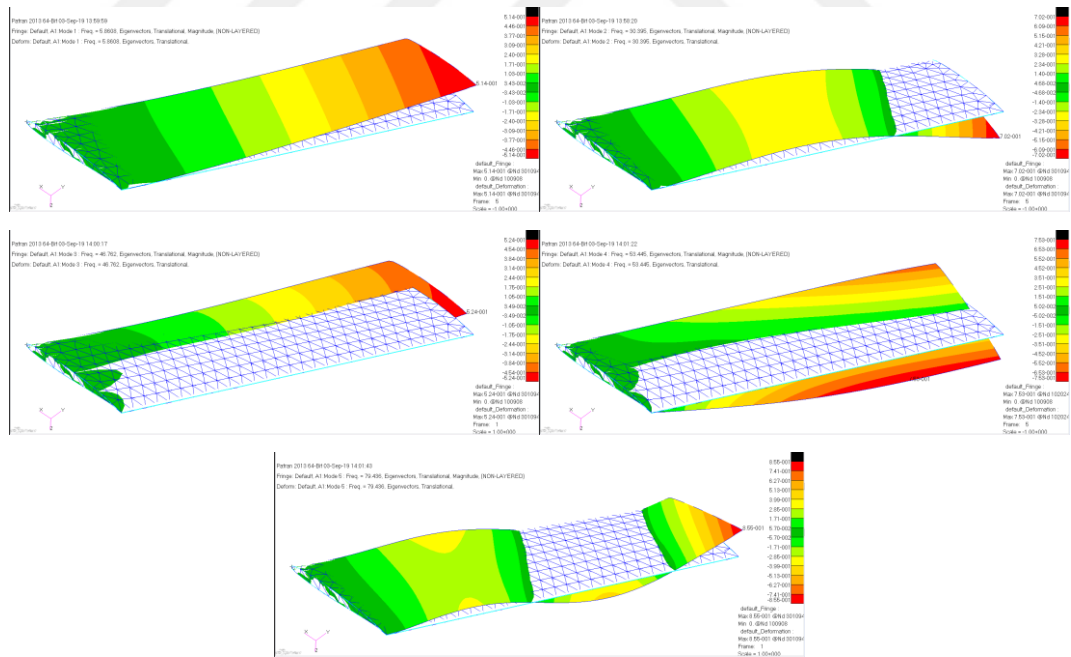


Figure A.22. First five mode shapes of the Wing 2

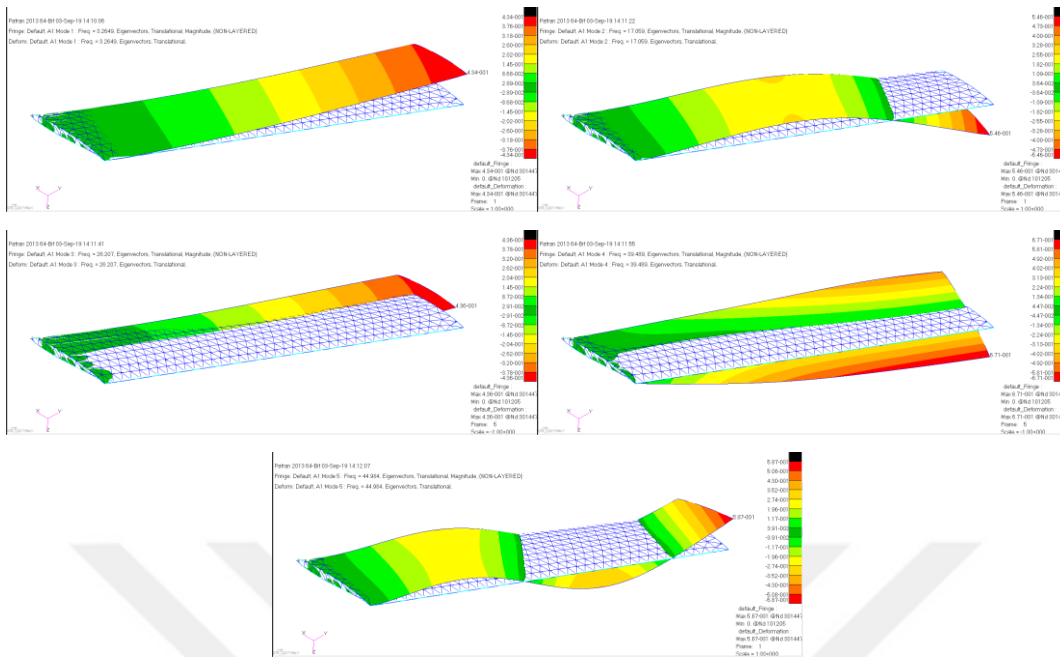


Figure A.23. First five mode shapes of the Wing 3

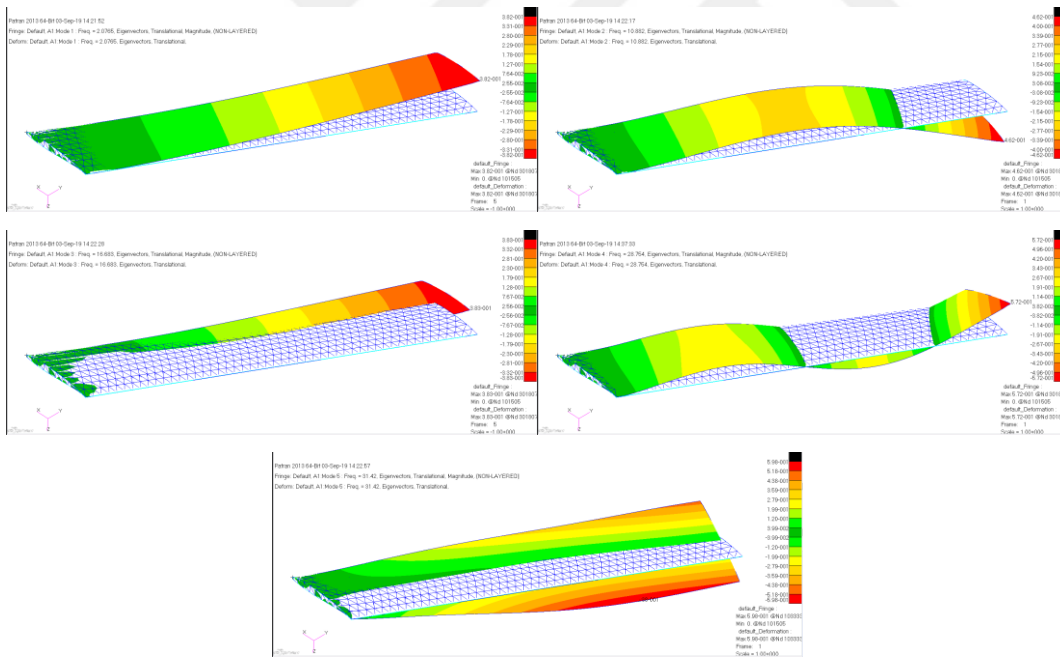


Figure A.24. First five mode shapes of the Wing 4

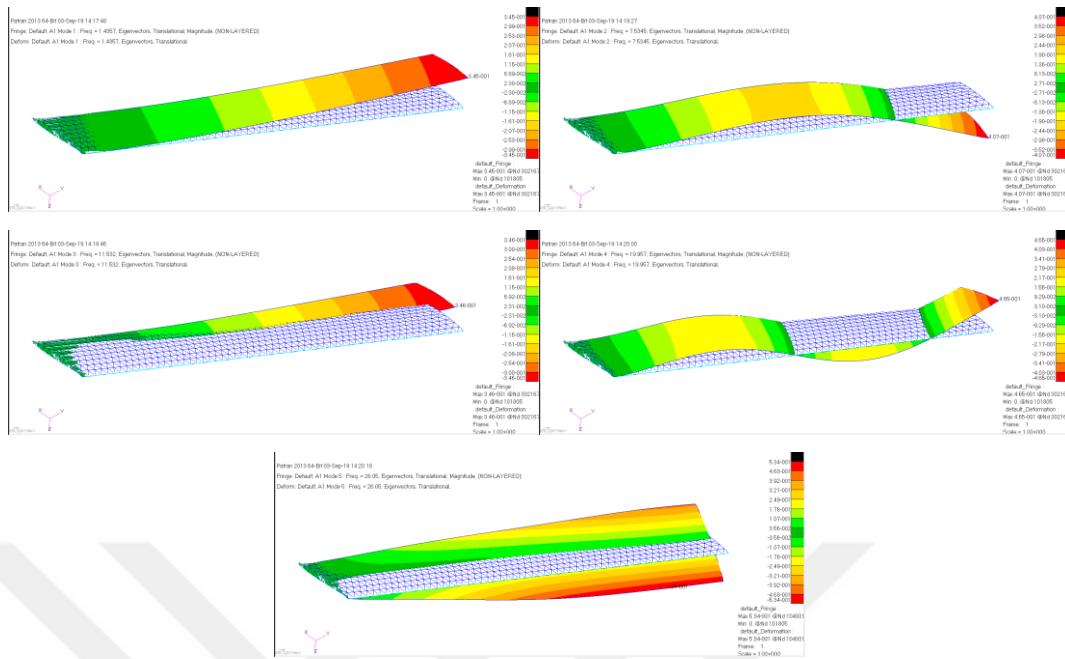


Figure A.25. First five mode shapes of the Wing 5

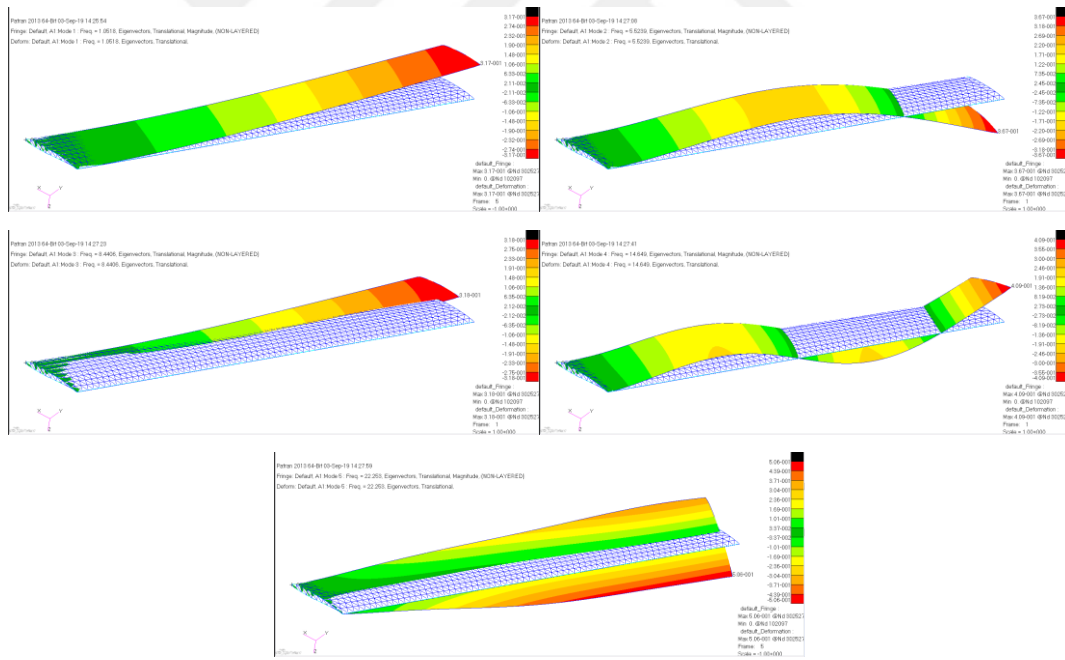


Figure A.26. First five mode shapes of the Wing 6

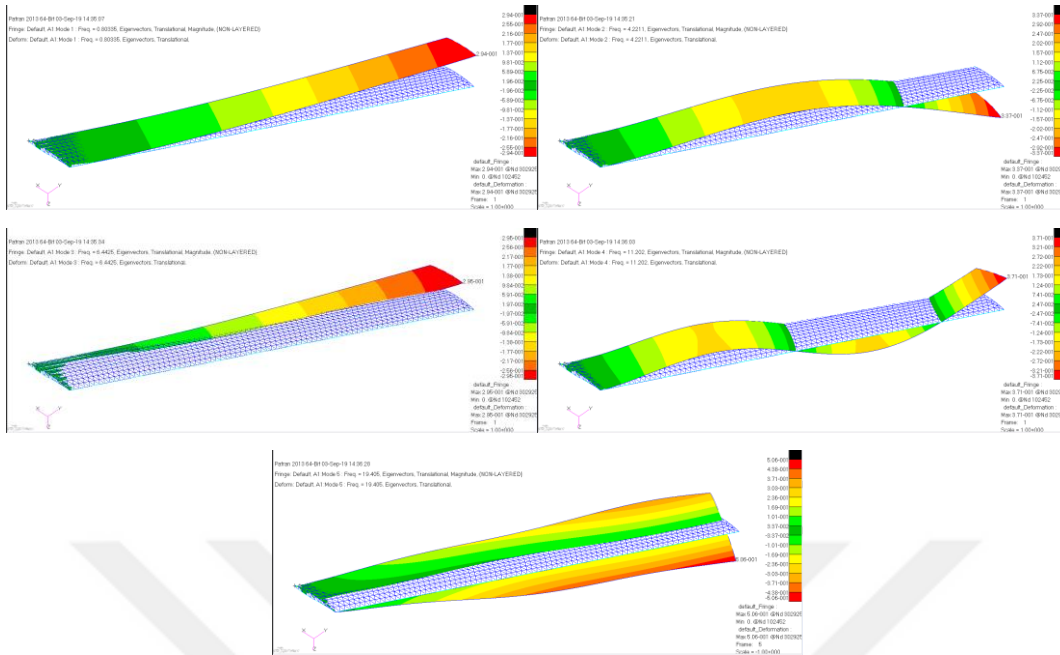


Figure A.27. First five mode shapes of the Wing 7

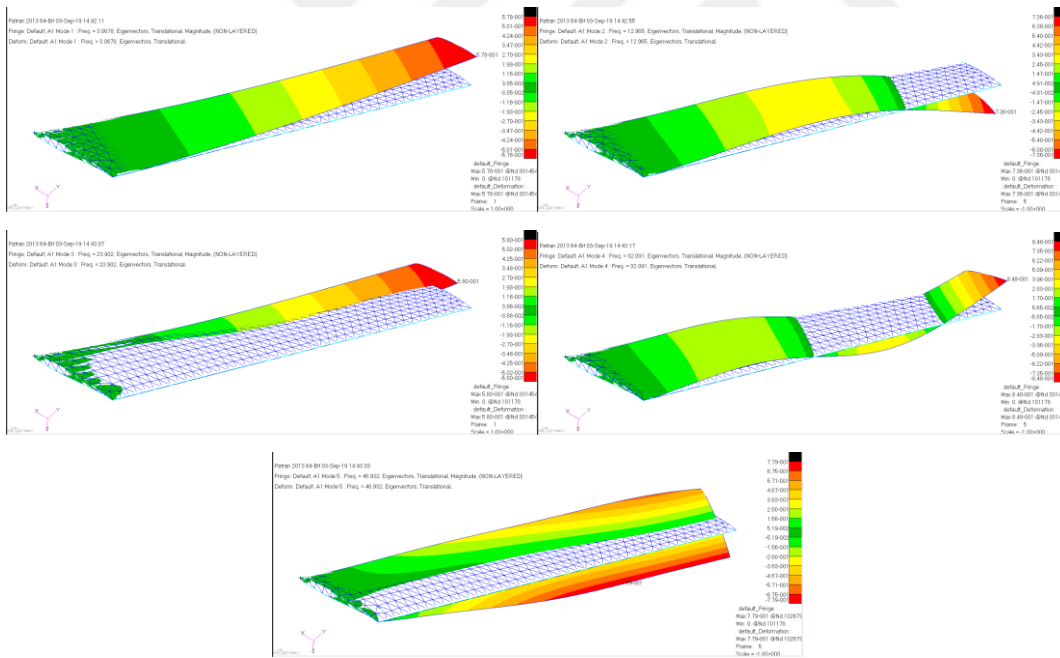


Figure A.28. First five mode shapes of the Wing 8

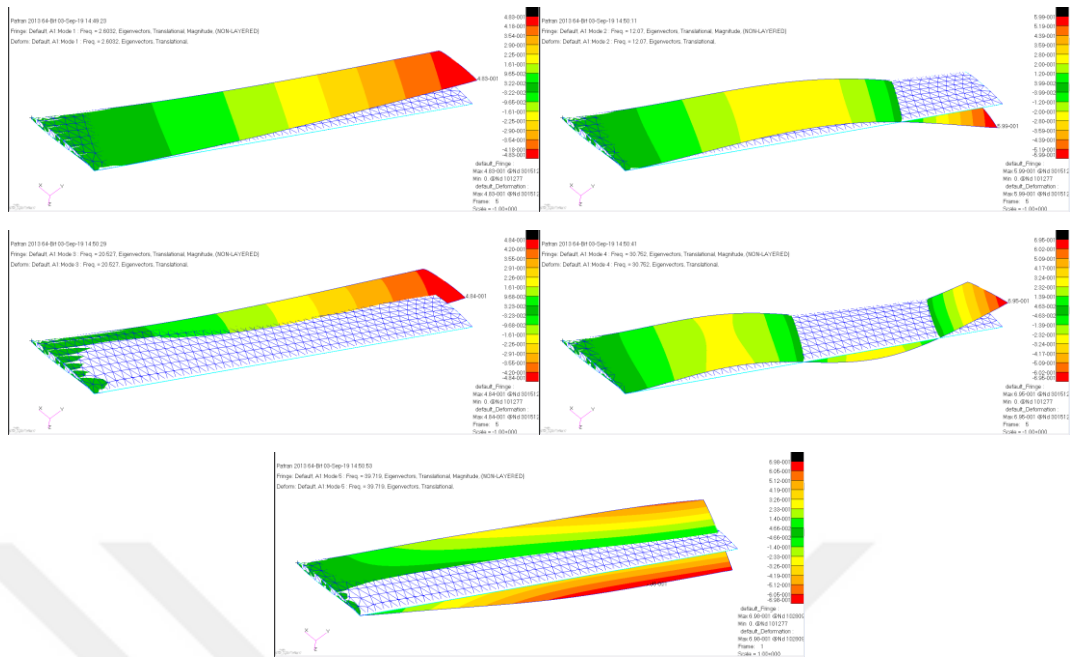


Figure A.29. First five mode shapes of the Wing 9

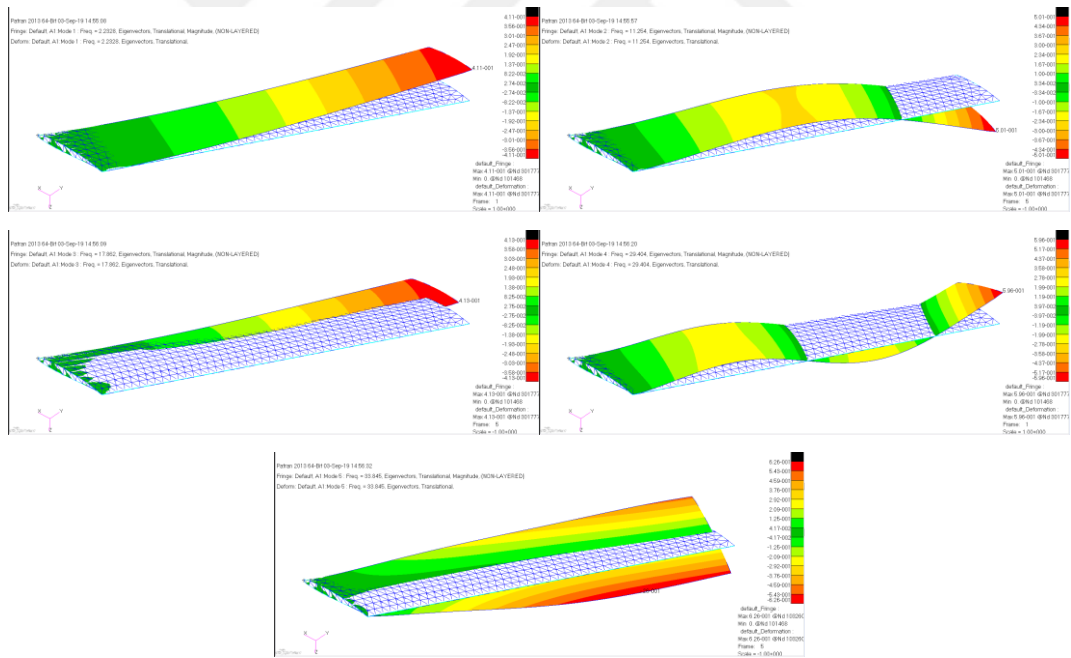


Figure A.30. First five mode shapes of the Wing 10

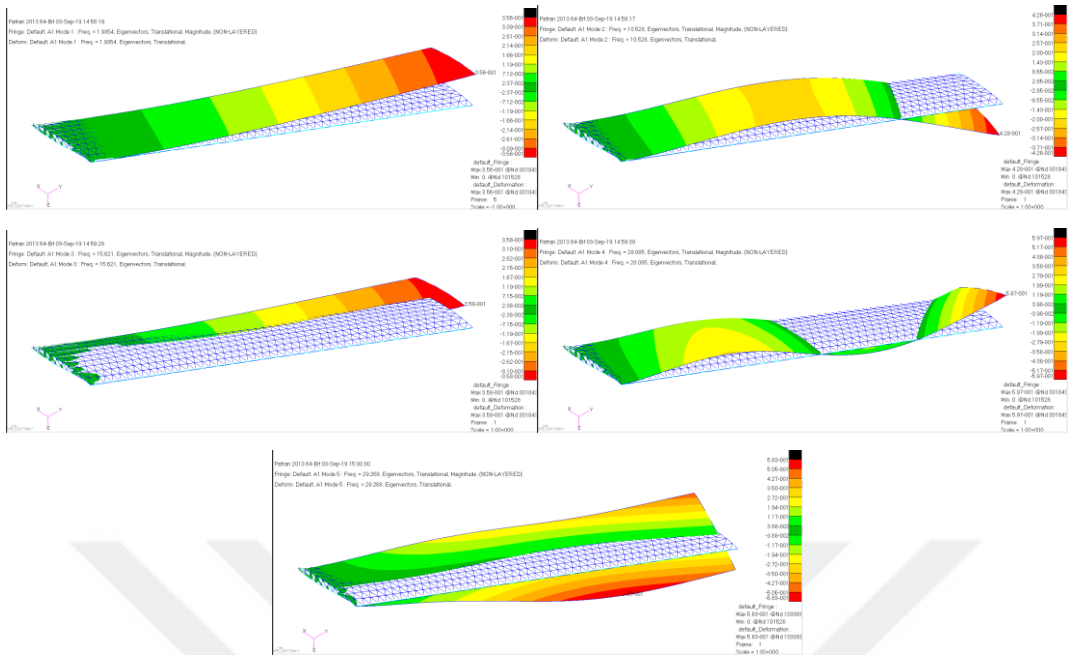


Figure A.31. First five mode shapes of the Wing 11

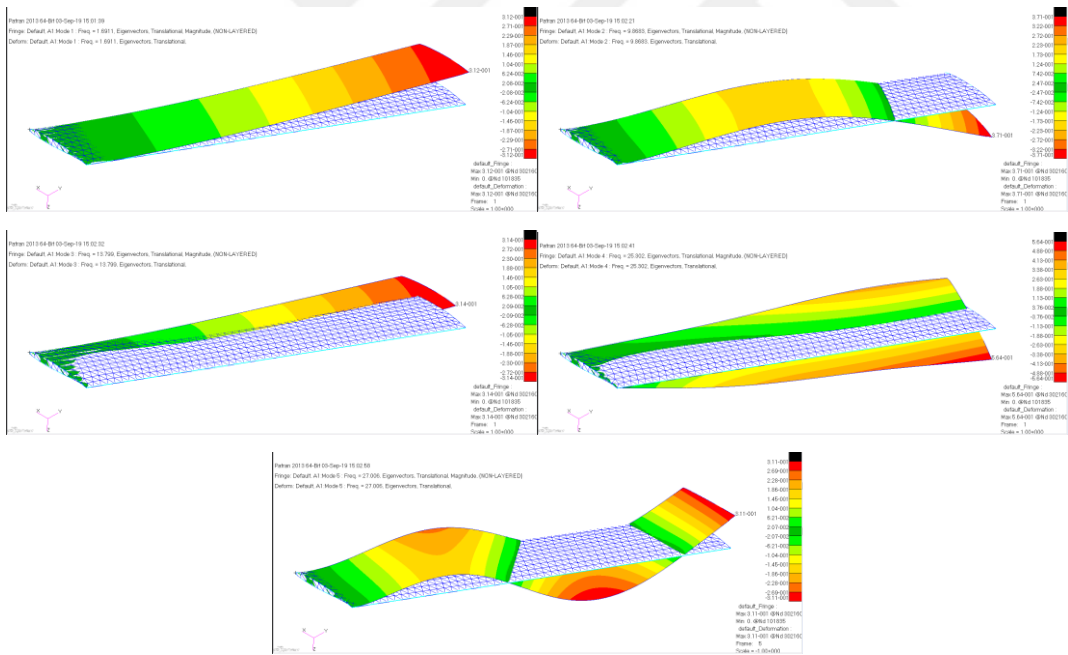


Figure A.32. First five mode shapes of the Wing 12

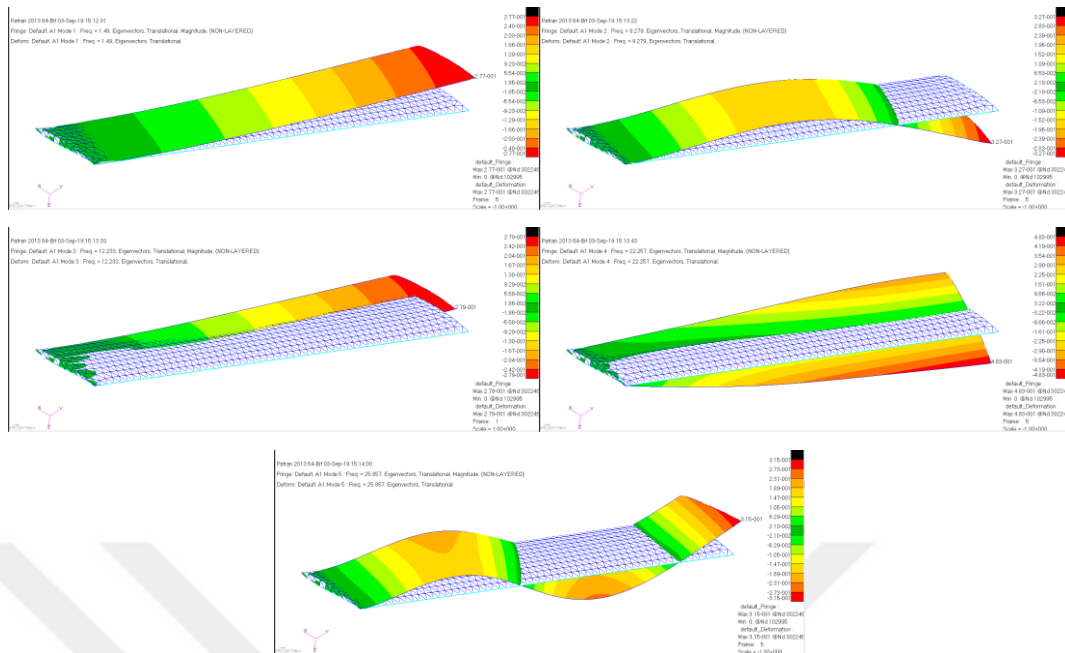


Figure A.33. First five mode shapes of the Wing 13

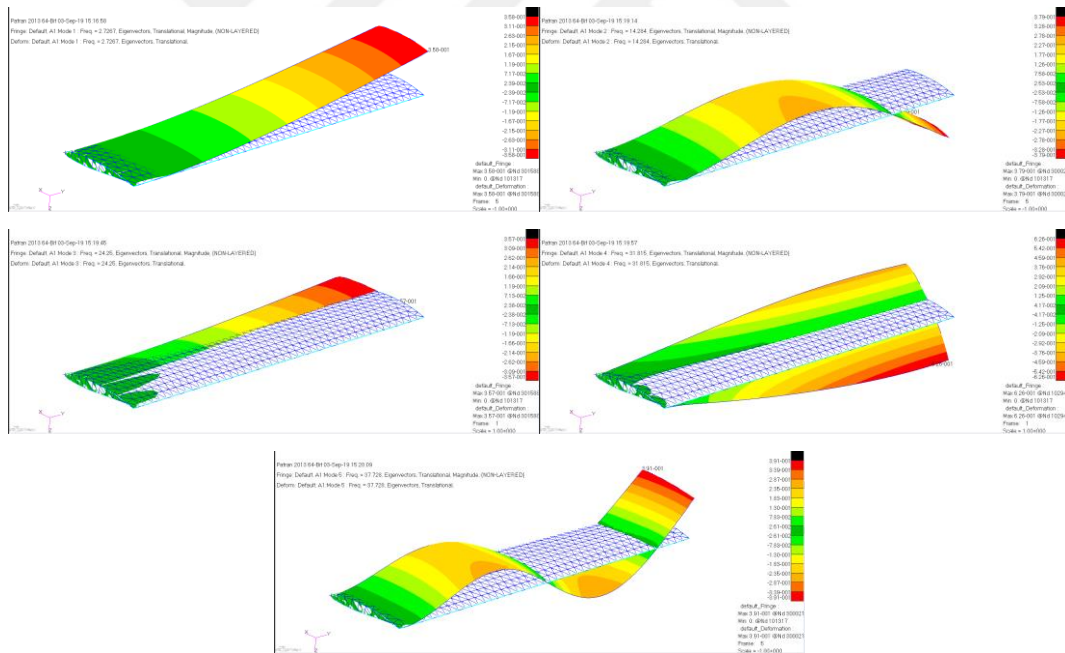


Figure A.34. First five mode shapes of the Wing 14

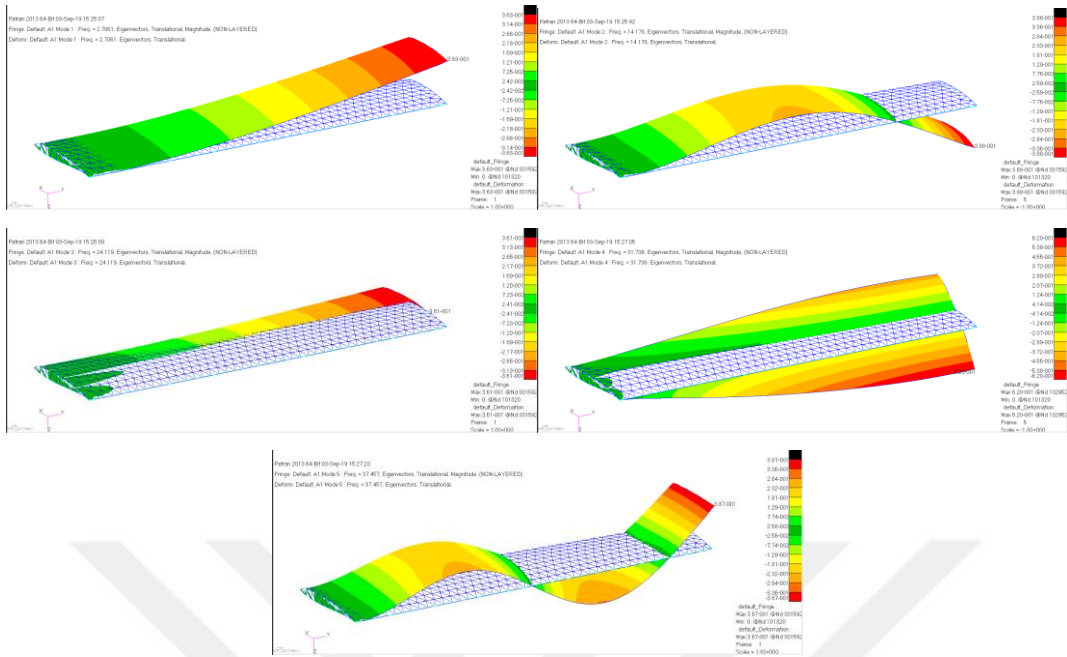


Figure A.35. First five mode shapes of the Wing 15

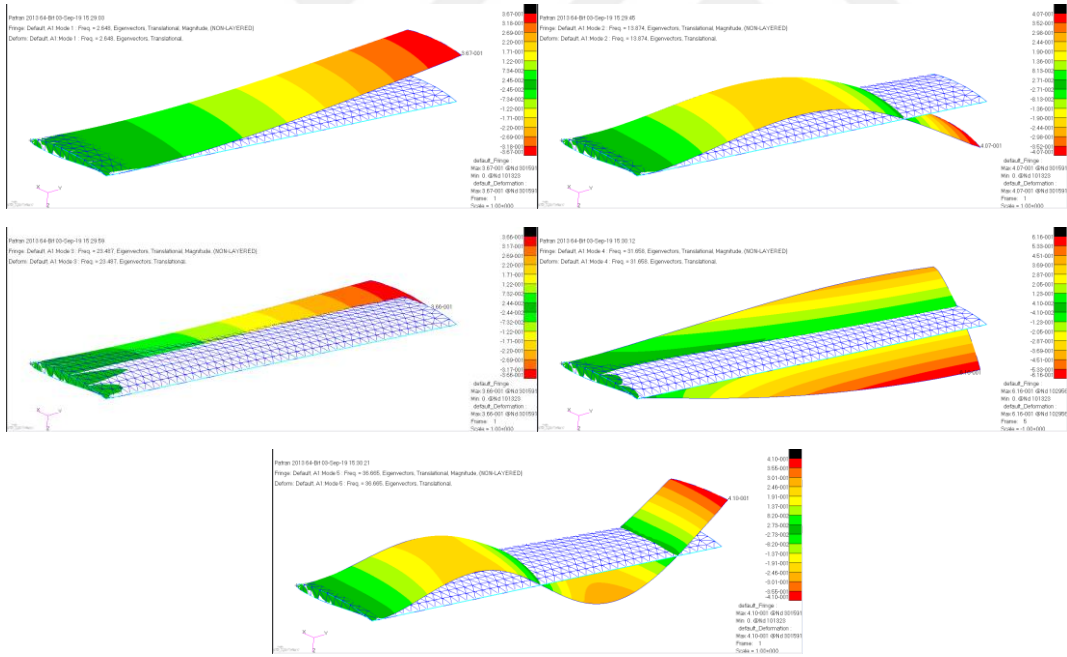


Figure A.36. First five mode shapes of the Wing 16

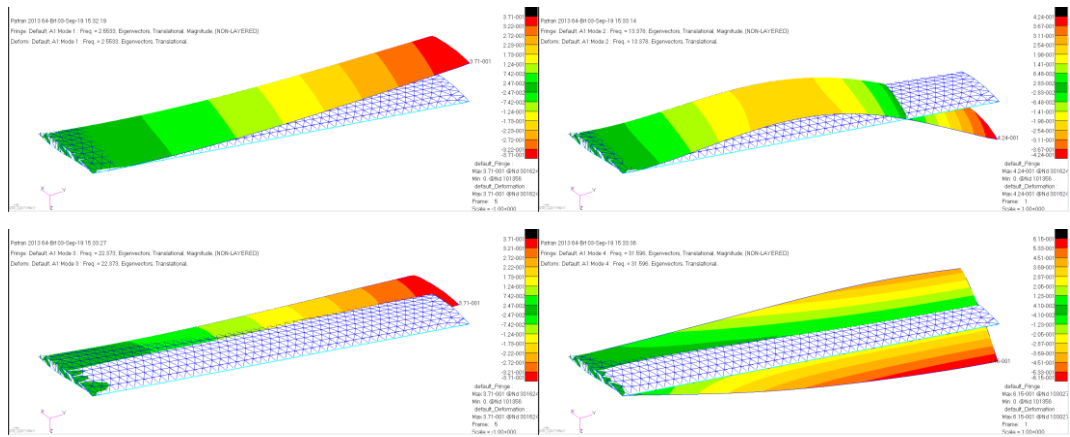


Figure A.37. First five mode shapes of the Wing 17

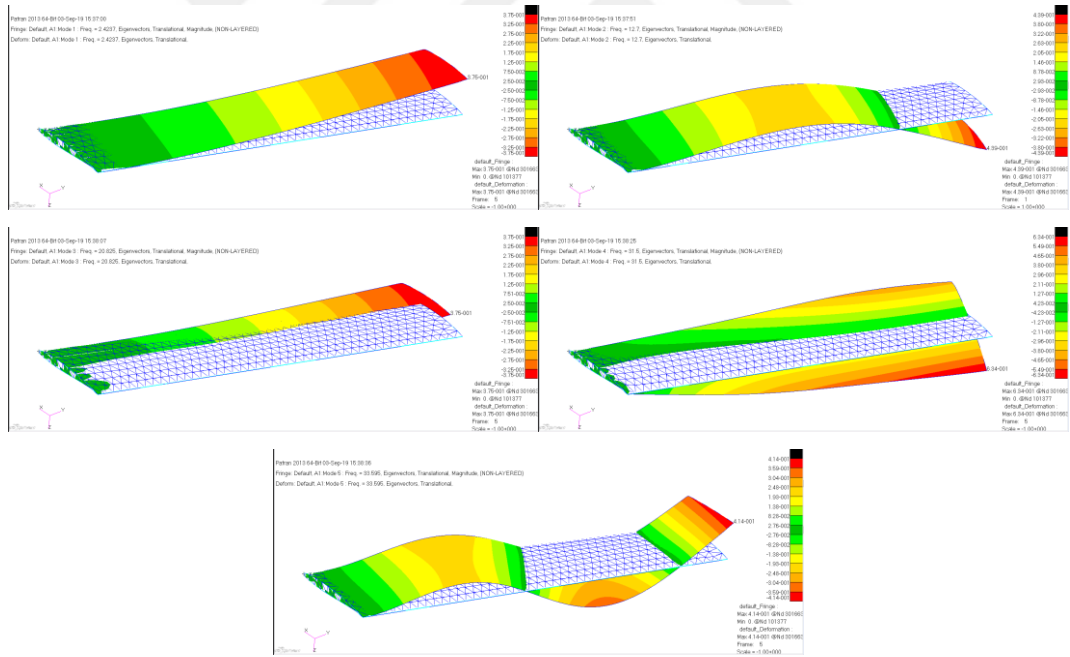


Figure A.38. First five mode shapes of the Wing 18

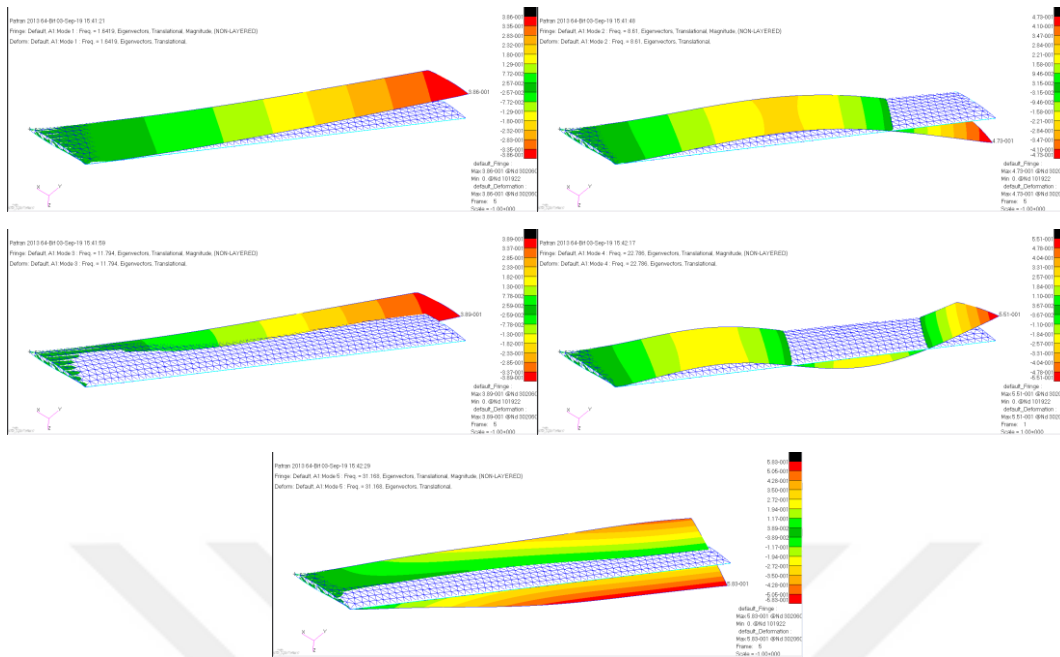


Figure A.39. First five mode shapes of the Wing 19

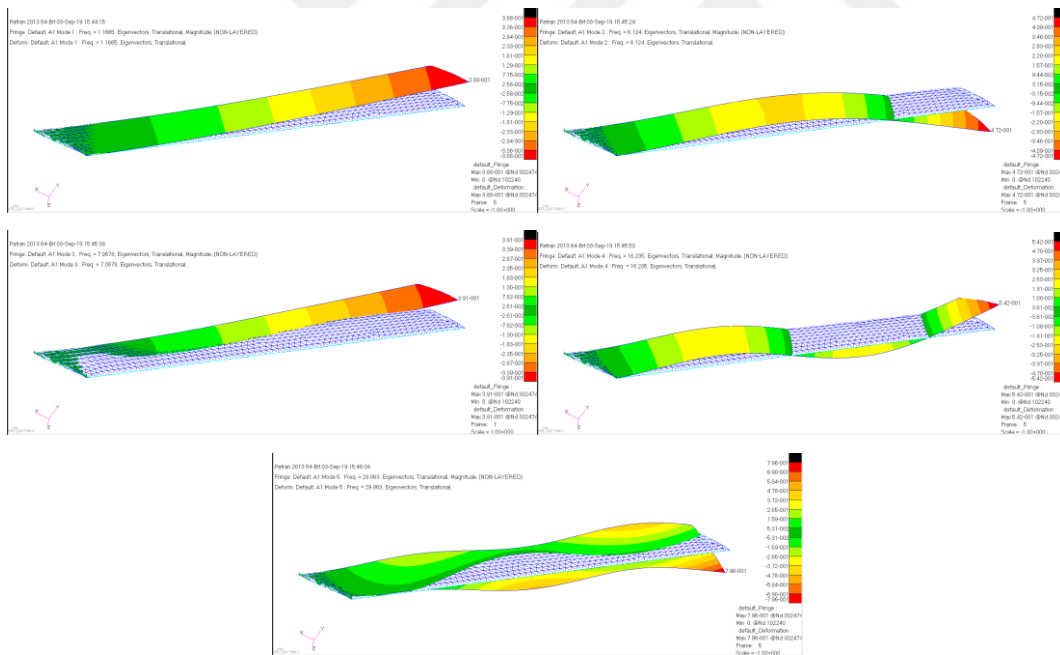


Figure A.40. First five mode shapes of the Wing 20

C. Flutter Analysis Results

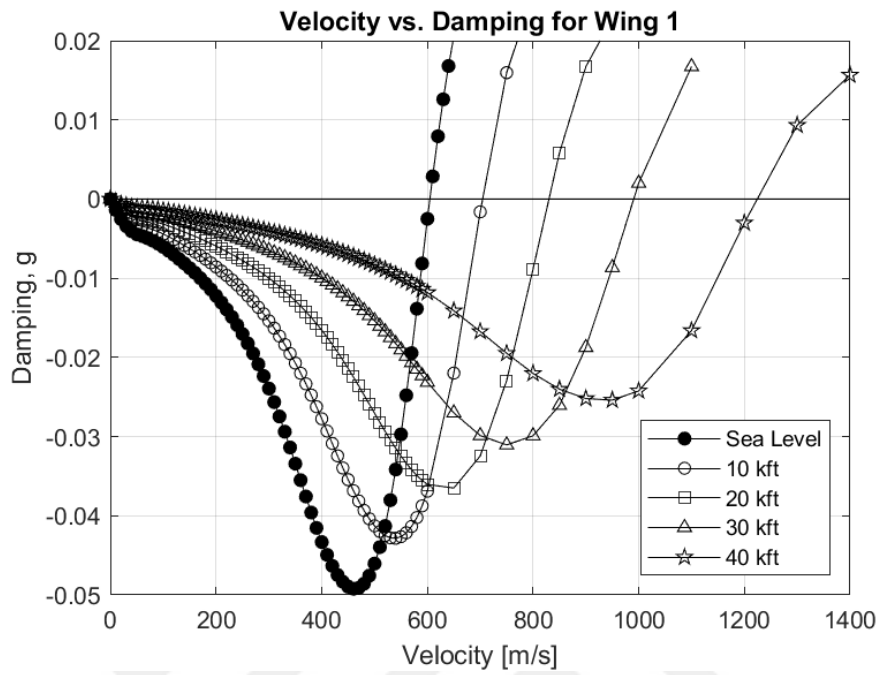


Figure A.41. Velocity vs. Damping plots for the Wing 1

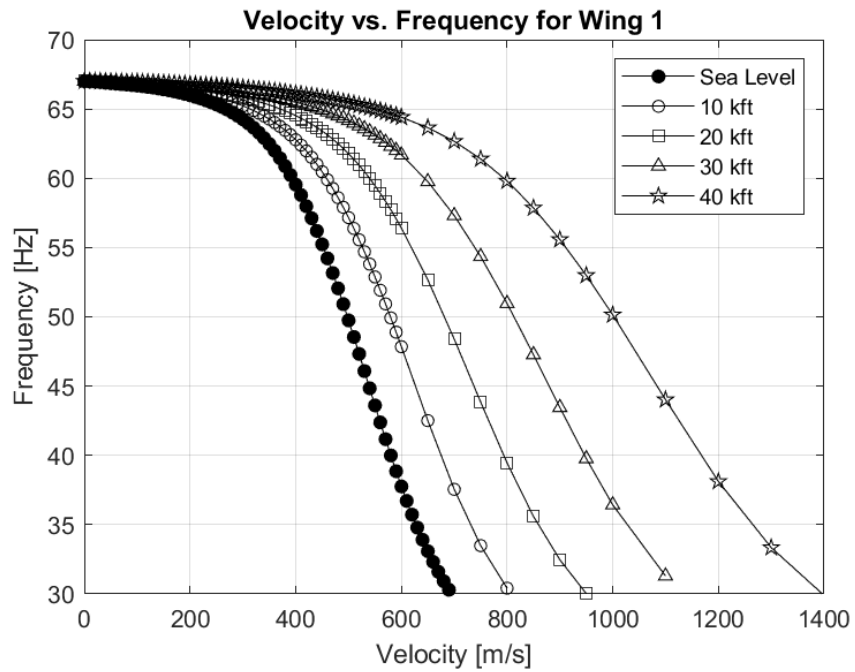


Figure A.42. Velocity vs. Frequency plots for the Wing 1

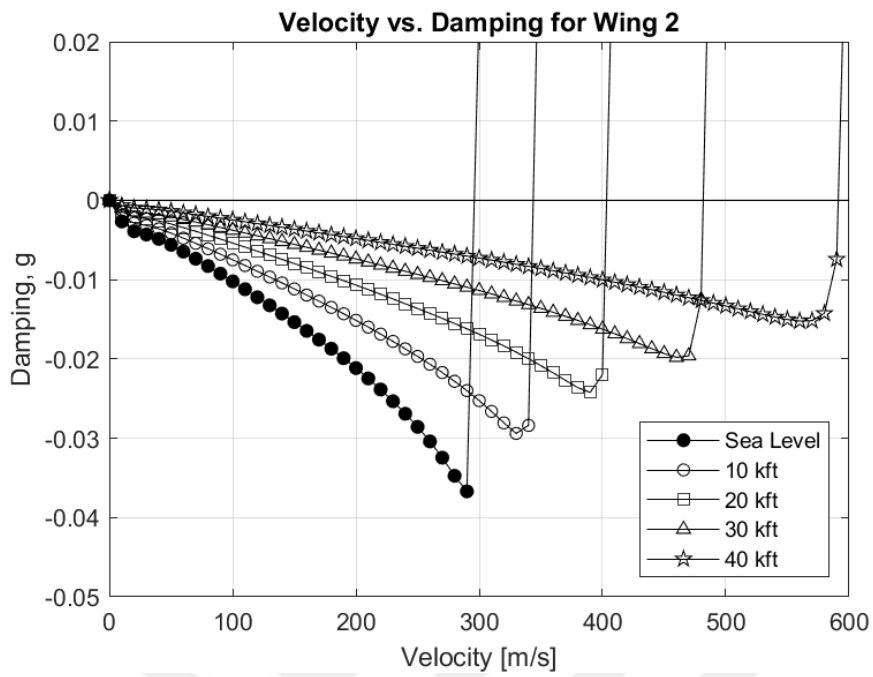


Figure A.43. Velocity vs. Damping plots for the Wing 2

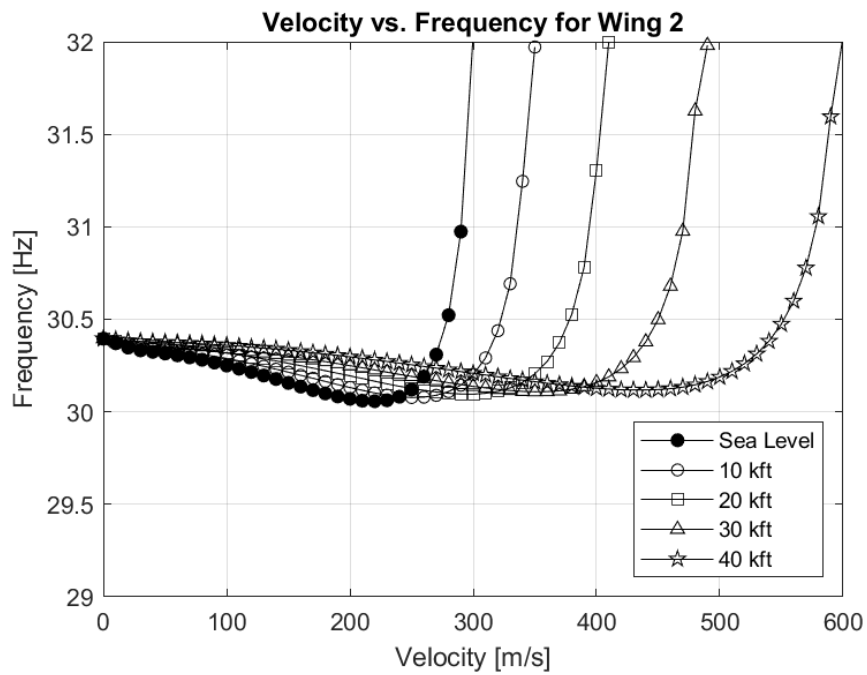


Figure A.44. Velocity vs. Frequency plots for the Wing 2

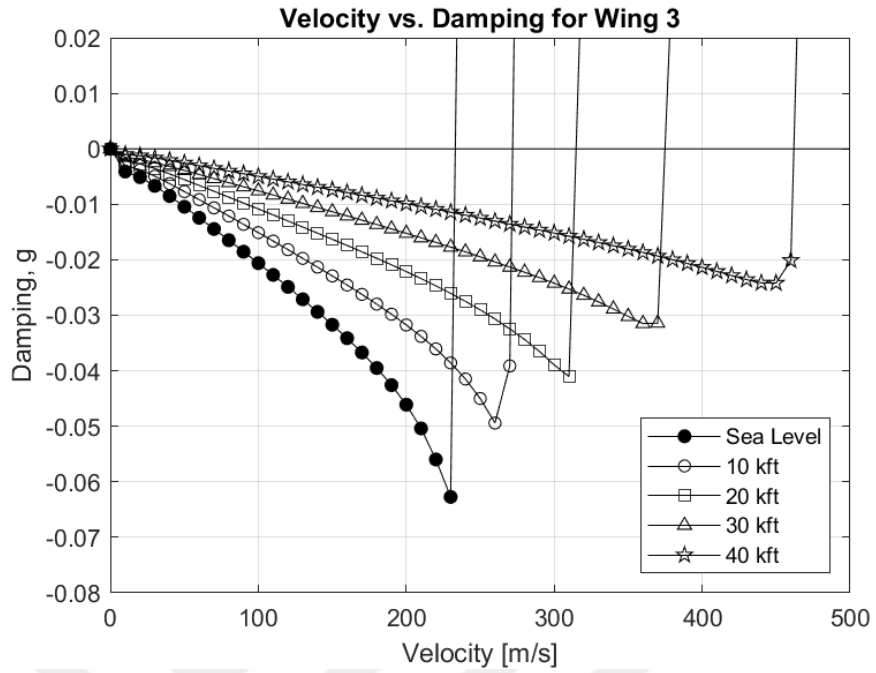


Figure A.45. Velocity vs. Damping plots for the Wing 3

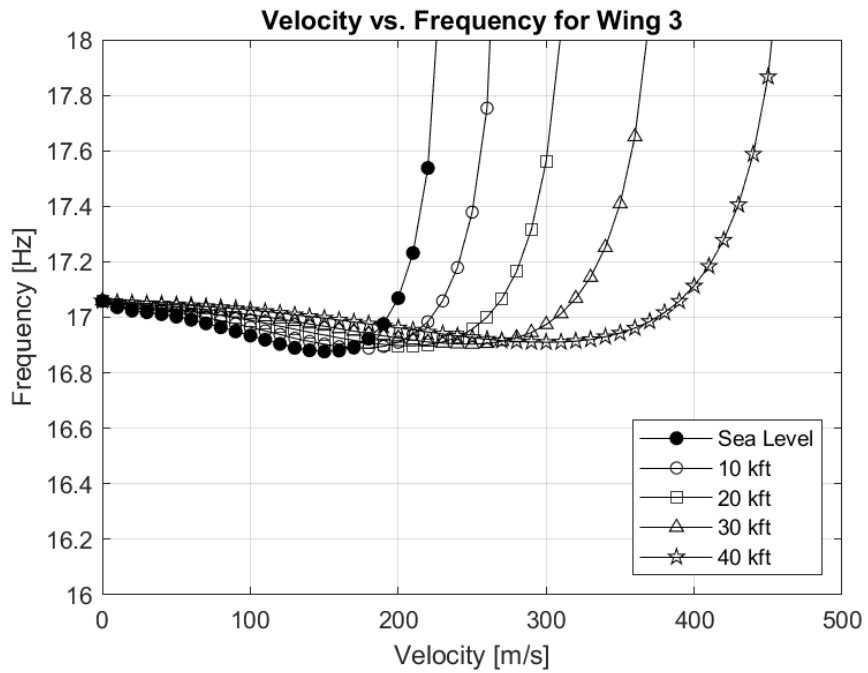


Figure A.46. Velocity vs. Frequency plots for the Wing 3

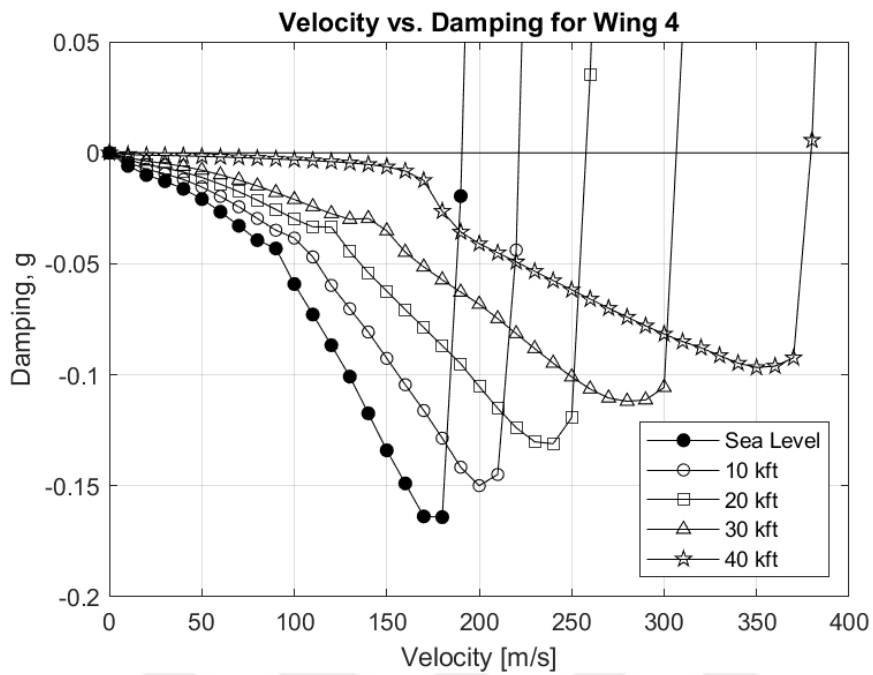


Figure A.47. Velocity vs. Damping plots for the Wing 4

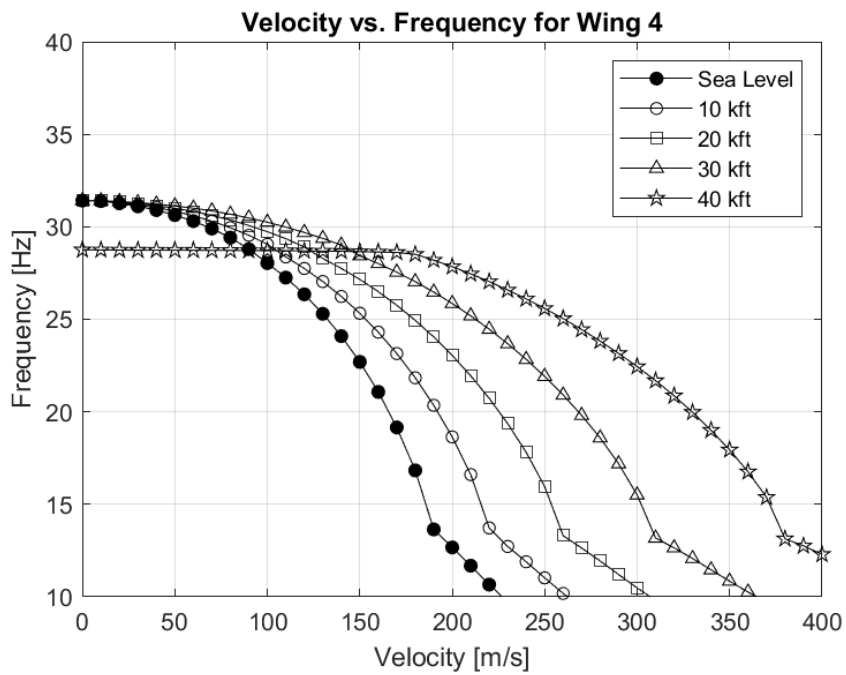


Figure A.48. Velocity vs. Frequency plots for the Wing 4

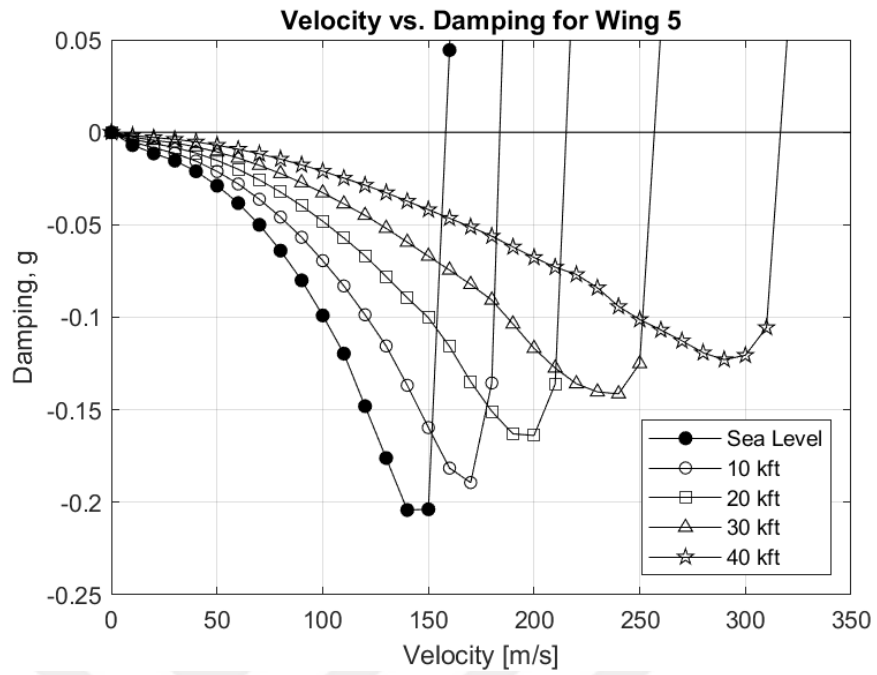


Figure A.49. Velocity vs. Damping plots for the Wing 5

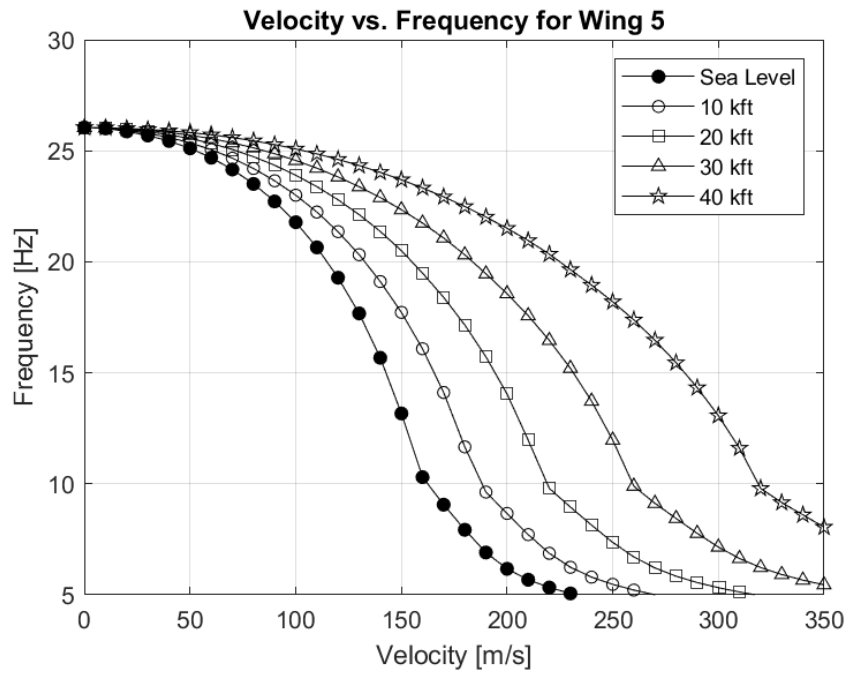


Figure A.50. Velocity vs. Frequency plots for the Wing 5

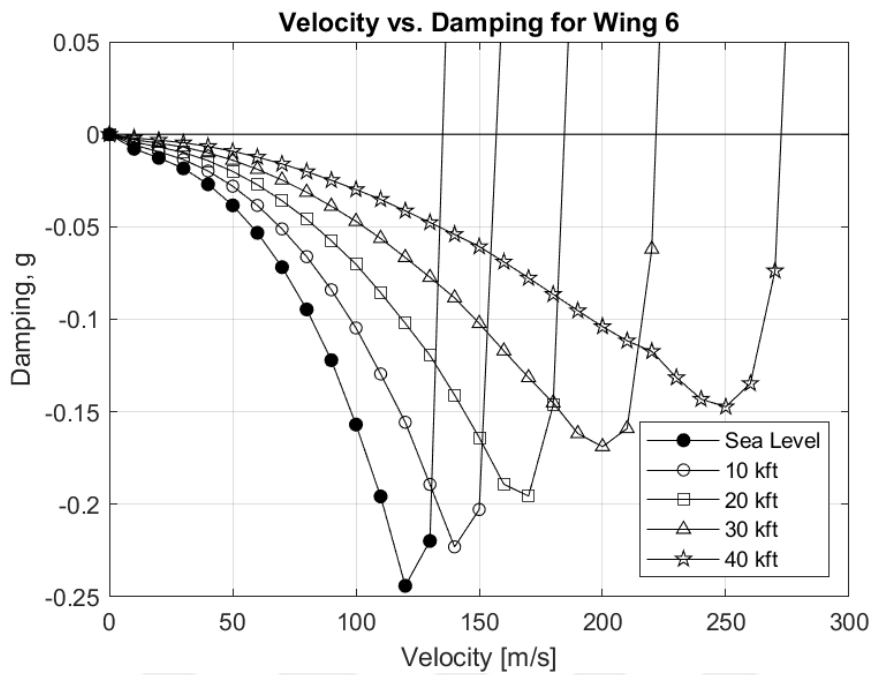


Figure A.51. Velocity vs. Damping plots for the Wing 6

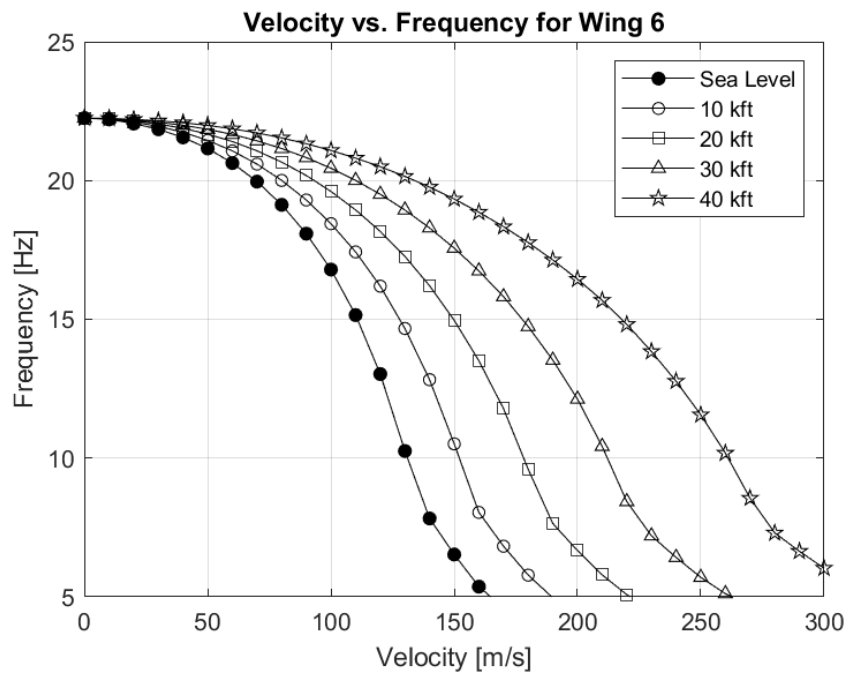


Figure A.52. Velocity vs. Frequency plots for the Wing 6

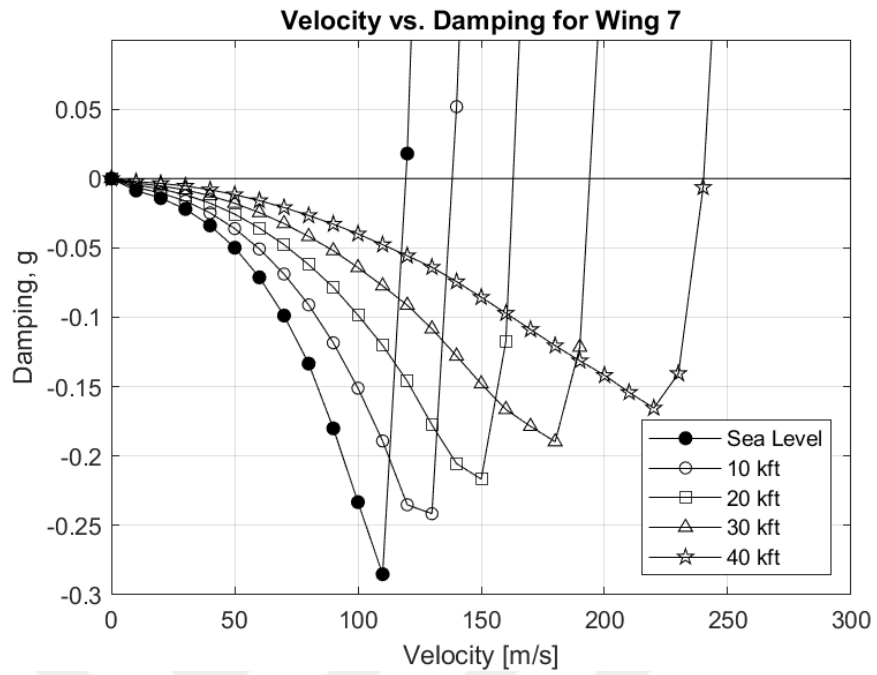


Figure A.53. Velocity vs. Damping plots for the Wing 7

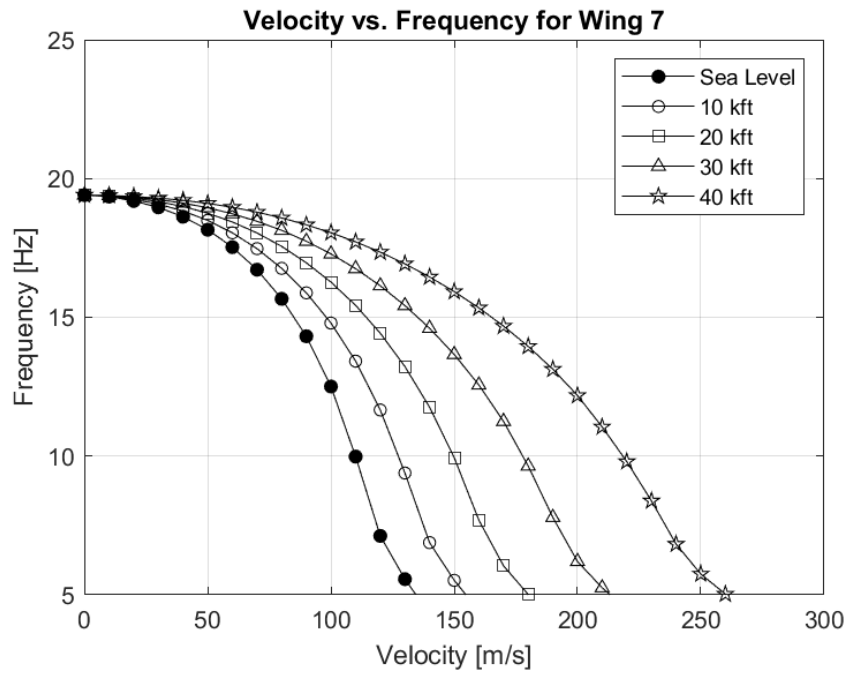


Figure A.54. Velocity vs. Frequency plots for the Wing 7

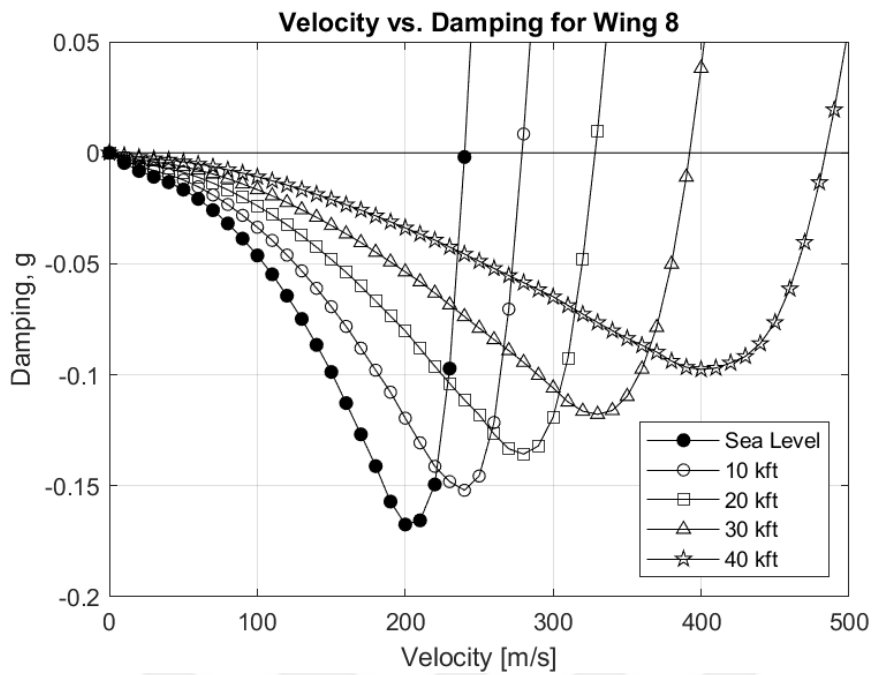


Figure A.55. Velocity vs. Damping plots for the Wing 8

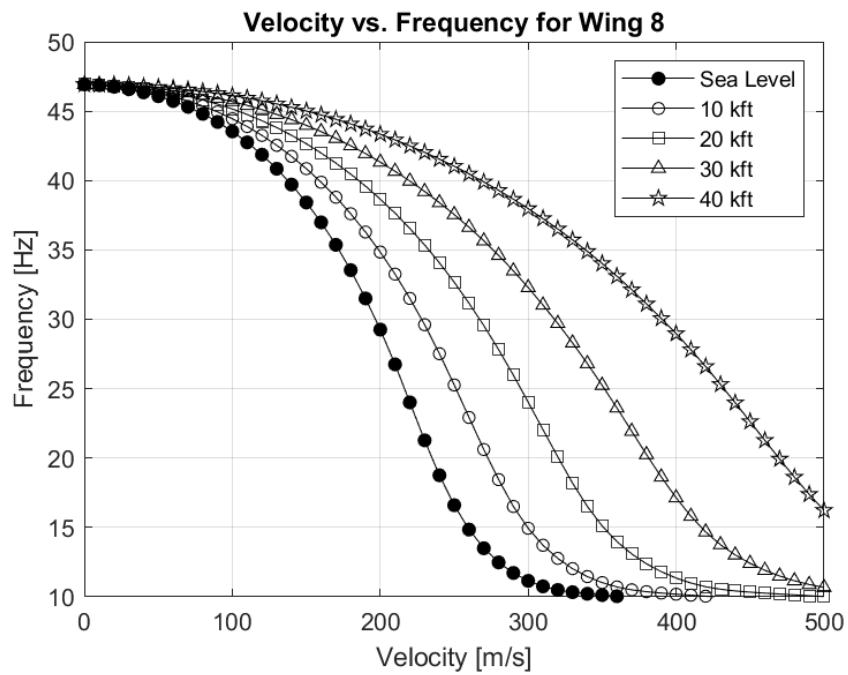


Figure A.56. Velocity vs. Frequency plots for the Wing 8

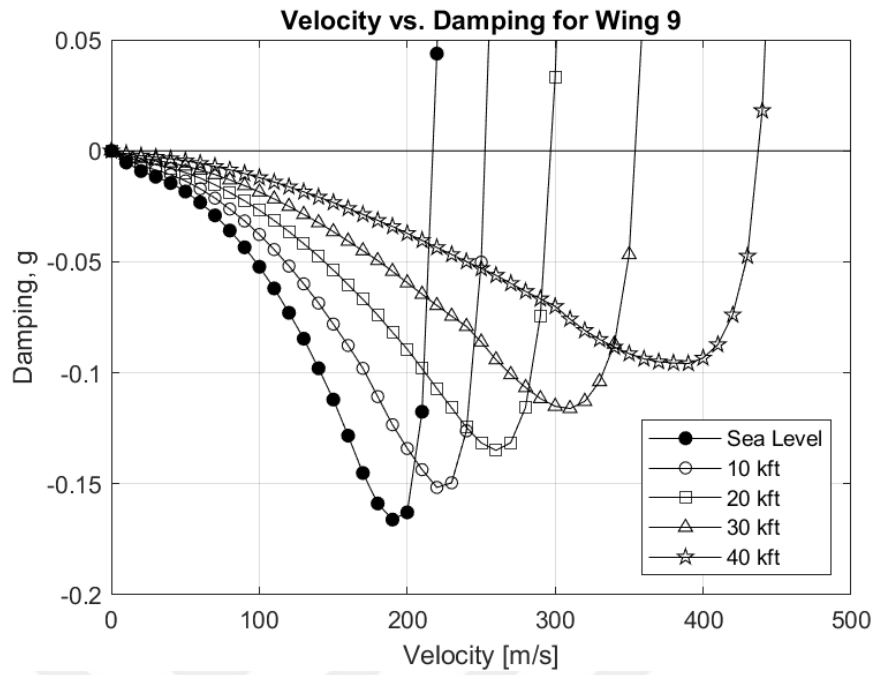


Figure A.57. Velocity vs. Damping plots for the Wing 9

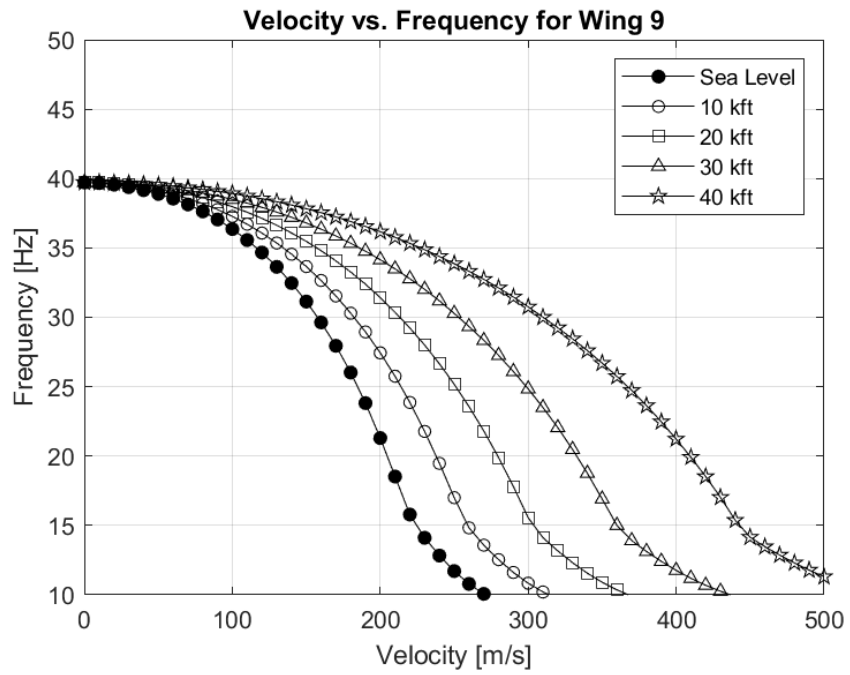


Figure A.58. Velocity vs. Frequency plots for the Wing 9

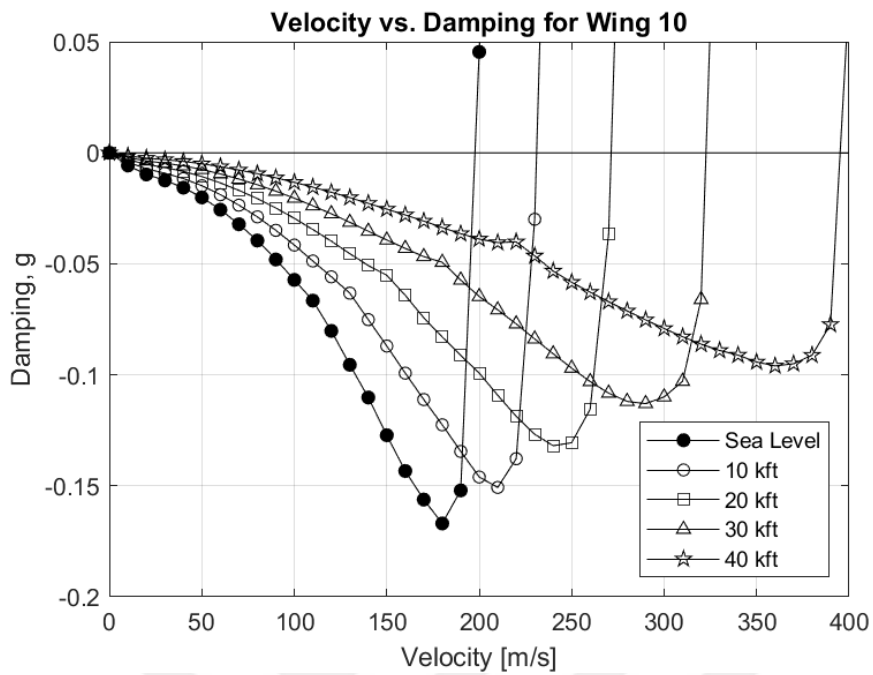


Figure A.59. Velocity vs. Damping plots for the Wing 10

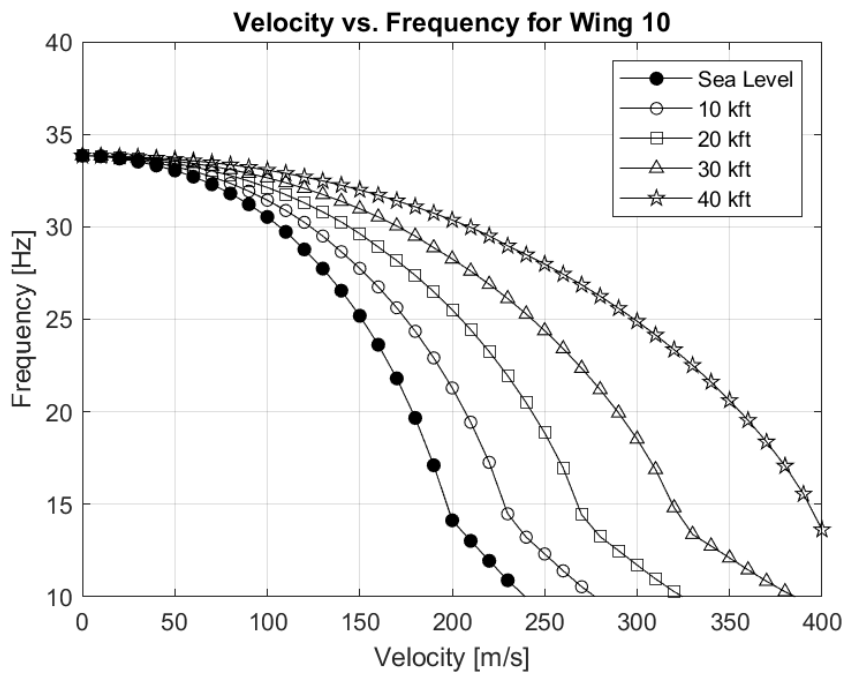


Figure A.60. Velocity vs. Frequency plots for the Wing 10

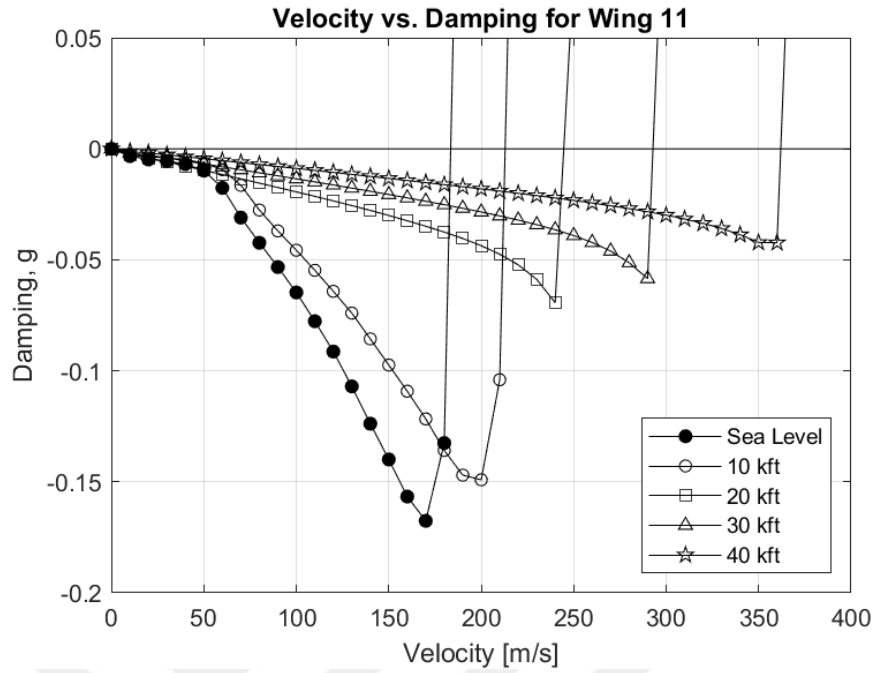


Figure A.61. Velocity vs. Damping plots for the Wing 11

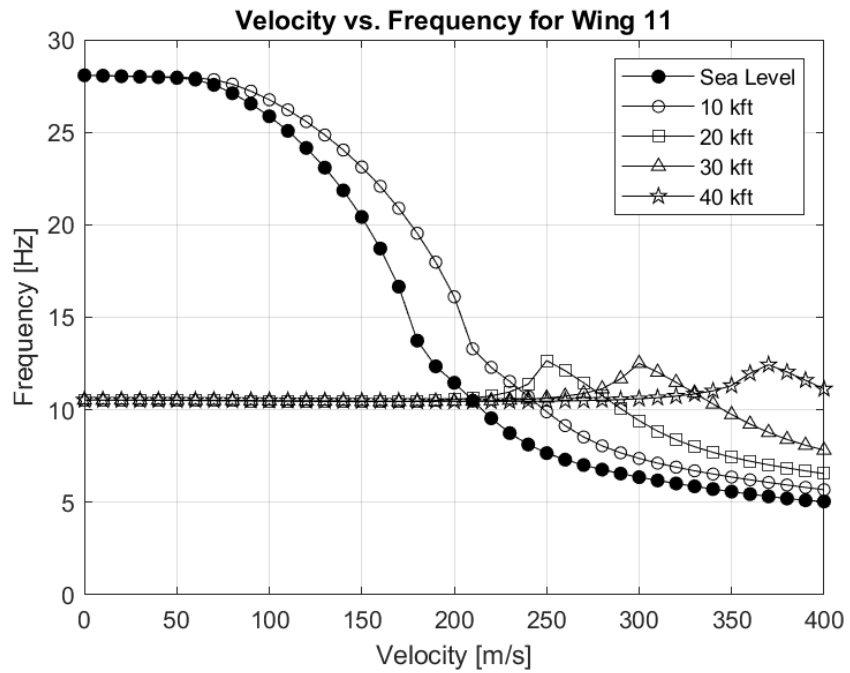


Figure A.62. Velocity vs. Frequency plots for the Wing 11

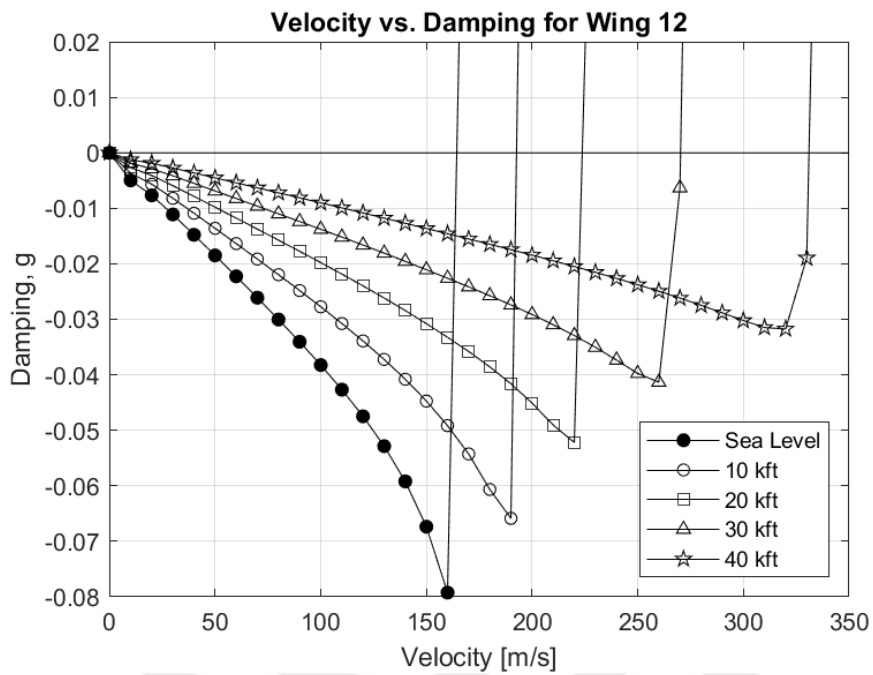


Figure A.63. Velocity vs. Damping plots for the Wing 12

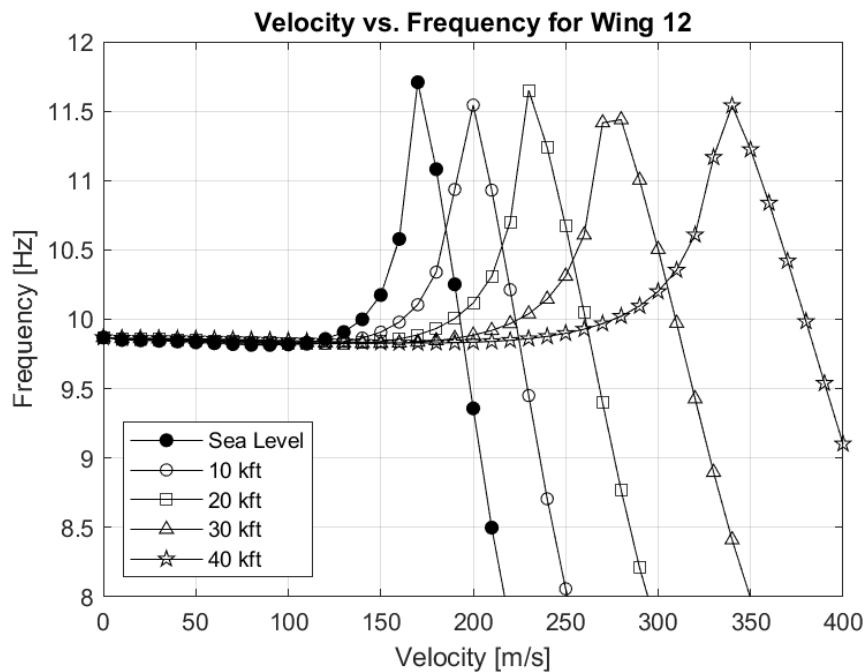


Figure A.64. Velocity vs. Frequency plots for the Wing 12

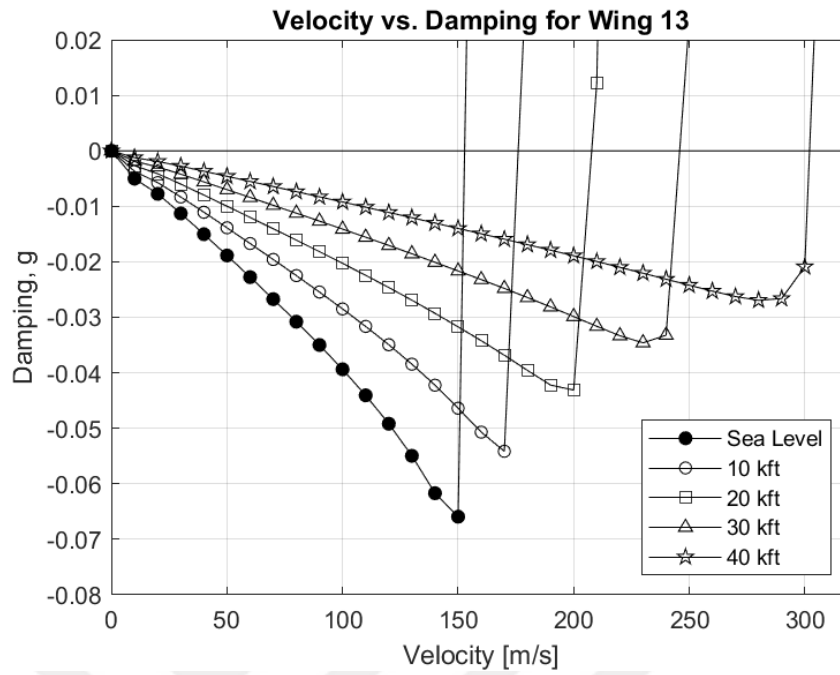


Figure A.65. Velocity vs. Damping plots for the Wing 13

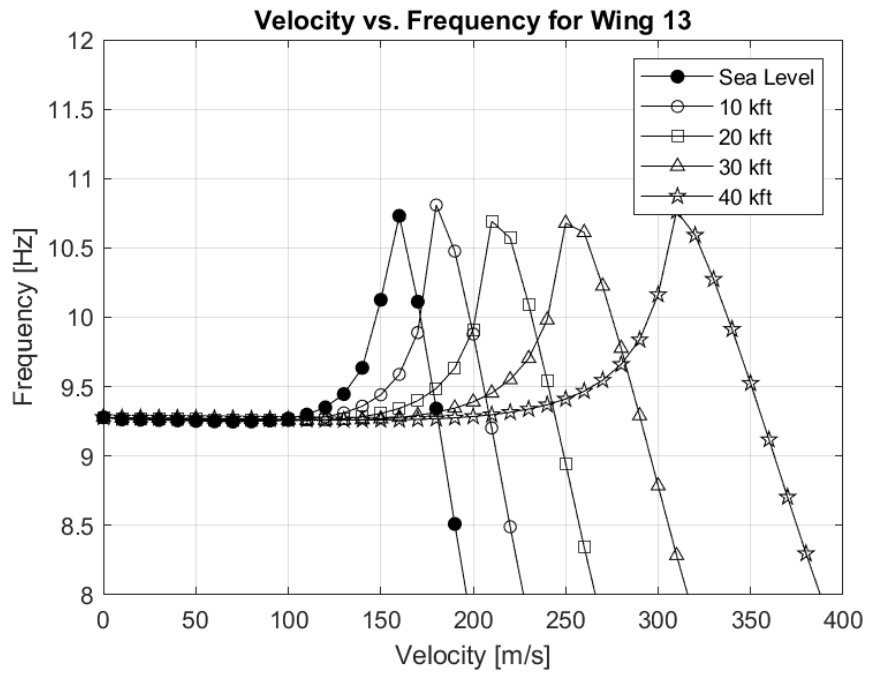


Figure A.66. Velocity vs. Frequency plots for the Wing 13

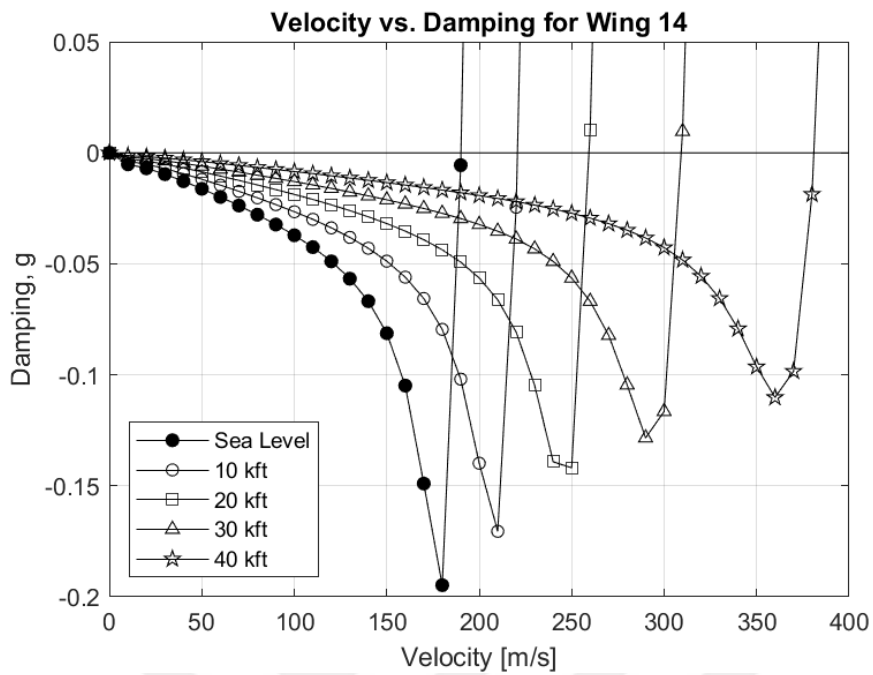


Figure A.67. Velocity vs. Damping plots for the Wing 14

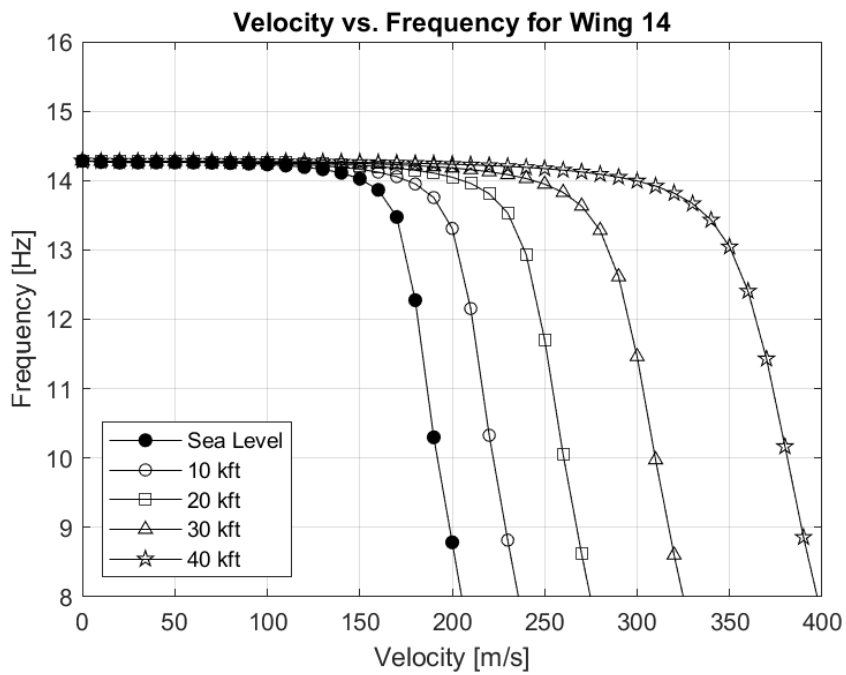


Figure A.68. Velocity vs. Frequency plots for the Wing 14

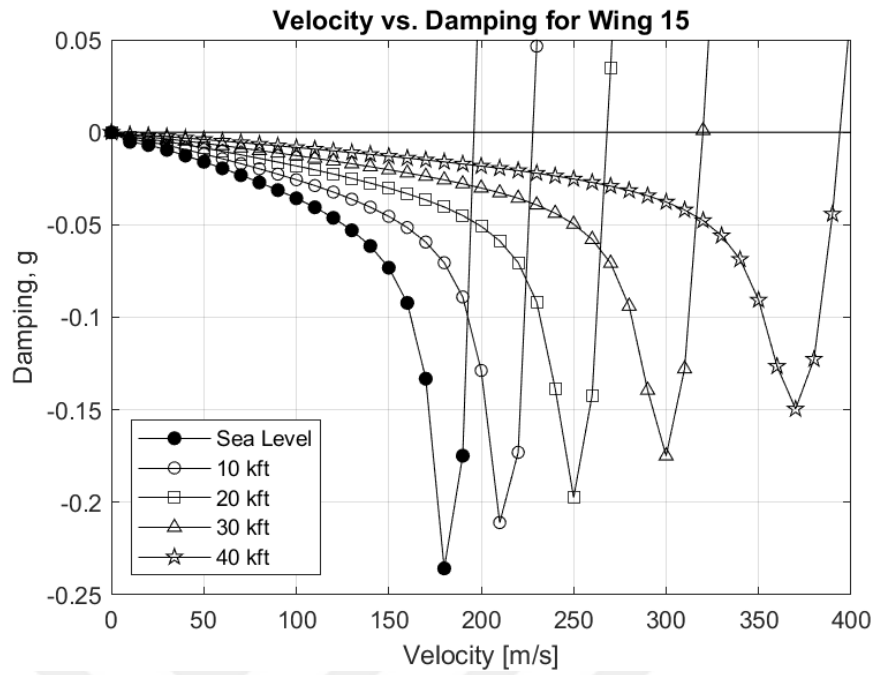


Figure A.69. Velocity vs. Damping plots for the Wing 15

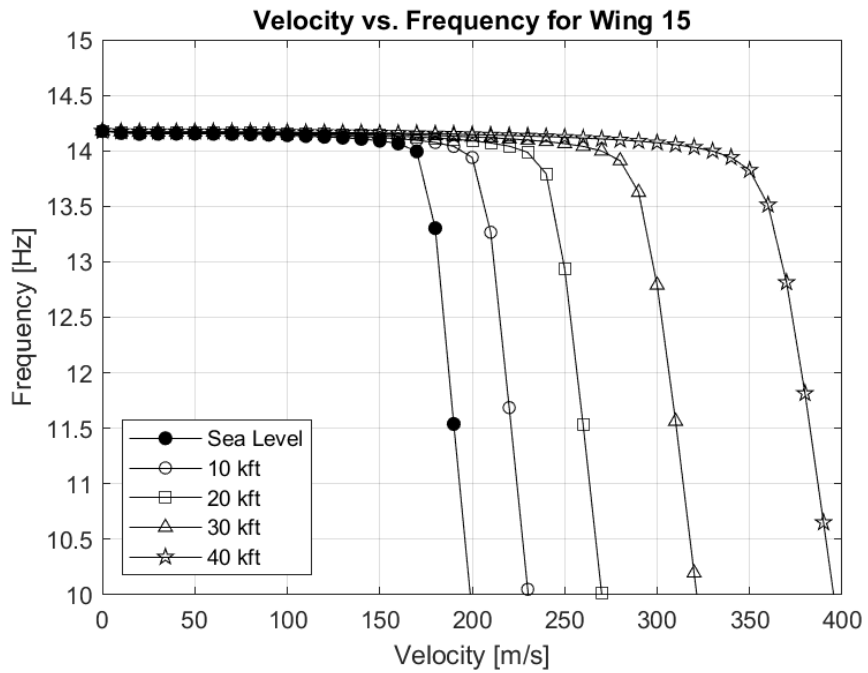


Figure A.70. Velocity vs. Frequency plots for the Wing 15

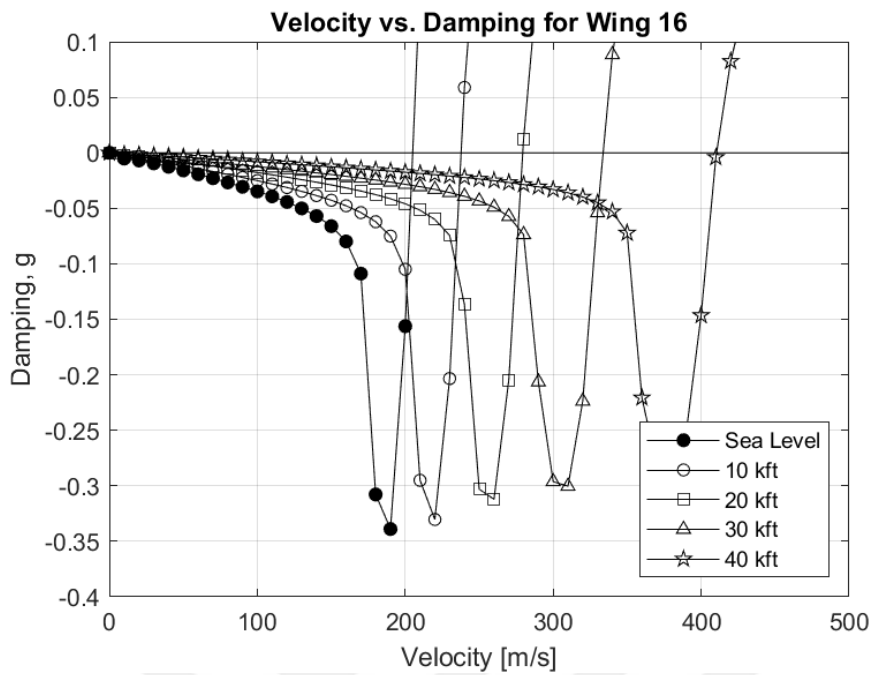


Figure A.71. Velocity vs. Damping plots for the Wing 16

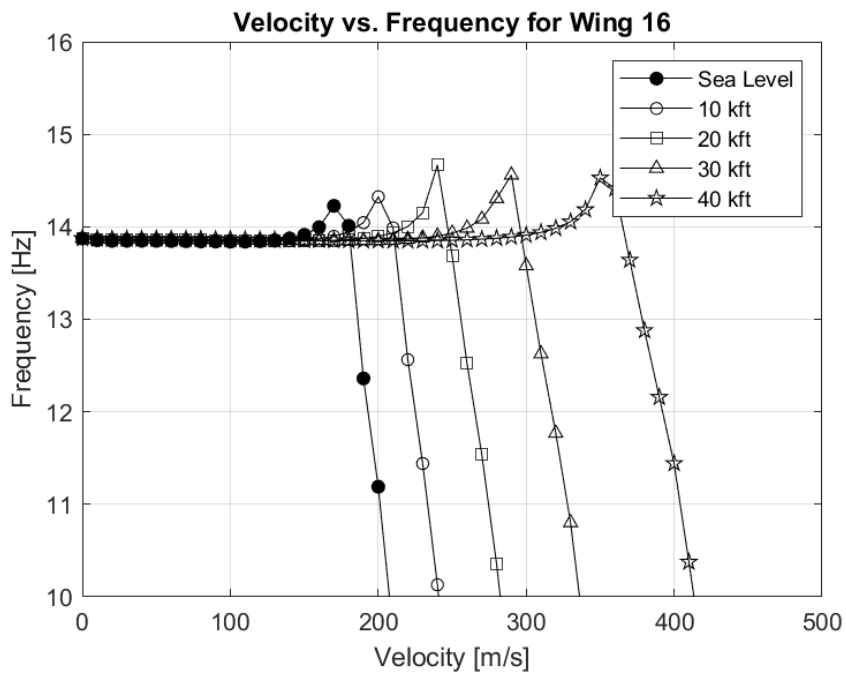


Figure A.72. Velocity vs. Frequency plots for the Wing 16

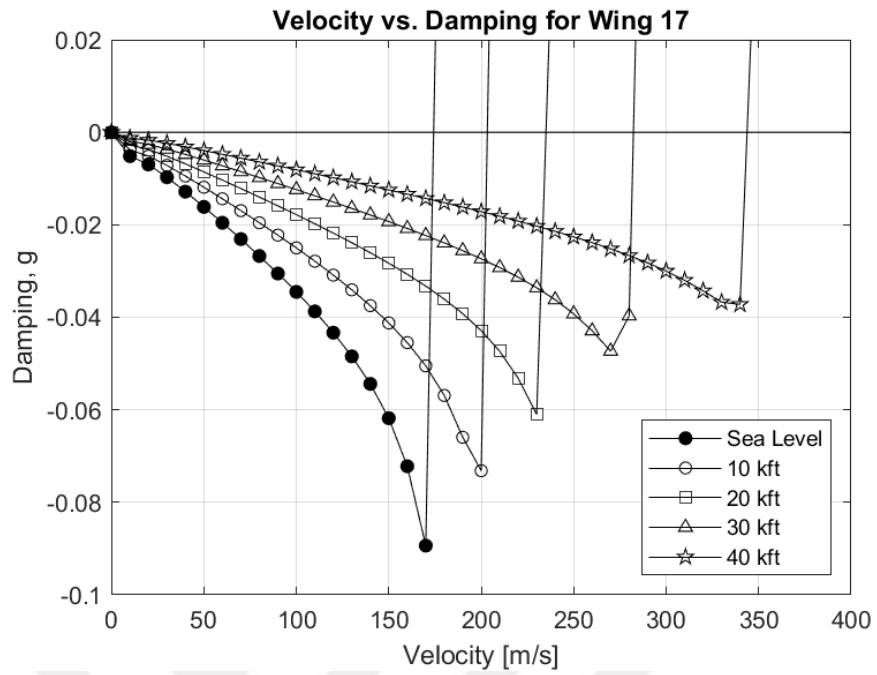


Figure A.73. Velocity vs. Damping plots for the Wing 17

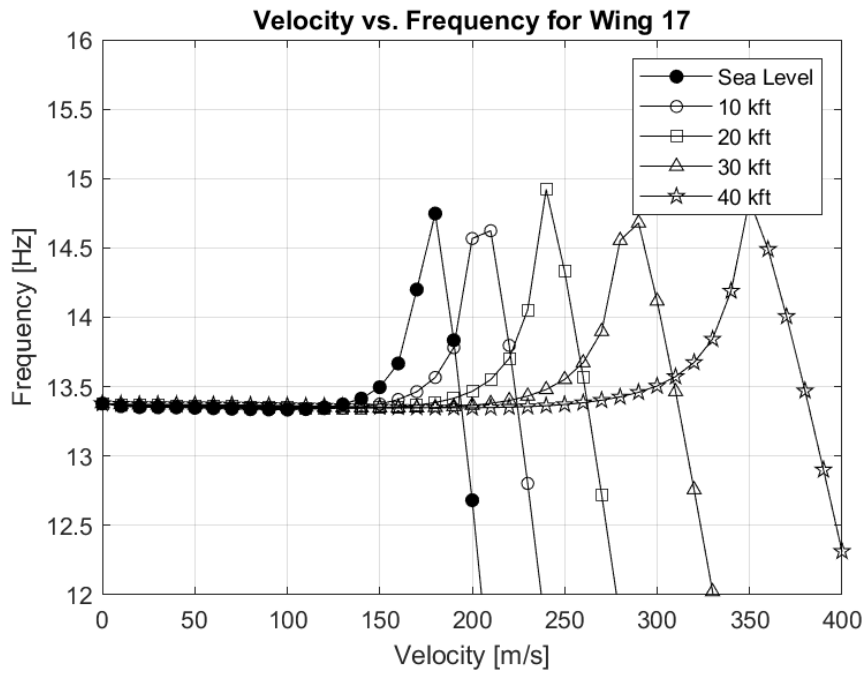


Figure A.74. Velocity vs. Frequency plots for the Wing 17

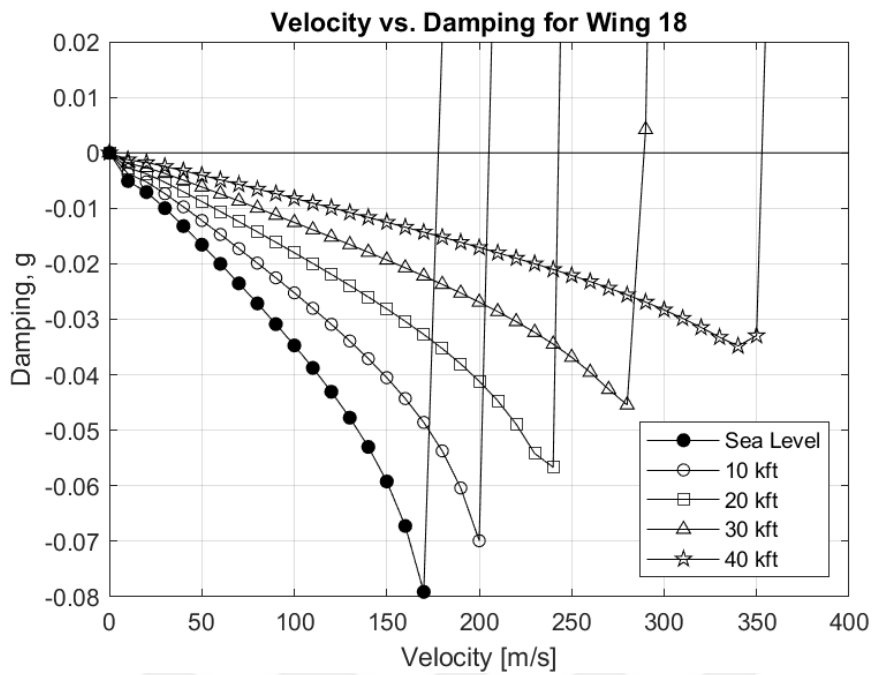


Figure A.75. Velocity vs. Damping plots for the Wing 18

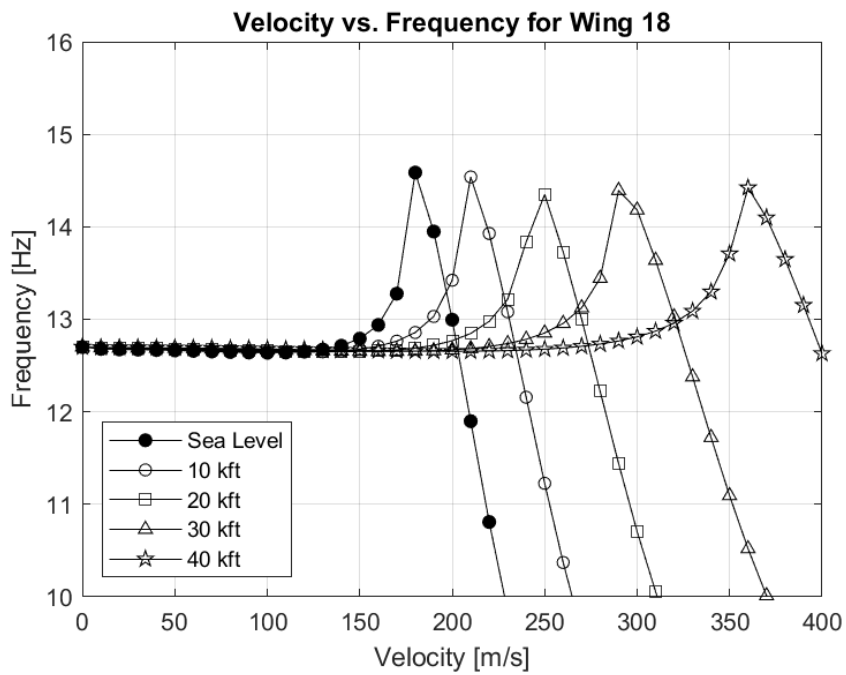


Figure A.76. Velocity vs. Frequency plots for the Wing 18

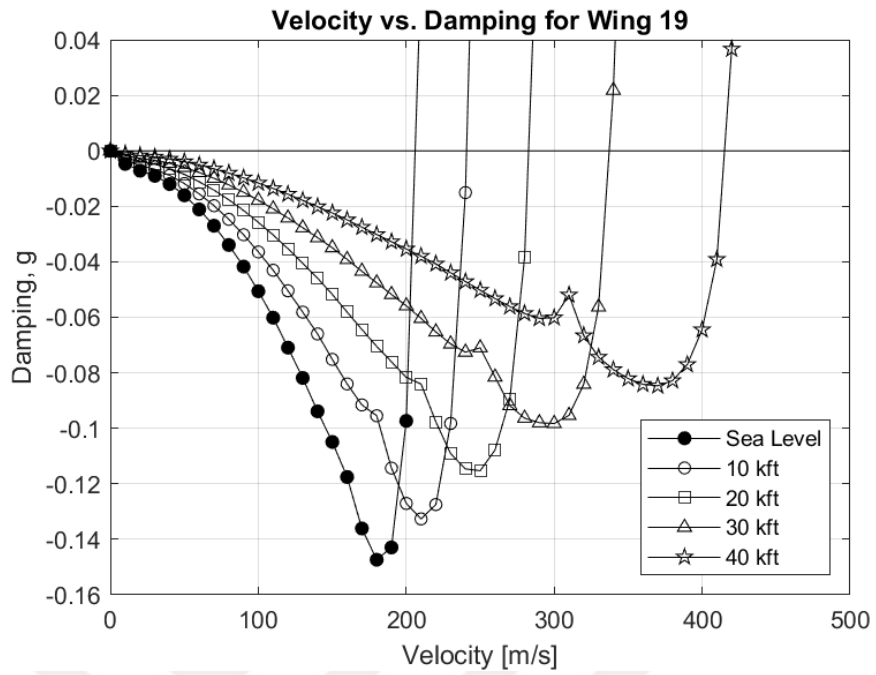


Figure A.77. Velocity vs. Damping plots for the Wing 19

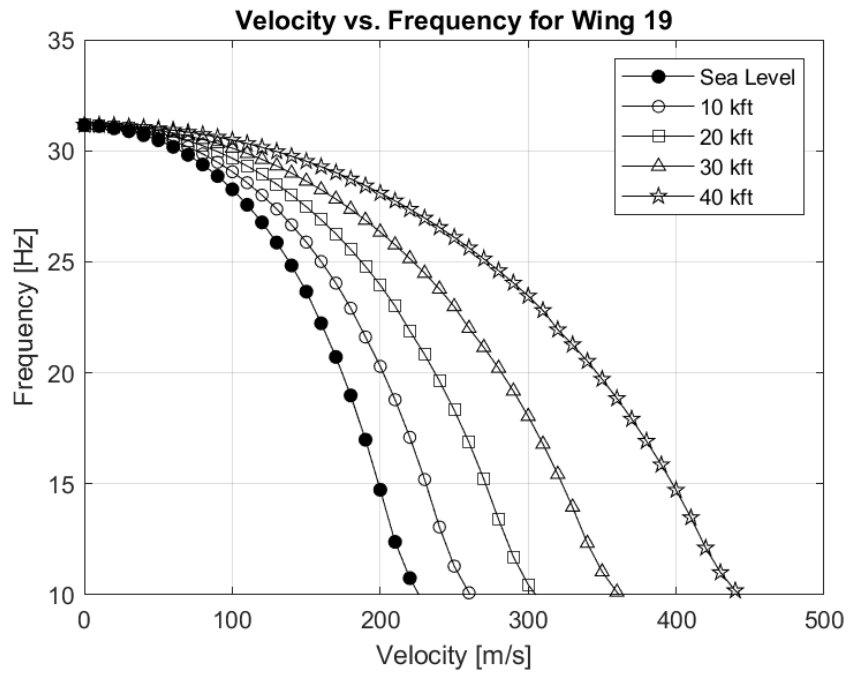


Figure A.78. Velocity vs. Frequency plots for the Wing 19

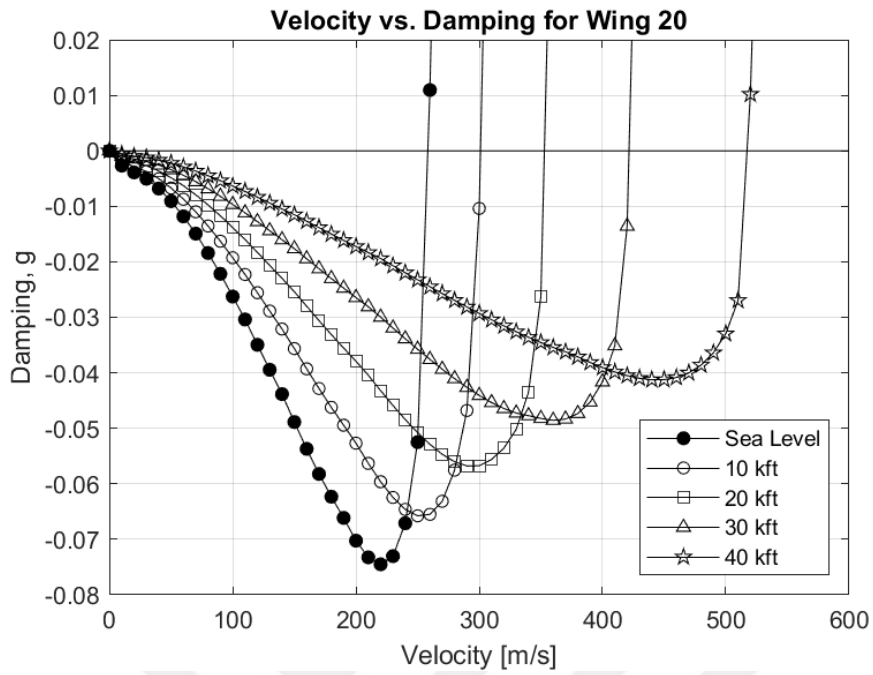


Figure A.79. Velocity vs. Damping plots for the Wing 20

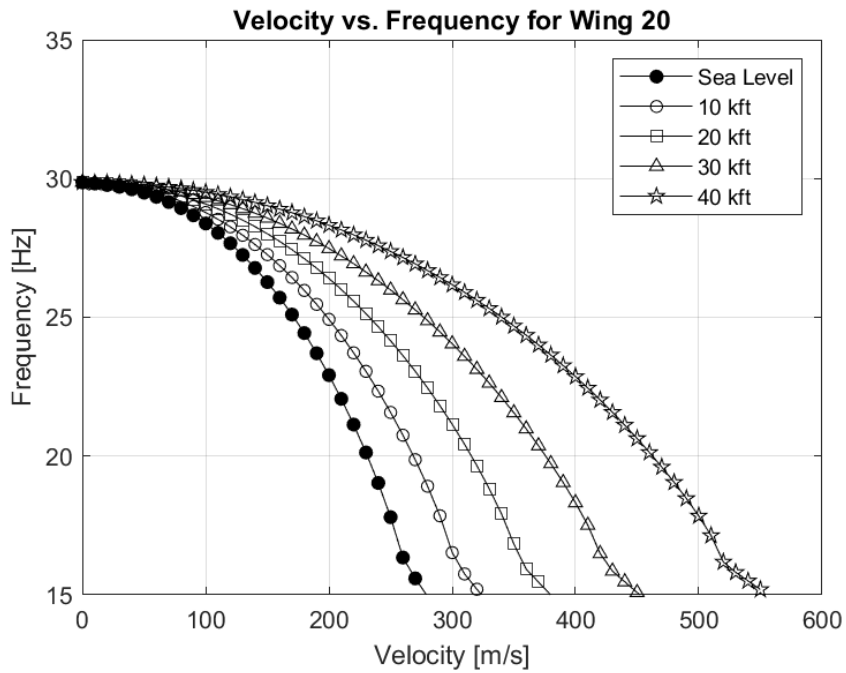


Figure A.80. Velocity vs. Frequency plots for the Wing 20